PATH INTEGRAL METHODS FOR QUANTUM DYNAMICS IN CONDENSED PHASES

BY

TUSEETA BANERJEE

DISSERTATION

Submitted in partial fulfillment of the requirements
for the degree of Doctor of Philosophy in Chemistry
in the Graduate College of the
University of Illinois at Urbana-Champaign, 2015

Urbana, Illinois

Doctoral Committee:

Professor Nancy Makri, Director of Research
Professor Zan Luthey-Schulten
Professor So Hirata
Professor Kenneth Schweizer

Abstract

Quantum mechanical effects play an important role in dynamics of condensed phases. It is also well known that the difficulty of solving the full Schrödinger equation grows exponentially with time. One approach to cope up with this difficulty is to restrict quantum treatment to a few particles (system) and treat the dynamics of the rest of particles (bath) using classical trajectories. Path integral methods due to their trajectory like nature provide excellent tool to develop quantum-classical methods, but to capture long time dynamics, the number of classical trajectories grow exponentially.

A part of this work focuses on improving Quantum-Classical Path Integral (QCPI) treatments that allow for larger path integral time step by building "smarter" propagators. These improved solvent-driven reference propagators is developed by incorporating physically motivated approximations to the solvent. When used in QCPI expression they allow convergence with larger time steps leading to an exponential reduction of the number of trajectories required. Further advantages of these propagators include improvements in path filtering techniques, smaller number of path integral steps for achieving the memory decoherence time, and smoothing of the integrand which leads to convergence with fewer Monte Carlo sample points.

These ideas have been validated on the spin boson model - a prototypical model to study condensed phase dynamics, which consists of a two-level system coupled to a harmonic bath. The new approach of building the reference propagators combined with their iterative evaluation and filtering is validated using parameters that mimic the first electron transfer in wild-type photosynthetic reaction centres. A real-world dynamical simulation contains various anharmonic effects, Ferrocene (donor) - Ferrocenium (acceptor) system in liquid Benzene was studied where the anharmonic effects of the bath of liquid Benzene on the dynamics of the system were treated using Ensemble Averaged Classical Path.

The process of electron or proton transfer occurs between two species having different charges and fluctuations in the solvent plays a key role in determining the rates of such reaction dynamics. To correctly account for the effects of initial distribution of the solvent on the dynamics of the quantum system, the concept of equilibrating the bath to the donor state of the system is used. Two different approaches have been used within the influence functional framework.

To Ma, Baba, Didi, Pankaj Da,

and my nephews Soumyo and Shubhra

Acknowledgements

I would like to thank my advisor, Prof. Nancy Makri for her guidance over the last four years. She has supported me during very difficult times and has provided me the necessary encouragement to complete the thesis – this thesis literally would not have been completed without her support. Again, during this time I was not just developing my ideas in the field of quantum dynamics but also honing my culinary skills. It was an absolute delight to take two courses from her. The clarity with which she explained the most difficult concepts and most importantly the transitions from classical to quantum or to semiclassical theories, helped me gain many concepts required in my research.

I would like to thank my committee members Prof. Luthey-Schulten, Prof. Hirata and Prof. Schweizer for agreeing to be in my committee. I am also indebted for learning various computational biology tools in Prof. Luthey-Schulten's class which later helped me a lot in one of the projects. It was also fun to learn how the concepts of stochastic methods (a tool which I was learning for my research project) could be applied to determine outcomes of different coupled enzymatic reactions in a lac genetic switch. I am also very grateful to Prof. Hirata for teaching me how various size consistent electronic structure theory calculations are done, and the significance of the diagrammatic approaches, and their relations with Green Functions. I would like to thank Prof. Schweizer and Prof. Luthey-Schulten for finding the time to go over my final presentation and offering useful insights and comments.

I would like to take this opportunity to thank all my previous teachers and professors, especially my masters' thesis advisor Prof. Anindya Datta. This Ph.D would not be possible without the education and the basic concepts and principles I have developed over my high school, my college, and my master's education.

I would like to thank my group members, Dr. Roberto Lambert, Dr. Mohammad Sahrapour, Peter Walters, Thomas Allen, Amartya Bose, Sambarta Chatterjee for making the office such a fun place to work. The random chats on random topics at random hours for random stretch of times is what kept most of stochastic dynamics moving forward. (apart from the random numbers)

I would like to thank all my friends at UIUC. I guess if I start to list everyone, I would literally run out of space. To everyone whom I met in Champaign-Urbana in the last four and half years, a big thank you for being a part of this journey and for sharing the laughter along with the tears. I would like to thank all my friends from my college and masters' whose constant support have helped me overcome different

challenges I faced in the last four years. Distance and time have caused differences in a few of these friendships, but I hope that the same distance and time would heal most of the differences.

Almost last, and definitely the most, I would like to thank my family, for constantly supporting my education, my decision to move to another state, and then another country to further pursue my education. This thesis would not have been possible without their sacrifices, their well-wishes, and their blessings. To Ma, Baba, Didi, Pankaj Da, Soumyo and Subhra, “I am here because of all of you”. The constant skype calls to my nephews to cheer me up, watching the first rice-eating, the first time they crawled, they stood up, their first few steps, hearing their first words, to the first day at school, to now their texts and messages over skype has kept me going through this journey. I guess they are too young to realize how much I love them!

Finally, I would like to thank the Department of Chemistry, NSF Grants CHE 11-12422 and CHE 13-62826 for providing the necessary funding for this work.

Table of Contents

Chapter 1. Introduction and Background

Most of the macroscopic objects around us, the relatively "large" and "heavy" ones obey the laws of classical mechanics. Classical mechanics is an extremely well developed field, and is still used in majority of dynamical simulations, because the most of the universe (the way we see it), lie in the classical domain. It is applicable for performing atomistic simulations of fluids, proteins, and polymers. To solve classical mechanics one needs to evaluate Hamilton's equations of motions, i.e. solve a set of *2N* coupled first order differential equations, for *N* degrees of freedom - thus classical mechanics is linearly growing. Classical mechanics is also the basis of understanding chaotic motions, and it provides insights and foundations for developing many concepts of quantum mechanics.

Quantum effects, on the other hand, are seen in "smaller" and "lighter" particles and grow exponentially with the number of particles. This is because, the exact formulation of quantum mechanics requires specifying grid points that scales exponentially with the number of degrees of freedom. On this grid a particular function is evaluated, that needs to be integrated to obtain the probability of the particles at that point. The process of chemistry which involves bond formation and bond breaking cannot occur without the transfer of the electrons, protons or energy. All of these fundamental particles demonstrate certain dynamical effects which cannot be explained using classical mechanics. Few of such effects are interference, zero-point energy and tunneling. To explain quantum tunneling let us consider a heavy ball dropped along the wall of the left well in Fig 1. If the ball has enough energy then it will overcome the tunneling barrier and cross to the right side, as shown by the curved arrow. If not, then it will lose its remaining potential energy and come to a stop in the left side, when all of its energy is absorbed by the surroundings. Now let's imagine a light ball in the left side of the well, and assume that it does not have enough energy to cross the barrier. The ball still has a probability to be found in the other well, because it can "tunnel" its way to the other side, as shown by the wiggly arrow. Also, the ball will never stop its motion, owing to the zero-point energy it possess. Quantum tunneling is a very fundamental quantum phenomena and is seen in metallic hydrides, ammonia, is responsible for spontaneous DNA mutations, cold emissions, and lays down the principle for construction of Josephson's Junctions and scanning tunneling electron microscopes [1-5]. Tunneling is often represented using a two state basis for the transferring quantum particle, i.e. the "right" $|r\rangle$ and the "left" $|l\rangle$ basis, as represented using the double wells in the potential diagram. The following Hamiltonian defines the energy and the state of the quantum system,

$$H_0 = -\hbar\Omega\sigma_x$$

Which is characterized by the tunneling splitting $2\hbar\Omega$, and σ_x is the standard 2×2 Pauli spin matrix. Such systems would coherently tunnel from one well to the other with a tunnelling frequency of Ω. However, in reality, a bare quantum particle can never be realised. Thus we assume that it is often coupled to other particles which would bring about dissipative effects in the coherent, i.e. oscillatory dynamics. This gives rise to the concept of partitioning all the degrees of freedom of the ensemble into system and bath, much like introductory thermodynamics. The system is often the quantum degrees of freedom, whose dynamics we are interested in solving, and the rest of the degrees of freedom can be referred to as the bath as shown in Figure 2. Most often, we partition it so that the bath contains heavier particles which can be treated using classical mechanics. This helps restrict the exponential scaling to only the relevant degrees of freedom and majority of the rest of the degrees of freedom are treated using a linear theory.

Traditional quantum dynamical methods involve solving Schrodinger's equation using wave-based methods. Extracting the probability for the few interesting degrees of freedom from such an approach is not an easy task if the total correlation between the system-bath has to be considered. To achieve the system-bath partitioning in a very natural way, the path integral formulation [6, 7] of quantum mechanics is very insightful. In the path integral formulation, the probability amplitude of a particle going from an initial time point, t_i, to a final time point, t_f, is given by the sum of probability over all possible paths connecting the two time points. The weight of each path is given by the exponential of the corresponding Lagrangian action. In this formulation we start with the initial probability distribution that is defined in the full system-bath Hilbert space. To achieve the system-bath partitioning, we simply need to integrate out the degrees of freedom associated with the bath. Once we have accomplished that we obtain a probability density which exists only in the system-subspace. We started with an exponentially growing grid in the system-bath space, but we restricted the exponential growth to only the system degrees of freedom. Thus starting from an exponential growing problem, we ended up with a quasi-exponential growth. This had been analytically derived in the framework of a quantum system bi-linearly coupled to a harmonic bath. [7]

$$\begin{aligned}\rho_{\mathrm{red}}(s_n^{\pm};n\delta t) = \int ds_0^{\pm}\int ds_1^{\pm}\cdots\int ds_{n-1}^{\pm}\left\langle s_n^{+}\left|e^{-iH_0\delta t/\hbar}\right|s_{n-1}^{+}\right\rangle\cdots\left\langle s_1^{+}\left|e^{-iH_0\delta t/\hbar}\right|s_0^{+}\right\rangle\left\langle s_0^{+}\left|\rho_0\right|s_0^{-}\right\rangle \\ \times\left\langle s_0^{-}\left|e^{iH_0\delta t/\hbar}\right|s_1^{-}\right\rangle\cdots\left\langle s_{n-1}^{-}\left|e^{iH_0\delta t/\hbar}\right|s_n^{-}\right\rangle F\left(s_0^{\pm},s_1^{\pm},...,s_n^{\pm}\right)\end{aligned} \quad (1.1)$$

where $\left\langle s_n^{+}\left|e^{-iH_0\delta t/\hbar}\right|s_{n-1}^{+}\right\rangle$ and $\left\langle s_{n-1}^{-}\left|e^{iH_0\delta t/\hbar}\right|s_n^{-}\right\rangle$ denotes the time evolution propagator and its adjoint used to propagate the system to time *t*, and F, the influence functional is given by

$$F\left(s_0^{\pm},s_1^{\pm},...,s_n^{\pm}\right)=\exp\left(-\frac{1}{\hbar}\int_0^t dt'\int_0^{t'}dt''\left(s^{+}(t')-s^{-}(t')\right)\left(\alpha(t'-t'')s^{+}(t'')-\alpha^{*}(t'-t'')s^{-}(t'')\right)\right) \quad (1.2)$$

contains all the interactions of the bath on the system. This influence functional is non local in time, and this means Markovian property of the multidimensional density matrix will not hold. The computational power of evaluating such integrals will grow exponentially as the system is propagated forward in time, i.e as the number of integration variables grows. In order to tackle such problems, Makarov and Makri [8-11] observed that although the dynamics is clearly non-Markovian, the dissipative effects from the bath quenches quantum oscillations, as a result of which the range of non-Markovian nature, i.e. the memory is lost after a finite length of time. Using this physical motivation, they propagated the system in presence of a bath to achieve long time dynamics, systematically converging the memory or the length of non-locality. Since the initial conceptualization of iterative dynamics, lots of variants and further developments [12-15] of the method have been reported in literature. Few methods formulated recently in our group, [16, 17] have also obviated the need for such iterative decomposition, by exploiting other physical phenomena relevant to the bath. One such method, namely the path-integral renormalization technique was formulated for a bath which contained distinct high frequency and low frequency modes. The high frequency modes required a shorter time step but lower memory, while the low frequency modes required larger time steps but longer memory. By "renormalizing" the propagator, a part of the most the significant or numerically important short-time interactions are taken inside the propagator, which then allows for a longer time step propagation for the renormalized propagators, thus allowing shorter time steps for the high frequencies, but longer length of propagation required for the low frequency modes.[16]. On the other hand, the blip decomposition of the path integral was motivated for a very slow bath strongly coupled to the system. In this case, the system is near the incoherent, exponentially decaying regime, where the dissipative nature of the surroundings quenches most of the oscillations. Thus instead of starting with the bare propagators that contain all the coherences, it is more insightful to start with the fully incoherent regime, i.e. the zero-blip regime, and carefully adding the coherences arising from higher order blip terms. [17]

However, all of the above methods, aim at solving the system-bath problem for a Gaussian bath linearly coupled to a system. Clearly the above methods will not be valid for a generalized bath which contains anharmonic effects. The various methods mentioned below have been summarized in introduction of Ref [18] and has been mentioned in this part as well. Many such system-bath formalisms exist in literature that try to tackle the problem of anharmonicity in a rather *ad hoc* fashion. The simplest and the most approximate would be the classical path model, or the 'no back-reaction model'. This is often called the unperturbed reference, where in terms of wave-based quantum mechanics, the quantum mechanical wavefunction of the quantum mechanical system is allowed to propagate along the solvent trajectory and this solvent trajectory does not feel the quantum system. However, it is an absolute necessity to take into account the nature of the effects of the system on the trajectories of the bath, i.e. "back reaction". The easiest way to accomplish

this task is to incorporate the back reaction via the Ehrenfest model [19] which is very related variant of the time dependent self-consistent approximation [21, 22]. There is also Pechukas' self-consistently determined semiclassical approximation, which is evaluated simultaneously along with the quantum mechanical wave function between the initial and final time points. Although the procedure is rigorous, with controlled approximations, and accurate, it is extremely computationally demanding, and often cannot be computed for large-scale systems and/or longer times. [23]

Surface hopping methods, that try to circumvent the averaging problem of Ehrenfest dynamics, is a very widely used branch of mixed quantum-classical approximations, and have been very successful in dealing with larger systems for longer dynamics. It was first proposed by Tully [20, 24], and is based on "hops" that the quantum trajectory is allowed to take, between different quantum or electronic states. The likelihood of this jump is determined by the strength of the non-adiabatic coupling strength of the states, which is a very explanation. Instead of being propagated in a single average branch, like in Ehrenfest dynamics, surface hopping allows for population or trajectory branching [25] and has been applied very widely to proton transfer reactions, [26] multiple proton transfer and proton-coupled electron transfer.[27] There are variants of surface hopping methods that evaluates the mean-field or the self-consistently determined Pechukas force for shorter time integrals [28-31] and can lead to capture of the back reaction in a more rigorous manner. Instead of dynamical or exponentially growing basis set methods, trajectory spawning methods, or multiple spawning methods determines the quantum mechanical transition amplitudes using local basis set in the vicinity of the classical trajectories [32]. There are reported methods in literature which use Bohm's quantum trajectories to simulate approximate non-adiabatic dynamics [33-35]. Another approximate treatment using an alternate formalism for dynamics, i.e. the quantum-classical Liouville equation is based on different low-order expansions of the same according to the ratio masses of the concerned quantum classical particles. [36, 37] An idea that avoids the system-bath partitioning and is capable of treating all particles in the same footing was first proposed by Meyer and Miller [38] and developed later by Stock and Thoss [39]. This allows classical trajectories to propagate in more than one Born-Oppenheimer state and that is achieved by mapping each electronic state on a pair of action-angle variables. So each discrete quantum state is now represented by continuous degrees of freedom and this can be now treated using classical or semiclassical trajectory methods on a single potential surface. [40]

Again, the path integral formulation of quantum mechanics [41] comes to rescue here and offers a great tool for the development of quantum-classical propagation methods, because the local, trajectory-like character of the quantum paths circumvents many of the above approximations. However, simulation of a dynamical process typically requires hundreds or thousands of path integral steps. Chapter 2 deals with the

various ways the number of time steps required for such path integral based quantum-classical treatments to converge can be reduced. We have validated the improvements against existing methods using the cherished spin-boson model which is a prototypical model to study tunneling dynamics of a quantum system in a dissipative bath.

For a real-world problem, that involves atoms of the solvent, or a protein backbone, or a chromatophore, the bath is generally solved using traditional molecular dynamics software. The potential in such case, is given by the sum of bonded and non-bonded interactions and include,

$$U\left(\overrightarrow{R}\right)_{bonded} = \sum_{bonds} k_i^{bond}\left(r_i - r_0\right)^2 + \sum_{angles} k_i^{angle}\left(\theta_i - \theta_0\right)^2 + \sum_{dihedrals} k_i^{dihe}\left[1+\cos\left(n_i\phi_i + \delta_i\right)\right] \tag{1.3}$$

$$U\left(\overrightarrow{R}\right)_{non-bonded} = \sum_i \sum_{j\neq i} 4\varepsilon_{ij}\left[\left(\frac{\sigma_{ij}}{r_{ij}}\right)^{12} - \left(\frac{\sigma_{ij}}{r_{ij}}\right)^{6}\right] + \sum_i \sum_{j\neq i} \frac{q_i q_j}{\varepsilon r_{ij}} \tag{1.4}$$

These potentials are far from Gaussian and in fact the non-bonded interactions contain very long-range interactions. However, if a statistically significant number of degrees of freedom are perturbed, the central limit theorem can be invoked and irrespective of the nature of the initial distribution of the potentials, the final distribution will be Gaussian. This equivalence forms the basis of Marcus' electron-transfer theory. Marcus's theory often also rely on other ad-hoc approximations: the solvent modes are purely classical; the potential is essentially diabatic with very low diabatic-coupling terms, and the rates are obtained using second order perturbative treatments. To move beyond Marcus's theory and even the linear approximation, we have studied the full-atom simulations of solvent-solute interactions including charge and non-bonding interactions in the Ferrocene - Ferrocenium system in a bath of Benzene molecules in Chapter 3. We have quantitatively proved how to systematically map the inherently anharmonic bath to produce a Gaussian bath with the closest resemblance to initial distribution.

The process of electron or proton transfer occurs between two species that have different charges. As a result the solvent molecules, depending on its polarity will distribute itself quite differently around these species. This is pictorially represented in Figure 3. The fluctuations in the solvent or the bath plays a critical role in determining the dynamics of the charge transfer. Two cases may arise in such situations: in the first case, the timescale of the bath is much faster than that of the dynamics of the charge transfer. In such a scenario, the bath or the solvent molecules may reorient itself quickly, and the initial distribution does not

affect the nature of such electron transfer reactions. On the other hand, if the bath is sluggish and is slower or in comparable time scales of the electron transfer reaction, the initial distribution of the bath or the solvent molecules become very important. In Chapter 4 we discuss two equivalent procedures for generalizing the influence functional approach to situations where the bath is initially in equilibrium with the localized state of the system. The first approach [41] involves evaluation of the influence functional with a shifted bath. The alternative, second approach consists of shifting the coordinate of the system to bring its initial state in equilibrium with the unshifted bath. This approach requires no modification of the influence functional and has already been used in earlier work by our group. [42]

Another important quantum mechanical phenomenon is vibrational energy relaxation as depicted using the toy model in Figure 4. To switch from tunneling to vibrational energy relaxation experimentally, one needs to change from a H-NMR to a Time Resolved 2D-IR. Theoretically, we can just take a canonical transformation of the system-bath Hamiltonian and use the same methods developed for studying quantum tunneling. Now the system, unlike the case of tunneling is expressed in terms of the excited and ground states. Since these states are Eigenstate of the system, if prepared in the excited state, an isolated system would continue to be in that state. The dynamics in this case is completely driven by the dissipative nature of the bath. The dynamics of such a bath is studied in Chapter 5 demonstrating the diffused nature of the coherent to incoherent transitions with changes in system-bath coupling, bath frequency modes and temperature.

1.1 Figures:

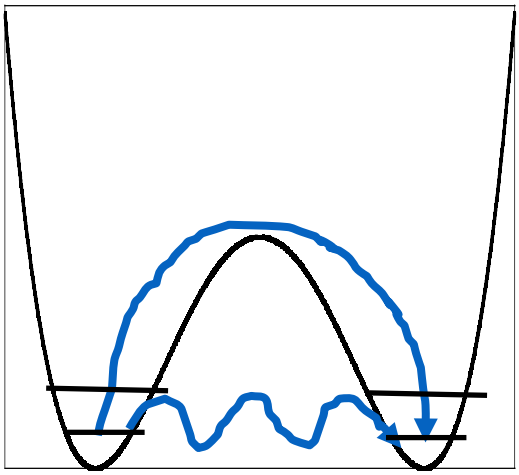

Figure 1.1: The double well indicates the right and the left states in a quantum tunneling system. The curved arrow shows "classically allowed transitions" while the wiggly arrow represents "classically forbidden tunneling transition" The difference of energies levels is related to the tunneling frequency, Ω by the relation $E^{+} - E^{-} = \Delta = 2\hbar\Omega$

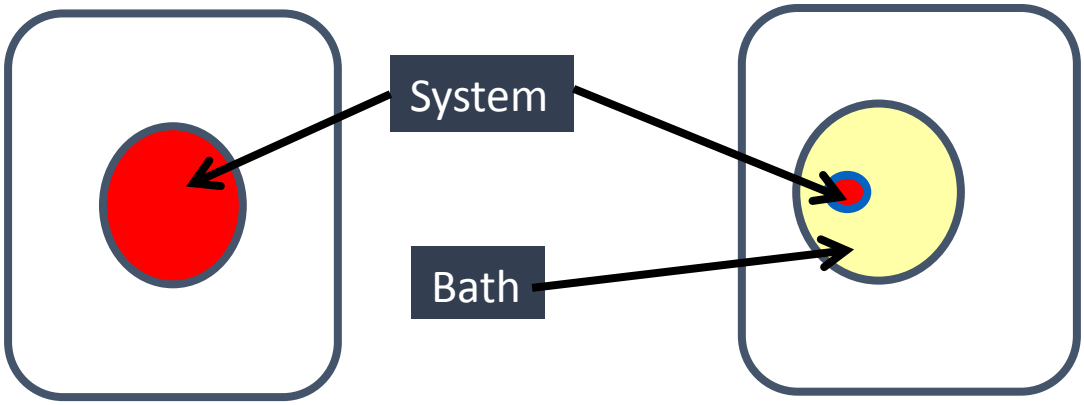

Figure 1.2: A model picture to show the system-bath partitioning of the total degrees of freedom of the ensemble (the circular area). The entire ensemble is placed in the surroundings, which act as the heat bath (denoted by the outer square)

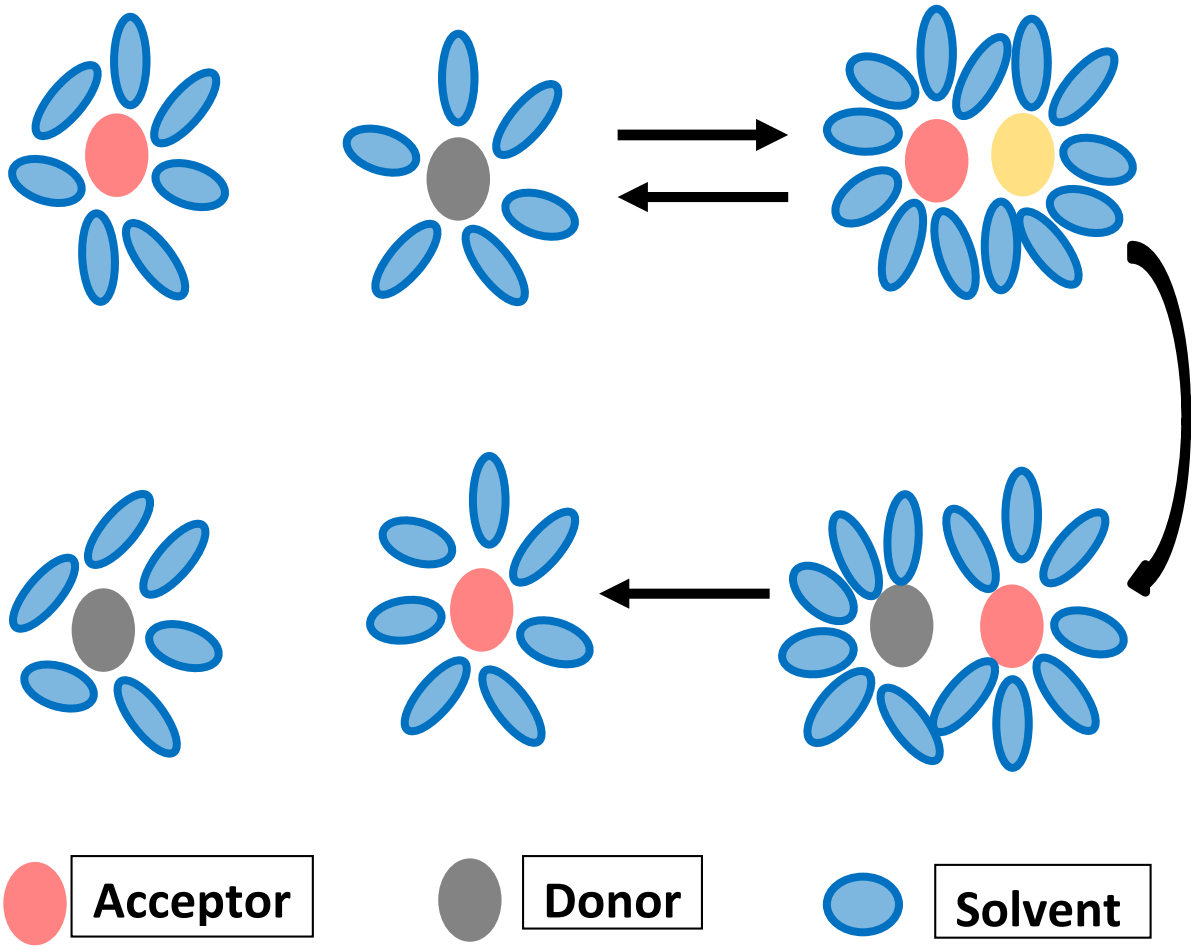

Figure 1.3: A toy model depicting the orientation of a non-polar solvent organized around a charged and uncharged species. This depicts the difference of interaction of the solvent with the donor and the acceptor species.

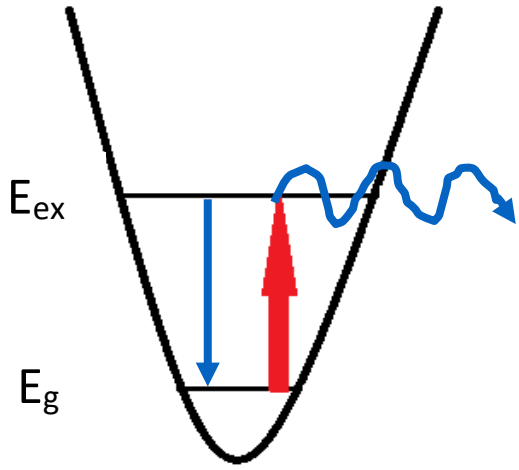

Figure 1.4 : A simple model picture to depict vibrational energy transfer with the excited and the gorund state. The wiggly arrow shows dissipation to the bath degrees of freedom while the arrow represents decay to the ground state.

1.2 References:

1. Sabo-Etienne, Sylviane, and Bruno Chaudret. "Quantum mechanical exchange coupling in polyhydride and dihydrogen complexes." *Chemical reviews* 98.6 (1998): 2077-2092.

2. Heinekey, D. M., Millar, J. M., Koetzle, T. F., Payne, N. G., & Zilm, K. W. (1990). Structural and spectroscopic characterization of iridium trihydride complexes: evidence for proton-proton exchange coupling. *Journal of the American Chemical Society*, *112*(3), 909-919

3. McGrady, G. Sean, and Gemma Guilera. "The multifarious world of transition metal hydrides." *Chemical Society Reviews* 32.6 (2003): 383-392.

4. Zilm, K. W., Heinekey, D. M., Millar, J. M., Payne, N. G., & Demou, P. (1989). Proton-proton exchange couplings in transition-metal polyhydrides. *Journal of the American Chemical Society*, *111*(8), 3088-3089.

5. Jarid, A., Moreno, M., Lledos, A., Lluch, J. M., & Bertran, J. (1993). Ab initio calculations of the quantum mechanical hydrogen exchange coupling in the [(C5H5) Ir (PH3) H3]+ complex. *Journal of the American Chemical Society*, *115*(13), 5861-5862.

6. Feynman, Richard Phillips. "Space-time approach to non-relativistic quantum mechanics." *Reviews of Modern Physics* 20.2 (1948): 367.

7. R. P. Feynman and A. R. Hibbs, *Quantum Mechanics and Path Integrals.* (McGraw-Hill, New York, 1965).

8. Makri, Nancy, and Dmitrii E. Makarov. "Tensor propagator for iterative quantum time evolution of reduced density matrices. I. Theory." *The Journal of chemical physics* 102.11 (1995): 4600-4610.

9. Makri, Nancy, and Dmitrii E. Makarov. "Tensor propagator for iterative quantum time evolution of reduced density matrices. II. Numerical methodology." *The Journal of chemical physics* 102.11 (1995): 4611-4618.

10. Makarov, Dmitrii E., and Nancy Makri. "Path integrals for dissipative systems by tensor multiplication. Condensed phase quantum dynamics for arbitrarily long time." *Chemical physics letters* 221.5 (1994): 482-491.

11. Makarov, Dmitrii E., and Nancy Makri. "Tunneling dynamics in dissipative curve-crossing problems." *Physical Review A* 48.5 (1993): 3626.

12. Sim, Eunji, and Nancy Makri. "Tensor propagator with weight-selected paths for quantum dissipative dynamics with long-memory kernels." *Chemical physics letters* 249.3 (1996): 224-230.

13. Sim, Eunji, and Nancy Makri. "Filtered propagator functional for iterative dynamics of quantum dissipative systems." *Computer physics communications* 99.2 (1997): 335-354.

14. Sim, Eunji. "Quantum dynamics for a system coupled to slow baths: On-the-fly filtered propagator method." *The Journal of Chemical Physics* 115.10 (2001): 4450-4456.

15. Lambert, Roberto, and Nancy Makri. "Memory propagator matrix for long-time dissipative charge transfer dynamics." *Molecular Physics* 110.15-16 (2012): 1967-1975.

16. Makri, Nancy. "Blip decomposition of the path integral: Exponential acceleration of real-time calculations on quantum dissipative systems." *The Journal of chemical physics* 141.13 (2014): 134117.

17. Makri, Nancy. "Path integral renormalization for quantum dissipative dynamics with multiple timescales." *Molecular Physics* 110.9-10 (2012): 1001-1007.

18. Banerjee, Tuseeta, and Nancy Makri. "Quantum-Classical Path Integral with Self-Consistent Solvent-Driven Reference Propagators." The Journal of Physical Chemistry B 117.42 (2013): 13357-13366.

19. Ehrenfest, P. Bemerkung über die angenäherte Gültigkeit der klassischen Mechanik innerhalb der Quantenmechanik. Zeitschrift für Physik A Hadrons and Nuclei, 1927. 45(7): p. 455-457.

20. Tully, John C. "Molecular dynamics with electronic transitions." *The Journal of Chemical Physics* 93.2 (1990): 1061-1071.

21. Gerber, R. B., and Mark A. Ratner. "Self-consistent-field methods for vibrational excitations in polyatomic systems." *Advances in Chemical Physics, edited by I. Prigogine and SA Rice (Wiley, 1988)* 70 (2009): 97-132.

22. Billing, Gert D. "Classical path method in inelastic and reactive scattering." *International Reviews in Physical Chemistry* 13.2 (1994): 309-335.

23. Pechukas, P. (1969). Time-dependent semiclassical scattering theory. II. Atomic collisions. *Physical Review*, *181*(1), 174.

24. Tully, John C., and Richard K. Preston. "Trajectory surface hopping approach to nonadiabatic molecular collisions: the reaction of H+ with D2." *The Journal of Chemical Physics* 55.2 (1971): 562-572.

25. Herman, Michael F. "Dynamics by semiclassical methods." *Annual review of physical chemistry* 45.1 (1994): 83-111.

26. Hammes-Schiffer, Sharon, and John C. Tully. "Proton transfer in solution: Molecular dynamics with quantum transitions." *The Journal of chemical physics* 101.6 (1994): 4657-4667.

27. Hammes-Schiffer, Sharon. "Theory of proton-coupled electron transfer in energy conversion processes." *Accounts of chemical research* 42.12 (2009): 1881-1889.

28. Webster, Frank J., Schnitker, J.; Friedrichs, M. S.; Friesner, R. A.; Rossky, P. J."Solvation dynamics of the hydrated electron: a nonadiabatic quantum simulation." *Physical review letters* 66.24 (1991): 3172.

29. Webster, Frank, P. J. Rossky, and R. A. Friesner. "Nonadiabatic processes in condensed matter: semi-classical theory and implementation." *Computer Physics Communications* 63.1 (1991): 494-522.

30. Coker, D. F., and L. Xiao. "Methods for molecular dynamics with nonadiabatic transitions." *The Journal of chemical physics* 102.1 (1995): 496-510.

31. Prezhdo, Oleg V., and Peter J. Rossky. "Mean-field molecular dynamics with surface hopping." *The Journal of chemical physics* 107.3 (1997): 825-834.

32. Ben-Nun, M., Jason Quenneville, and Todd J. Martínez. "Ab initio multiple spawning: Photochemistry from first principles quantum molecular dynamics." *The Journal of Physical Chemistry A* 104.22 (2000): 5161-5175.

33. Burant, John C., and John C. Tully. "Nonadiabatic dynamics via the classical limit Schrödinger equation." *The Journal of Chemical Physics* 112.14 (2000): 6097-6103.

34. Wyatt, Robert E., Courtney L. Lopreore, and Gérard Parlant. "Electronic transitions with quantum trajectories." *The Journal of Chemical Physics* 114.12 (2001): 5113-5116.

35. Prezhdo, Oleg V., and Craig Brooksby. "Quantum backreaction through the Bohmian particle." *Physical review letters* 86.15 (2001): 3215.

36. Donoso, Arnaldo, and Craig C. Martens. "Simulation of coherent nonadiabatic dynamics using classical trajectories." *The Journal of Physical Chemistry A* 102.23 (1998): 4291-4300.

37. Kapral, Raymond, and Giovanni Ciccotti. "Mixed quantum-classical dynamics." *The Journal of chemical physics* 110.18 (1999): 8919-8929.

38. Meyera, Hans-Dieter, and William H. Miller. "A classical analog for electronic degrees of freedom in nonadiabatic collision processes." *The Journal of Chemical Physics* 70.7 (1979): 3214-3223.

39. Stock, Gerhard, and Michael Thoss. "Semiclassical description of nonadiabatic quantum dynamics." *Physical review letters* 78.4 (1997): 578.

40. Miller, William H. "Electronically nonadiabatic dynamics via semiclassical initial value methods." *The Journal of Physical Chemistry A* 113.8 (2009): 1405-1415.

41. Feynman, Richard Phillips. "Space-time approach to non-relativistic quantum mechanics." *Reviews of Modern Physics* 20.2 (1948): 367.

42. Sim, Eunji, and Nancy Makri. "Path integral simulation of charge transfer dynamics in photosynthetic reaction centers." *The Journal of Physical Chemistry B* 101.27 (1997): 5446-5458.

Chapter 2. Quantum-Classical Path Integral with Solvent-Driven Reference Propagators

2.1 Introduction:

Sections 2.1 to 2.4 and 2.7 is based on the paper [Banerjee, Tuseeta, and Nancy Makri. "Quantum-Classical Path Integral with Self-Consistent Solvent-Driven Reference Propagators." The Journal of Physical Chemistry B 117.42 (2013): 13357-13366].

Since the solution of full Schrödinger equation becomes very difficult with increase in the number of degrees of freedom that are coupled to one another, one often relies on making simplifications, or assumptions to account for quantum mechanical effects in dynamics of condensed phase processes. One of such approximations is to treat a few degrees of freedom using quantum mechanical treatments, and use classical trajectories to capture the nature of the dynamics of the rest of the degrees of freedom. Owing to the fundamental differences between the trajectory-based classical mechanical formalism and the wave-based solutions of Schrödinger equation this task becomes extremely difficult.

Fortunately, path integral formulation, like classical mechanics is also based on trajectories, and these quantum paths are local, and can be a great tool for developing quantum-classical methods. Unfortunately, simulating such dynamics for practical purposes might require a great number of path integral time steps. There is a proliferation in the number of quantum paths, with the number of time steps and these calculations become computationally very challenging. In this chapter, we discuss a method to overcome this problem and accelerate the path integral calculations to make them feasible for practical applications. Simple trajectory-based mixed formalisms, like the classical path approximation (which needs to be adequately averaged over many solvent trajectories or many classical paths, so as to get a non-varying density matrix for the solvent) or Ehrenfest model, i.e. the self-consistent model are quite exact within short time scales. Knowing this, we can use this approximation within a single time step of the total path integral calculation. This effectively leads to the system being perturbed by a time dependent reference (here the reference of the approximate solvent trajectory) to build the propagators themselves. We can capture very important physical aspects of the dynamics, i.e. include classical decoherence when using the averaged classical path approximation or capturing the averaged- “back reaction” in Ehrenfest approximation) in the single-step of path integral propagation which can increase the time step allowed for the system propagation. The

complete “back reaction” when classical path approximation is considered or the remainder of the “back reaction” when Ehrenfest is considered can be captured through full summation over system paths. The self-consistent field (or the Ehrenfest) model can allow for path integral time steps approximately as large as the “solvent-induced decoherence time”. These are two candidates which are considered here, but in general this scheme can be extended to global system-independent trajectories. These system independent trajectories can be evaluated from any of the methods described in literature for mixed quantum-classical methods and be used to construct the solvent-driven propagators. These propagators when constructed from any of these approximations will allow for larger time step convergence and hence exponential reduction in the computational time, allowing less trajectory proliferation, promising a new method for condensed phase and biological applications. Using the QCPI framework, we have also devised a method to make corrections for these approximate theories.

In Section 2.2 we review the QCPI formulation and describe the construction of propagators from a generalized solvent reference. In section 2.3 we discuss two excellent candidates for such a reference, the unperturbed solvent and the TDSCF or Ehrenfest models. In section 2.4, these ideas are illustrated with applications on a two-level system coupled to a harmonic bath, for which accurate results for comparison are available. [3,4] Section 2.5 and 2.6 describes the application of the iterative and filtering algorithm to model electron transfer in challenging regimes while Section 2.7 presents some concluding remarks.

2.2 Quantum-Classical Path Integral with Time-Dependent Reference:

The total Hamiltonian comprises of the system Hamiltonian, the bath Hamiltonian and their coupling. The system part is fully described using the coordinate S and momentum p_s. The bath Hamiltonian which we have decided to treat via classical mechanics, is defined using the vectors x, p which consists of the positions and the momenta of the coordinates of the bath or the solvent particle(s) with the mass m_{b} (note the masses can be different or same depending on the solvent)

$$\hat{H} = H_0(\hat{s}, \hat{p}_s) + T_{\mathrm{b}}(\hat{p}) + V_{\mathrm{b}}(\hat{x}) + V_{\mathrm{int}}(\hat{s}, \hat{x}) \tag{2.1}$$

where H_0 is the Hamiltonian of the quantum system, T_{b} is the kinetic energy of the bath or environment, V_{b} is the potential of the bare solvent, and V_{int} is the potential for interaction between the solvent and the quantum system. The time evolution of the system’s reduced density matrix is given by,

$$\rho_{\mathrm{red}}(s_n^{\pm}; n\delta t) = \mathrm{Tr}_{\mathrm{b}} \left\langle s_n^{+} \left| e^{-i\hat{H}t/\hbar} \hat{\rho}(0) e^{i\hat{H}t/\hbar} \right| s_n^{-} \right\rangle, \tag{2.2}$$

where δt is an elementary time step that is maximally allowed after convergence. We had already decided for a classical or semiclassical prescription for the solvent dynamics. In such cases, the reduced density matrix given in Eqn 2.2 is expressed the form [5-8]

$$\rho_{\text{red}}(s_n^{\pm}; n\delta t) = \int dx_0 \int dp_0 \; P(x_0, p_0) Q(x_0, p_0; s_n^{\pm}) \tag{2.3}$$

where $P(x_0, p_0)$ is the solvent phase space density and $Q\left(x_0, p_0; s_n^{\pm}\right)$ is the "quantum influence function" . Q describes the effects that the quantum system has on the dynamics of the solvent. It is expressed in terms of a sum with respect to all (forward and backward) system paths, and as a product of all exponential terms formed by splitting the time integral and also a phase whose implication is discussed immediately later. Q is given according to the expression

$$\begin{aligned} Q\left(x_0, p_0; s_n^{\pm}\right) = \int ds_0^{\pm} \cdots \int ds_{n-1}^{\pm} \left\langle s_n^{+} \middle| e^{-i\hat{H}_0 \delta t/\hbar} \middle| s_{n-1}^{+} \right\rangle \cdots \left\langle s_1^{+} \middle| e^{-i\hat{H}_0 \delta t/\hbar} \middle| s_0^{+} \right\rangle \rho_{\text{red}}(s_0^{\pm}; 0) \\ \times \left\langle s_0^{-} \middle| e^{i\hat{H}_0 \delta t/\hbar} \middle| s_1^{-} \right\rangle \cdots \left\langle s_{n-1}^{-} \middle| e^{i\hat{H}_0 \delta t/\hbar} \middle| s_n^{-} \right\rangle e^{i\Phi(x_0, p_0; s_0^{\pm}, s_1^{\pm}, \ldots, s_n^{\pm})/\hbar} \end{aligned} \tag{2.4}$$

Φ is the trapezoid-discretized action integral which is computed for each of exponentially growing system paths formed and evaluated along the classical trajectory emanating from the initial condition x_0, p_0 according to the force which is determined by the instantaneous coordinate of the system along the particular path. Here δt is the path integral time step which is a convergence parameter and depends on the particular system - bath parameters. Each of the terms, *P, Q,* Φ and even the method of evaluation of the solvent trajectory depends on what formalism we decide to use for QCPI. A brief introduction of the formalisms are given in Ref[7] and any of them can be adapted and the concepts discussed in this chapter can be extended to it. If we consider a classical or linearized path integral (LPI) treatment [8-11], the process of linearization, avoids the propagation of the classical trajectory explicitly in forward and backward in time, like the system, but instead it leads to classical trajectories experiencing the average of the forces exerted by the system at its instantaneous forward and backward configurations,

$$f(x, k\delta t) = -\frac{\partial}{\partial x}\left[V_{\text{b}}(x) + \frac{1}{2}\left(V_{\text{int}}(s_k^{+}, x) + V_{\text{int}}(s_k^{-}, x) \right) \right], \tag{2.5}$$

The forward-backward semiclassical treatment of the solvent dynamics (FBSD) [3,4], on the other hand, will lead to separate forward and backward trajectories along the system forward and backward configurations, and is more accurate. The linearization of semiclassical formalism leading to quasi-classical treatments can also be considered as a potential candidate. All these different formalisms can be adapted depending on the desired level of accuracy and available resources. Let us now focus on just one of these formalisms, say the LPI treatment, where phase space density is given by the Wigner transform [12] of the initial density operator,

$$P(x_0, p_0) = (2\pi\hbar)^{-1} \int d\Delta x_0 \left\langle x_0 + \tfrac{1}{2}\Delta x_0 \middle| \hat{\rho}(0) \middle| x_0 - \tfrac{1}{2}\Delta x_0 \right\rangle e^{-ip_0 \Delta x_0/\hbar} \; , \tag{2.6}$$

and the action is given by

$$\Phi(x_0, p_0; s_0^{\pm}, s_1^{\pm}, \ldots, s_n^{\pm}) = \Bigg(\tfrac{1}{2} V_{\text{int}}(s_0^{+}, x_0) + \sum_{k=1}^{n-1} V_{\text{int}}(s_k^{+}, x_k) + \tfrac{1}{2} V_{\text{int}}(s_n^{+}, x_n) \\ - \tfrac{1}{2} V_{\text{int}}(s_0^{-}, x_0) - \sum_{k=1}^{n-1} V_{\text{int}}(s_k^{-}, x_k) - \tfrac{1}{2} V_{\text{int}}(s_n^{-}, x_n) \Bigg) \delta t \tag{2.7}$$

where $x_k = x(k\delta t)$. The solvent potential V_b is the same as the forward and the backward trajectory and thus cancels, leaving just the bath interaction terms in Eq.(2.7) This term expressed Eq. (2.7) is a product when for very short time ($n\delta t \to 0$) or very low magnitudes of V_{int}, i.e. in the weak system-bath coupling.

Since we are interested in the quantum-classical formulation, we need to evaluate the propagators using full quantum mechanics. The quantum part of the system can also be treated using semiclassical theory where we could have evaluated semiclassical propagators and then we would have had to evaluate the classical trajectories for both the system and the bath. [13-14] Although such methods would avoid the proliferation of trajectories with system propagation, i.e not have the exponential growth the main difficulty in mixed semiclassical-classical system is the convergence of highly oscillatory Monte-Carlo phase space integrals. In QCPI the phase space integrals are much less oscillatory and after the treatments we have done in this chapter, the phase-space integrals are further smoothed out.

Unlike the semi-classical treatments the main difficulty in quantum-classical treatments is the exponential growth in the number of terms in the system path sum, as the number of steps of propagation of the system increases. To illustrate this difficulty let us consider that the quantum system is represented in terms of *M* states or sites. If we incorporate the concept of discrete variable representation [15] of the system coordinate then we can replace the system integrals in Eq. (2.4) by discrete sum over the M system states. The DVR states are local and have position operator like characteristics, as a result the system-bath interaction potential can be very conveniently represented in these states. [16] If we consider a system propagation of n steps and there are separate forward-backward paths, then we could have to evaluate M^{2n} classical trajectories. Just like harmonic influence functional treatments of "memory" [7], each time point was connected to the other time points via correlation functions, in QCPI the classical trajectories become dependent on system. This memory or the non-Markovian character prevent the iterative evaluation of the path sum into single-step decompositions. Also, due to the exponential proliferation, the full path sum can only be evaluated if n is small.

As we had discussed before, we aim at incorporating a part of the system-bath interaction inside the system-propagators. We had also decided that this system bath interaction will not be dependent on the system trajectories explicitly. To achieve this we consider that the action Φ can be divided into two separate components. The first component comprises of "explicit dependence" [33] of the reference Lagrangian which is based on local trajectories, i.e. trajectories which are not dependent on system coordinates. The second part of the action consists of "implicit dependence" [33], i.e.this chunk of the action arises from the part of the trajectories that depend on system coordinates. Observing this, we can separate the action into two parts

$$\Phi\left(x_0, p_0; s_0^{\pm}, s_1^{\pm}, \ldots, s_n^{\pm}\right) = \Phi_{\text{ref}}\left(s_0^{\pm}, s_1^{\pm}, \ldots, s_n^{\pm}; x^{\text{ref}}(x_0, p_0)\right) + \Delta\Phi\left(x_0, p_0; s_0^{\pm}, s_1^{\pm}, \ldots, s_n^{\pm}\right) \tag{2.8}$$

The reference part has only explicit dependence, and the "reference trajectory" $x^{\text{ref}}(t')$ is the same for a particular initial condition. Similar to calculation of the action, the reference action is calculated from the reference trajectory, where $x_k^{\text{ref}} \equiv x^{\text{ref}}(k\delta t),\ k = 0, \ldots, n$, and the reference action is

$$\begin{aligned}\Phi_{\text{ref}}\left(s_0^{\pm}, s_1^{\pm}, \ldots, s_n^{\pm}; x^{\text{ref}}(x_0, p_0)\right) = \Bigg(& \tfrac{1}{2} V_{\text{int}}\left(s_0^{+}, x_0^{\text{ref}}\right) + \sum_{k=1}^{n-1} V_{\text{int}}\left(s_k^{+}, x_k^{\text{ref}}\right) + \tfrac{1}{2} V_{\text{int}}\left(s_n^{+}, x_n^{\text{ref}}\right) \\ & - \tfrac{1}{2} V_{\text{int}}\left(s_0^{-}, x_0^{\text{ref}}\right) + \sum_{k=1}^{n-1} V_{\text{int}}\left(s_k^{-}, x_k^{\text{ref}}(k\delta t)\right) + \tfrac{1}{2} V_{\text{int}}\left(s_n^{-}, x_n^{\text{ref}}\right) \Bigg)\end{aligned} \tag{2.9}$$

To motivate the use of larger time steps, we need to observe that the interaction with the system changes the solvent trajectory very less for times up to $\Delta t = n_{\text{ref}}\,\delta t$. As a result $\Delta\Phi$ along a path $\{ s_0^{\pm}, s_1^{\pm}, \ldots, s_{n_{\text{ref}}}^{\pm} \}$ is small and thus be replaced by its trapezoid rule approximation,

$$\begin{aligned}&\Delta\Phi(x_0, p_0; s_0^{\pm}, s_1^{\pm}, \ldots, s_{n_{\text{ref}}}^{\pm}) \\ &\simeq \frac{1}{2}\Big[\Delta V_{\text{int}}(s_0^{+}, x_0) + \Delta V_{\text{int}}(s_n^{+}, x_{n_{\text{ref}}}) - \Delta V_{\text{int}}(s_0^{-}, x_0) - \tfrac{1}{2}\Delta V_{\text{int}}(s_n^{-}, x_{n_{\text{ref}}})\Big]\Delta t\end{aligned} \tag{2.10}$$

where $\Delta V_{\text{int}}(s_k^{\pm}, x_k) = V_{\text{int}}(s_k^{\pm}, x_k) - V_{\text{int}}(s_k^{\pm}, x_k^{\text{ref}})$. With this assumption, Eq. (2.4) becomes

$$\begin{aligned}Q\left(x_0, p_0; s_{n_{\text{ref}}}^{\pm}\right) = \int ds_0^{\pm} \cdots \int ds_{n_{\text{ref}}-1}^{\pm}\, & e^{-iV_{\text{int}}(s_{n_{\text{ref}}}^{+}, x_{n_{\text{ref}}}^{\text{ref}})\delta t/2\hbar} \left\langle s_{n_{\text{ref}}}^{+} \middle| e^{-i\hat{H}_0\delta t/\hbar} \middle| s_{n_{\text{ref}}-1}^{+} \right\rangle e^{-iV_{\text{int}}(s_{n_{\text{ref}}-1}^{+}, x_{n_{\text{ref}}-1}^{\text{ref}})\delta t/\hbar} \cdots \\ & \times e^{-iV_{\text{int}}(s_1^{+}, x_1^{\text{ref}})\delta t/\hbar} \left\langle s_1^{+} \middle| e^{-i\hat{H}_0\delta t/\hbar} \middle| s_0^{+} \right\rangle e^{-iV_{\text{int}}(s_0^{+}, x_0^{\text{ref}})\delta t/2\hbar} \rho_{\text{red}}(s_0^{\pm}; 0) \\ & \times e^{iV_{\text{int}}(s_0^{-}, x_0^{\text{ref}})\delta t/2\hbar} \left\langle s_0^{-} \middle| e^{i\hat{H}_0\delta t/\hbar} \middle| s_1^{-} \right\rangle e^{iV_{\text{int}}(s_1^{-}, x_1^{\text{ref}})\delta t/\hbar} \cdots \\ & \times e^{iV_{\text{int}}(s_{n_{\text{ref}}-1}^{-}, x_{n_{\text{ref}}-1}^{\text{ref}})\delta t/\hbar} \left\langle s_{n_{\text{ref}}-1}^{-} \middle| e^{i\hat{H}_0\delta t/\hbar} \middle| s_{n_{\text{ref}}}^{-} \right\rangle e^{iV_{\text{int}}(s_{n_{\text{ref}}}^{-}, x_{n_{\text{ref}}}^{\text{ref}})\delta t/2\hbar} \\ & \times e^{i\left[\Delta V_{\text{int}}(s_0^{+}, x_0) + \Delta V_{\text{int}}(s_{n_{\text{ref}}}^{+}, x_{n_{\text{ref}}}) - \Delta V_{\text{int}}(s_0^{-}, x_0) - \frac{1}{2}\Delta V_{\text{int}}(s_{n_{\text{ref}}}^{-}, x_{n_{\text{ref}}})\right]\Delta t/2\hbar}\end{aligned} \tag{2.11}$$

So the next step would be to insert the reference trajectory phase factors into the short time propagators. (we had all the way planned to do this step, and hence motivated the discussion on the reference). Also it should be noted that the reference trajectory values x_k^{ref} are independent of the path integral variables $s_k^{\pm}$,

because of the construction (that was the criteria we set for constructing the reference). Thus now the system Hamiltonian is given by the following "reference Hamiltonian" comprising of the original system Hamiltonian and also the reference interaction.

$$\hat{H}_{\text{ref}}(t) = \hat{H}_0 + \hat{V}_{\text{int}}\left(x^{\text{ref}}(t)\right) \tag{2.12}$$

and the quantum influence function will be given as the product of the propagators constructed from the above Hamiltonian and the difference in action because of the remaining interaction,

$$\begin{aligned} Q\left(x_0, p_0; s^{\pm}_{n_{\text{ref}}}\right) = \int ds_0^{\pm} \left\langle s^{+}_{n_{\text{ref}}} \middle| U_{\text{ref}}(\Delta t, 0; x_0, p_0) \middle| s_0^{+} \right\rangle \rho_{\text{red}}(s_0^{\pm}; 0) \left\langle s_0^{-} \middle| U^{\dagger}_{\text{ref}}(0, \Delta t; x_0, p_0) \middle| s^{-}_{n_{\text{ref}}} \right\rangle \\ \times e^{-\frac{i\Delta t}{2\hbar}\left[\Delta V_{\text{int}}(s_0^{+}, x_0) + \Delta V_{\text{int}}(s^{+}_{n_{\text{ref}}}, x_{n_{\text{ref}}}) - \Delta V_{\text{int}}(s_0^{-}, x_0) - \frac{1}{2}\Delta V_{\text{int}}(s^{-}_{n_{\text{ref}}}, x_{n_{\text{ref}}})\right]} \end{aligned} \tag{2.13}$$

where U_{ref} is the time evolution operator corresponding to the time-dependent "reference Hamiltonian", Eq. (2.12). The matrix elements of the time evolution operator is evaluated by solving the time-dependent Schrödinger equation in the system basis,

$$i\hbar \frac{\partial}{\partial t} \left\langle s' \middle| \hat{U}_{\text{ref}}\left(t; t_0; x_0, p_0\right) \middle| s'' \right\rangle = \left\langle s' \middle| \hat{H}_{\text{ref}}(t) \hat{U}_{\text{ref}}\left(t; t_0; x_0, p_0\right) \middle| s'' \right\rangle, \tag{2.14}$$

The other way of obtaining it would be to iteratively evaluate Eq. (2.11) by $M^2 \times M^2$ short-time propagator matrix multiplication n_{ref} times. As we had pointed out before that the reference trajectory is different for each initial condition as a result the reference propagators need to be re-evaluated for each (x_0, p_0) pair.

To evaluate the advantage of these propagators, let us consider that Δt is small, (i.e., $n_{\text{ref}} \sim 1$). In this case Eq. (2.13) is equivalent to the original expression and we are not taking the full utilization of the propagators. As Δt increases, we see the exponential gain in the computational costs. It may so happen that the system-bath interaction become very strong and the single step approximation of (2.10) will break down, and we need to take larger time steps. Even then, this method of constructing the propagators in its single step evaluation of path integrals captures the qualitative nature of the dynamics for the complete time.

Now let us consider the scenario when the above approximation will not hold true, say when temperature is lowered, time of propagation is large, and/or the system-bath coupling is increased. In such cases the above approximation will be valid only for short times. Now all variables from time 0 to n_{ref} are contained in the long-time propagator and the variables $s_1^{\pm}, \ldots, s^{\pm}_{n_{\text{ref}}-1}$ lose their significance. Since we can take larger time step, Δt using this propagator, we can say that the system position at the end of this time Δt is $s_1^{\pm}$. Thus Eq. (2.13) is written as

$$Q\left(x_0,p_0;s_1^{\pm}\right)=\int ds_0^{\pm}\left\langle s_1^{+}\left|U_{\mathrm{ref}}\left(\Delta t,0;x_0,p_0\right)\right|s_0^{+}\right\rangle\rho_{\mathrm{red}}(s_0^{\pm};0)\left\langle s_0^{-}\left|U_{\mathrm{ref}}^{\dagger}\left(0,\Delta t;x_0,p_0\right)\right|s_1^{-}\right\rangle \times e^{-\frac{i\Delta t}{2\hbar}\left[\Delta V_{\mathrm{int}}(s_0^{+},x_0)+\Delta V_{\mathrm{int}}(s_1^{+},x_1)-\Delta V_{\mathrm{int}}(s_0^{-},x_0)-\frac{1}{2}\Delta V_{\mathrm{int}}(s_1^{-},x_1)\right]} \tag{2.15}$$

Once the single step propagation fails, we can use these reference propagators as we had decided before in full QCPI expressions to make the corrections that arise of the system-bath coupling. This would allow propagation of the density matrix to longer times without compromising the accuracy of results. It is possible because the reference propagators being constructed from a physically motivated reference will allow much larger time steps than conventional propagators. This implies that the final time is obtained in fewer number of path integral time splitting and if it so happens that the allowed time step is larger than the quantum memory, iterative evaluation [17] should become very cheap.

We can now put together all the separate parts, i.e. the larger time-step propagators, the corrections to these approximations evaluated in terms of the actions, to obtain the quantum influence function

$$\begin{aligned}Q\left(x_0,p_0;s_N^{\pm}\right)=\int ds_0^{\pm}\cdots\int ds_{N-1}^{\pm}\left\langle s_N^{+}\left|\hat{U}_{\mathrm{ref}}\left(N\Delta t,(N-1)\Delta t;x_0,p_0\right)\right|s_{N-1}^{+}\right\rangle\cdots\\ \times\left\langle s_1^{+}\left|\hat{U}_{\mathrm{ref}}\left(\Delta t,0;x_0,p_0\right)\right|s_0^{+}\right\rangle\rho_{\mathrm{red}}(s_0^{\pm};0)\left\langle s_0^{-}\left|\hat{U}_{\mathrm{ref}}^{\dagger}\left(0,\Delta t;x_0,p_0\right)\right|s_1^{-}\right\rangle\cdots\\ \times\left\langle s_{N-1}^{-}\left|\hat{U}_{\mathrm{ref}}^{\dagger}\left((N-1)\Delta t,N\Delta t;x_0,p_0\right)\right|s_N^{-}\right\rangle\ e^{\frac{i}{\hbar}\Delta\Phi(x_0,p_0;s_0^{\pm},\ldots,s_N^{\pm})}\end{aligned} \tag{2.16}$$

where $\Delta\Phi$ is given by Eq. (2.8) but is discretized with the new time step Δt. In order to implement Eq. (2.16), first we need to propagate the solvent trajectory for a single initial condition, x_0, p_0 following the approximation we take into consideration. Next using the system-bath interaction along this trajectory, and the other parameters in the system Hamiltonian, we can solve the time-dependent Schrödinger equation to obtain the system propagators. For each of the set of forward-backward system path combination, we find the system-bath interaction for each of these trajectories experiencing the average of the unique combination fo the forward-backward system path combination. The difference between the system bath interaction of the reference and the system-force driven trajectory gives the net action $\Delta\Phi$. This phase obtained from this action difference captures the corrections to the reference approximation, Eq. (2.13).

2.3 Unperturbed Solvent and Self-Consistent Reference:

In this chapter we have considered two different approximation schemes for construction of different propagators. The first is the ensemble-averaged classical path (EACP) approximation, where the reference trajectory constructed from each initial condition is given by the motion of the pure solvent which neglects the system-bath interactions. Recent work in the group [7,17] has revealed that the EACP approximation is almost exact in the limit of high temperature and/or weak system-bath coupling. It has been shown that the

EACP approximation when integrated over phase space for a harmonic bath will result in the real part of the influence functional [7] and this becomes highly important in high-temperature/weak-coupling regimes. This is because the quantum effects of the system on most the bath trajectories is almost negligible at this extremes. If we are not at these parameter regimes, then the error from this approximation starts accumulating over time and as a result it will not give rise to the correct population dynamics. In such cases we can take advantage of the fact that the unperturbed solvent *ansatz* will still produce time steps that are larger than the conventional bare propagators.

To choose a better reference than the unperturbed *ansatz*, or the EACP approximation we need to take into account some part of the neglected "back-reaction" i.e. the system-bath interaction. On the other hand the constraint for choosing the reference trajectory is that it should not have the instantaneous system path dependence. Perhaps the best choice here would be to follow the *average* system path. This is known as the Ehrenfest model which is closely related to the time-dependent self-consistent field (TDSCF) approximation [25, 26] if the solvent is described in terms of classical trajectories. To obtain the TDSCF approximation, one needs to use the *ansatz* consisting of the product of wavefunctions and then use the time-dependent variational principle [27]. This leads to energy minimized single-particle wavefunctions. The TDSCF approximation provides a qualitative description of energy transfer, [25, 26], but it cannot account for probability splitting on two surfaces. [28] In the quantum-classical Ehrenfest version [29, 30] the solvent is considered classical and hence the when determining the driving position of the quantum particle, the average position of the solvents are not considered. This version of Ehrenfest prescription solves some of the problems of fully quantum TDSCF. Even so, Ehrenfest model leads to improper branching and equilibrium populations and cannot accurately describe proton transfer events or electronic transitions. Still, there is no harm in using it as a candidate for constructing the reference propagator, so that it can allow for larger time steps than possible by bare system.

Once we have an initial condition x_0, p_0 sampled from the Wigner distribution using Metropolis Monte Carlo, using the Ehrenfest model, the classical trajectory will be subject to the following force

$$-\frac{\partial}{\partial x_t}\left(V_{\mathrm{b}}(x_t)+\left\langle V_{\mathrm{int}}(\hat{s},x_t)\right\rangle\right) \tag{2.17}$$

where $\langle V_{\mathrm{int}}(\hat{s},x_t)\rangle$ is given by the instantaneous average of the system-bath interaction

$$\left\langle V_{\mathrm{int}}(\hat{s},x_t)\right\rangle = \mathrm{Tr}_{\mathrm{sys}}\left(\hat{\rho}_{\mathrm{sys}}(t)\,V_{\mathrm{int}}(\hat{s},x_t)\right) \tag{2.18}$$

where $\hat{\rho}_{\mathrm{sys}}(t)$ is the "density matrix of the system in the Ehrenfest approximation" and it is propagated according to the von Neumann equation

$$i\hbar \frac{d}{dt}\hat{\rho}_{\text{sys}}(t) = \left[\hat{H}_0 + V_{\text{int}}(\hat{s}, x_t),\ \hat{\rho}_{\text{sys}}(t)\right]. \tag{2.19}$$

2.4 Application to Model Systems:

We have applied the ideas developed in the previous section and validated answers on the symmetric "spin-boson" model for which numerically exact answers already exist. The Hamiltonian consists of a two-level system (TLS) coupled to a harmonic bath [31] and the quantum system is given by

$$H_0 = -\hbar\Omega\sigma_x, \tag{2.20}$$

It is mainly characterized by the tunneling frequency Ω and it is coupled to a dissipative bath bilenarly in the coordinate space,

$$H_{\text{b}} = \sum_j \left(\frac{\hat{p}_j^2}{2m} + \frac{1}{2} m\omega_j^2 \hat{x}_j^2 \right), \quad V_{\text{int}} = -\sigma_z \sum_j c_j \hat{x}_j . \tag{2.21}$$

where σ_x and σ_z are the standard 2×2 Pauli spin matrices. Depending on the initial conditions we chose, the Hamiltonian of Equations (3.4)-(3.5) can serve as an excellent model for studying the dynamics of electron transfer or the energy transfer in vibrational relaxation. In the calculations presented below we assume that the system is initially in the right-localized TLS state and that the bath is at thermal equilibrium at the temperature $k_B T = \beta^{-1}$. The bath frequencies and coupling coefficients are described collectively by the spectral density function [32]

$$J(\omega) = \frac{\pi}{2} \sum_j \frac{c_j^2}{m_j \omega_j} \delta(\omega - \omega_j) . \tag{2.22}$$

In particular, we choose the common Ohmic form, [31]

$$J(\omega) = \frac{1}{2} \pi\hbar\xi\omega\, e^{-\omega/\omega_c}, \tag{2.23}$$

where the dimensionless Kondo parameter ξ provides a measure of the dissipation strength (i.e., the magnitude of the system-bath coupling) and ω_c gives the maximum of the spectral density. In order to apply the QCPI methodology, we approximate the bath by a sum of 60 harmonic oscillators whose frequencies and coupling coefficients are evaluated using a logarithmic discretization of the spectral density[33] with a maximum frequency given by $\omega_{\max} = 4\omega_c$.

In order to assess the performance of the reference trajectory schemes described in the previous section, we show in Figure 1 the average TLS position $\langle \sigma_z(t) \rangle$ obtained via a single path integral propagation step.

The diagonal form of the initial density matrix of the system implies $s_0^+ = s_0^-$, while the trace operation imposes the condition $s_N^+ = s_N^-$. Since both endpoints of the forward and backward system paths are the same, these paths are identical within the single step treatment and $\Delta\Phi = 0$. In this case the two single-step QCPI schemes discussed in the previous section are equivalent to the corresponding approximations, i.e., the EACP approximation given by Eq. (2.11)-(2.14) and the self-consistent (Ehrenfest) approximation.

The calculations presented in Figure 1 compare results obtained with the two (unperturbed bath and Ehrenfest-based) time-dependent reference propagators, as well as the conventional propagator splitting based on the bare system Hamiltonian, for a symmetric TLS. The single-step QCPI results are compared to numerically exact results obtained with the iterative path integral methodology developed earlier in our group, [33,34] which is based on the analytical Feynman-Vernon influence functional. In all cases, the results obtained using the single-step system propagator derived from the bare TLS Hamiltonian are accurate only for a small fraction of the TLS period and are qualitatively wrong after $t \sim 0.5\Omega^{-1}$ or (in the case of Fig. 1a) even earlier.

Figure 1a shows the average TLS position in a high-temperature, overdamped regime, characterized by $\hbar\Omega\beta = 0.2$, $\omega_c = 2.5\Omega$ and $\xi = 1.2$. In this regime the behavior of the bath is almost completely classical, and the Wigner function may be replaced by the Boltzmann density. Because of the large system-bath coupling strength, the bare system propagator fails after about $0.2\,\Omega^{-1}$. This is in agreement with earlier QCPI calculations, where a time step $\Delta t = 0.125\Omega^{-1}$ was necessary to converge the path integral. [7] By contrast, the EACP approximation yields reasonable results over the entire propagation time. (The small deviations in the EACP approximation can be attributed to high-frequency bath oscillators in the tail of the spectral density, for which the bath trajectories are significantly perturbed by the system.) With these parameters, the Ehrenfest approximation yields results indistinguishable from those of the full path integral treatment.

In Fig. 1b we show results at a lower temperature, $\hbar\Omega\beta = 2.5$, and intermediate coupling strength characterized by $\xi = 0.6$. Even though the bath has the same frequency distribution, ($\omega_c = 2.5\Omega$), it exhibits more pronounced quantum mechanical effects at this lower temperature. The unperturbed solvent approximation leads to accurate results for $\Omega t \sim 1$, after which it is seen to exaggerate the oscillatory nature of the TLS dynamics. In this case the Ehrenfest model reproduces the underdamped oscillation of the TLS average position nearly quantitatively for all times.

A strongly quantum mechanical, high-frequency, low-temperature bath, characterized by $\omega_c = 5\Omega$, $\hbar\Omega\beta = 5$ and intermediate coupling strength ($\xi = 0.3$), is used in the calculations presented in Figure 1c. In this case the majority of the oscillators are practically at zero temperature. In this regime neither the EACP approximation nor the Ehrenfest approximation can reproduce the exact quantum mechanical results in a quantitative fashion. Specifically, the unperturbed solvent approximation exaggerates the oscillatory character of the motion because it neglects decoherence associated with quantum mechanical memory. On the other hand, the Ehrenfest approximation leads to faster damping of the TLS dynamics. Thus full QCPI calculations are necessary in this regime. Because both approximations seem adequate for times up to $t \sim \Omega^{-1}$, either one seems an excellent candidate for constructing a reference propagator that should allow large path integral time steps.

To explain the improvement offered by the mean field (Ehrenfest) approximation, we have studied the bath trajectories for a single bath degree of freedom experiencing a particular set of system forces along one particular forward-backward system paths. In Figure 2 we see such trajectories in the case of a single bath degree of freedom coupled to the TLS. (The system-bath coupling used to obtain the trajectories in Fig. 2 has been increased substantially compared to the values employed in the calculations of Fig. 1. so that the effects are more pronounced and we can draw the conclusions well.) The momentum of these trajectories displays discontinuities where the force from the quantum system changes. These changes are more prominent in lower-energy trajectories, whose dynamics can be changed more by the interaction of the bath with the system. This observation is the physical reason for the less significant role of the "back reaction" under high temperature conditions.

In figure 2 we have also compared the trajectory of the various approximations. The Ehrenfest reference follow closely the exact system propagation in shorter times. The trajectories are almost exact for a significant portion of the time but then finally fails. It is really beneficial at early times, and this can be used to construct larger time step propagators. However eventually, towards the end of the system propagation, the trajectories are significantly different and Ehrenfest trajectories over compensate for the classical path discrepancies.

In Figure 3 we present full QCPI calculations using propagators derived with the unperturbed solvent or the self-consistent (Ehrenfest) model as the reference Hamiltonian. The parameters are those employed in the calculations of Fig. 1. As can be seen in Fig. 3, the use of improved time-dependent reference propagators yields converged results with large time steps. As is expected, the most notable gain is again observed in the high-temperature case shown in Fig. 3a, where the Ehrenfest reference produces results that

are practically exact with a single time step. Thus, a single trajectory is required for each initial condition in this case. The propagator based on the unperturbed solvent reference leads to converged QCPI results with $\Delta t = \Omega^{-1}$. As seen in the figure, this time step is by far too large for the standard propagator splitting, which requires a step size $\Delta t = 0.125\Omega^{-1}$ for convergence. Propagation to the same final time with the time-independent system propagator would require 40 path integral steps and 2^{80} trajectories for each initial condition leading to a lot of computational savings.

Under the more challenging conditions of Figures 3b and 3c, the QCPI calculations with the two time-dependent reference models converged with $\Delta t = 0.625\Omega^{-1}$ and $\Delta t = 0.75\Omega^{-1}$ respectively. For comparison, the time step required with the standard propagator discretization was $\Delta t = 0.25\Omega^{-1}$. Perhaps the most significant consequence of a threefold gain in step size is that the important features of the system dynamics was captured with only 5 path integral time steps (i.e., 2^{10} trajectories from each initial condition), and hence an iterative decomposition of the path sum was not required.

As the reference part of the total action, Φ_{ref}, is taken into the system propagation, there is a reduction in phase of the Monte-Carlo integrand, i.e. we are now left with a phase factor of $e^{i\Delta\Phi}$. Thus the spread of the quantum influence functional is reduced as is evident from Figure 4. Figure 4a shows the spread of the quantum influence functional for the bare, the EACP and the TDSCF propagators for the high temperature case. The TDSCF propagators do not require full QCPI calculations as a result the corresponding quantum influence functional is restricted only to the magnitude between 0 and 1, i.e. the magnitude of the propagators. The quantum influence functional corresponding to classical propagators on the other hand spread to -0.25 to 1.25, while for the bare propagators it moves further to the negative regions from -0.75 to 1.75. Though the number of points spanning these inaccessible regions are low, there is still a wider spread than the TDSCF and the EACP propagators. Next we present the most challenging regime, when the spread of the Monte-Carlo integrand is considered. This is the most quantum mechanical case, or the low temperature regime. In this regime, the bare, quantum influence functional from the EACP and the TDSCF propagators is much more spread, and extended from -1.75 to 0.75. Here there is significant number of occurrences in the most extreme interval only for the bare propagators.

A direct consequence of the above observation is the reduced number of Monte Carlo samples required for convergence. The number of Monte Carlo samples was adjusted to produce statistical error bars comparable to or smaller than the size of the markers shown in Figure 3. This precision was achieved with 40,000

Monte Carlo points in the case of the bare (time-independent) system propagator, and 10,000-20,000 points when the time dependent reference propagators were used.

2.5 Iterative Evaluation of Quantum Classical Path Integral with Solvent Driven Propagators:

The iterative methodology for QCPI has been developed in previous publication [17], and has been adapted with the solvent-driven propagators in this work. Since there is an exponential growth in the number of trajectories with the system states, i.e. M^{2N} trajectories are created when the system is represented in terms of M states, the direct summation or full path sum is feasible for a 2 or 3 state system only for N<8 time steps. So if we have captured the major dynamics within ~8 path integral time steps as we have seen in the above sections, that should be fine. But for slower baths, if the dynamics requires long time propagation, we need to move to an iterative approach.

Makri *et. al* [3,4] had observed earlier that the correlation or the response function of the quantum memory is short lived and decays to zero beyond a certain time interval, $\tau_{\text{mem}} = m\Delta t$. This in turn implies in the QCPI picture that the dynamics of the system is governed by the forces that depends only on the m recent path time steps. In this section we discuss the implication of this idea and how it can be used in the QCPI framework with the improved propagators. Thus the classical trajectories now do not depend on all time points from evaluation time, but the force only extends to a pre-decided time length, which is equal to the decoherence time for that particular system- bath parameters.

We take the idea of memory (or decoherence) time to be same as that from the influence functional approach, $\tau_{\text{mem}} = m\Delta t$ and proceed using the method described in Ref [17]. Like in full step QCPI the first step is similar: we need to sample the function P (here the Wigner distribution) using Metropolis Monte Carlo procedures to obtain the initial phase space points. Unlike full QCPI, we create all trajectories that result from the different system forces along the $M^{2(m+1)}$ system paths only to define the rank-$2m$ path tensor with the improved propagators,

$$R_{m-1}\left(s_0^{\pm}, s_1^{\pm}, \ldots, s_{m-1}^{\pm}; x_0, p_0\right) = \left\langle s_{m-1}^{+}\left|\hat{U}_{\text{ref}}\left((m-1)\Delta t, (\text{m}-2)\Delta t; x_0, p_0\right)\right|s_{m-2}^{+}\right\rangle \cdots \left\langle s_1^{+}\left|\hat{U}_{\text{ref}}\left(\Delta t, 0; x_0, p_0\right)\right|s_0^{+}\right\rangle$$
$$\times \left\langle s_0^{+}\left|\hat{\rho}_0\right|s_0^{-}\right\rangle \left\langle s_0^{-}\left|\hat{U}_{\text{ref}}^{\dagger}\left(0, \Delta t; x_0, p_0\right)\right|s_1^{-}\right\rangle \cdots$$
$$\times \left\langle s_{m-2}^{-}\left|\hat{U}_{\text{ref}}^{\dagger}\left((m-2)\Delta t, (m-1)\Delta t; x_0, p_0\right)\right|s_{m-1}^{-}\right\rangle e^{\frac{i}{\hbar}\Delta\Phi(x_0, p_0; s_0^{\pm}, \ldots, s_{m-1}^{\pm})} \tag{2.24}$$

An important aspect to note that each of these propagators and the tensors, are different and unique to each trajectory, unlike the influence functional approach. Though symmetry in the harmonic system can be utilized to find out each non-unique combinations, but this is not a general method and cannot be extended to anharmonic bath. This means that the evaluation of such propagators must be done at each step of the propagation and for each initial condition in the Monte Carlo loop.

Next we construct the propagator tensor of rank $2(m+2)$,

$$T_m\left(x_0, p_0; s_0^{\pm}, s_1^{\pm}, \ldots, s_m^{\pm}\right) = \left\langle s_m^{+}\left|\hat{U}_{\text{ref}}\left(m\Delta t, (m-1)\Delta t; x_0, p_0\right)\right|s_{m-1}^{+}\right\rangle$$
$$\times \left\langle s_{m-1}^{-}\left|\hat{U}_{\text{ref}}^{\dagger}\left((m-1)\Delta t, m\Delta t; x_0, p_0\right)\right|s_m^{-}\right\rangle e^{\frac{i}{\hbar}\Delta\Phi(x_0, p_0; s_0^{\pm}, \ldots, s_m^{\pm})} \tag{2.25}$$

This propagator is used to propagate the tensor made in Eqn. 2.24 one step by simple matrix-vector multiplication as suggested in ref [17]. It is also different in different time step of propagation, and is given by the integration (i.e. the summation) of the product of the tensor (vector) and the propagator (matrix),

$$R_m\left(s_1^{\pm}, \ldots, s_m^{\pm}; x_0, p_0\right) = \int ds_0^{\pm}\, T_m\left(s_0^{\pm}, s_1^{\pm}, \ldots, s_m^{\pm}; x_0, p_0\right) R_{m-1}\left(s_0^{\pm}, s_1^{\pm}, \ldots, s_{m-1}^{\pm}; x_0, p_0\right) \tag{2.26}$$

To propagate this further in time, say one step at a time, the classical trajectories should be calculated for the next step. This would lead to an increase in the number of trajectories by a factor of M^2, which is not desired. To avoid this problem, we propagate only one of these trajectories, chosen randomly, by one time step to the time $(m+1)\Delta t$, thus still maintaining the number of trajectories to $M^{2(m+1)}$. This is how we avoid the exponential proliferation of the number of paths. Constructing the propagator tensor for the next step.

$$T_{m+1}\left(x_1, p_1; s_1^{\pm}, s_2^{\pm}, \ldots, s_{m+1}^{\pm}\right) = \left\langle s_{m+1}^{+}\left|\hat{U}_{\text{ref}}\left((m+1)\Delta t, m\Delta t; x_0, p_0\right)\right|s_m^{+}\right\rangle$$
$$\times \left\langle s_m^{-}\left|\hat{U}_{\text{ref}}^{\dagger}\left(m\Delta t, (m+1)\Delta t; x_0, p_0\right)\right|s_{m+1}^{-}\right\rangle e^{\frac{i}{\hbar}\Delta\Phi(x_1, p_1; s_1^{\pm}, \ldots, s_{m+1}^{\pm})} \tag{2.27}$$

leads to the following propagated result,

$$R_{m+1}\left(s_2^{\pm},\ldots,s_{m+1}^{\pm};x_0,p_0\right)=\int ds_1^{\pm}\,T_m\left(s_1^{\pm},\ldots,s_{m+1}^{\pm};x_0,p_0\right)R_m\left(s_1^{\pm},\ldots,s_m^{\pm};x_0,p_0\right). \tag{2.28}$$

We repeat the procedure described above till we reach the final time point. At each propagation step we obtain the quantum influence function as well as the reduced density matrix, by taking the Monte Carlo average of the quantum influence function, (this is done by repeating the above algorithm for all initial conditions)

$$Q\left(s_N^{\pm},x_0,p_0;N\Delta t\right)=\int ds_{N+1-m}^{\pm}\cdots\int ds_{N-1}^{\pm}\,R_N\left(s_{N+1-m}^{\pm},\ldots,s_N^{\pm};x_0,p_0\right), \tag{2.29}$$

$$\rho_{\mathrm{red}}\left(s_N^{\pm};N\Delta t\right)=\int dx_0\int dp_0\,Q\left(s_N^{\pm},x_0,p_0;N\Delta t\right),\quad N=m,m+1,\ldots \tag{2.30}$$

The memory length m is a convergence parameter. Using the solvent-driven propagators this memory length is achieved in much lower number of path integral slices. This has a two-way benefit, first there is exponential reduction in the number of terms required to obtain the desired memory length. Also, owing to the reduced number of terms, the dimension of the tensors and the propagators are highly reduced, requiring less storage requirements. This coupled advantage of using the solvent driven propagators make iterative evaluation possible for extremely slow and sluggish baths.

In Figure 6 we present iterative calculations using propagators derived with the unperturbed solvent as the reference Hamiltonian. The parameters are those employed in the calculations of Fig. 1. As we had seen in Fig. 3, the use of improved time-dependent reference propagators yields converged results with large time steps. The most notable gain is again observed in the high-temperature case shown in Fig. 4a, where the memory $\tau_{mem}=0.625\Omega^{-1}$ is practically achieved in a single time step of propagation $\Delta t=\Omega^{-1}$. This is the simplest version of the iterative QCPI scheme and it involves the storage of just M^4 trajectories from the forces corresponding to the forward-backward coordinates of each pair of adjacent time points. The tensors $\mathbf{R}_k$ have rank 2 and the propagator tensors $\mathbf{T}_k$ have rank 4. This becomes almost as computationally inexpensive as calculating the EACP approximation. On the other hand, for QCPI with bare propagators, in order to reach the desired memory of $\tau_{mem}=0.625\Omega^{-1}$, it required a memory span of $m=5$; thus requiring tensors $\mathbf{R}_k$ have rank 10 and the propagator tensors $\mathbf{T}_k$ have rank 12[7]. Even under more challenging regimes of Figure 6b. and 6c. we have achieved the required memory of $\tau_{mem}=1.25\Omega^{-1}$ by using just 3 and 2 steps respectively. The tensors $\mathbf{R}_k$ have rank 6 and 4 and the propagator tensors $\mathbf{T}_k$ have rank 8 and 6 respectively. As is seen in the figure the time step used with the solvent driven propagators are too large for the standard QCPI to converge. In comparison, for QCPI with bare propagators required

$m = 6$ to achieve the required memory length, thus implying that it needed tensors $\mathbf{R}_k$ have rank 10 and the propagator tensors $\mathbf{T}_k$ have rank 12 [7, 17].

2.6 Applications of Iterative Evaluation with Filtering to Challenging Regimes:

To move to more challenging regime we illustrate the iterative QCPI methodology with calculations on asymmetric dissipative two-level systems (TLS). The quantum system is described by the Hamiltonian

$$H_0 = -\hbar\Omega\sigma_x - \varepsilon\sigma_z \tag{2.31}$$

where σ_x and σ_z are the standard 2×2 Pauli spin matrices. If the absence of an energy bias ($\varepsilon = 0$) the bare TLS is characterized by the tunneling splitting $2\hbar\Omega$. The TLS is coupled to a harmonic bath as described in the previous sections.

First we present results for an asymmetric TLS with $\varepsilon = \hbar\Omega$, strongly coupled ($\xi = 1.2$) to a bath ($\omega_c = 2.5\Omega$) at an intermediate temperature ($\hbar\Omega\beta = 1$). This is a particularly challenging regime with the naïve QCPI evaluation. In order to obtain the total quantum non-locality the iterative QCPI scheme required $m = 10$ using a path integral time step $\Delta t = 0.125$. This is particularly challenging and computationally not feasible, because it requires a total of 2^{20} possible such segments. Thus it required filtering schemes to retain 1.25×10^5 system path segments to obtain converged results [17]. In Fig 7a. for the same parameters, in the single step propagation, we see that the bare propagators fails to capture the dynamics beyond a time step of $0.2\,\Omega^{-1}$. This confirms with earlier QCPI calculations, where a time step $\Delta t = 0.125\Omega^{-1}$ was necessary to converge the path integral. However we see that the EACP approximation is valid till a time of Ω^{-1} while the TDSCF reference is accurate till $1.5\,\Omega^{-1}$. Neither the EACP approximation nor the TDSCF reference in its single step, can correctly predict the equilibrium population, because they cannot account for the quantum decoherence in a quantitative fashion. To correct for that, we incorporate the EACP approximation in the iterative scheme of QCPI. In Fig 7b. we have accounted for the quantum non-locality by using $m = 5$ and a path integral time step $\Delta t = 0.25$. We just required 2^{10} paths, which can be easily done using modern computers thus obviating the need for filtering in this regime. QCPI with naïve propagators do not achieve the accurate results using such high time steps as is quite evident from the curve.

For very slow and sluggish baths, the solvent-induced memory spans many path integral time steps. In such cases, the computational cost of the iterative QCPI methodology becomes rather high. and we need to use

the scheme of filtering. To properly use the concept of filtering, consider two physically motivating aspects[17]: First, for a generalized Hamiltonian represented in continuous coordinates, if we construct propagators using energy filtered procedures, (e.g. discrete variable representation), the propagators will decay to zero if there is a difference in the starting and end system configuration. Thus the propagators which show a lot of system transitions will have very small magnitude and can be easily ignored. Second, the propagators whose weight is dependent on the classical particle, can take advantage of some dynamical information related to solvent reorganization. If the transition from one quantum state to another, requires a lot of energy in terms of solvent reorganization, then such processes will be unfavorable and hence the propagator which is dependent on the classical coordinates of the solvent will be of very low magnitude and can be ignored. Also, these propagators will avoid the region where the coupling between two quantum systems is low. The concept of filtering was first developed in our group in the influence functional or the harmonic bath framework [18-20]. Either a stochastic [18, 19] or a deterministic [20] criteria was used to throw away paths. This method of filtering depended on the weight of traditional propagators. Filtering with bare propagators utilized only the first criteria mentioned above. On the other hand, both of these physical phenomena are captured in the EACP propagators, which are constructed in the DVR representation and take some weight of the classical trajectories. It can be argued that the EACP propagators take into account fully the reorganization energy associated with the classical frequencies and should be ideal for filtering in case of very high temperatures where filtering schemes are most effective. The selection procedure for a path is kept very simple: The weight of the path is given by the weight of the solvent-driven propagator till the propagation time, if this weight is greater than the threshold θ then it is accepted otherwise it is rejected. The procedure is deterministic, and often results in elimination of majority of the non-important paths. All paths within the memory *m*, which is greater than the threshold are selected, and all of these segments are used for further propagation.

To demonstrate the ideas of filtering with iterative evaluation using EACP propagators, we apply the methodology to the TLS-Ohmic bath model presented in Ref. [18], where the parameters were chosen to resemble those in the early dynamics of bacterial photosynthesis. The system Hamiltonian takes the form

$$H_0 = \begin{pmatrix} \varepsilon_1 & V_{12} \\ V_{12} & \varepsilon_2 \end{pmatrix} \tag{2.32}$$

Where $\varepsilon_1 = 0$ cm^{-1}, $\varepsilon_1 = 400$ cm^{-1}, $V_{12} = 22$ cm^{-1}. The spectral density has the Ohmic form with $\omega_c = 150$ cm^{-1} and the reorganization energy as $2\eta\omega_c = 500$ cm^{-1}. The asymmetry in this case is very challenging and is almost 5 time the tunneling splitting. This presents a very difficult scenario for the convergence using naïve QCPI. Also, it has very high reorganization energy and the filtering scheme will help throw out most of the statistically insignificant paths.

Figure 8c shows the single step propagation with the bare and the EACP propagators. While the bare propagators cannot capture any dynamics of the electron transfer system, either quantitatively or qualitatively, the EACP propagators captures it at least qualitatively. It is accurate to the first 0.5 ps after which it starts to deviate and reaches the equilibrium population of 0, which is predicted by the classical limit. Owing to the high asymmetry present in the system, the equilibrium population predicted by the quantum mechanical treatment is significantly different as predicted from the classical limit, thus posing a major challenge for convergence. However, when we use the EACP approximation as a reference to construct propagators for iterative QCPI it converges using a time step of 10 fs. In comparison, naïve propagators required a time step of 5 fs. In order to converge the total quantum non-locality QCPI with EACP propagators we required $m=10$. Exploiting the concept of filtering as described above we could throw away majority of the paths, and required a cut off threshold of θ, which retained approximately 3000 paths. This is a dramatic save as compared to 2^{20}, this making this computation feasible. Figure 8d shows the convergence of the iterative QCPI with filtering with different number of oscillators. Owing to the ohmic nature of the spectral density, majority of the reorganization energy originates from the low frequency modes. Due to large reorganization energies, there is a high importance of including enough low frequency mode oscillators to converge at longer times. This is very well-explained in Figure 7b, where we have seen we require 200 oscillators to converge.

2.7 Concluding Remarks:

In this chapter we have taken the method of QCPI and have used a very simple, physically motivated idea to accelerate the evaluation of QCPI. QCPI itself is a very rigorous theory and can be used to benchmark calculations for electron and proton transfer reactions. Thus by incorporating the developments we have proposed here, we have made sure that such calculations become feasible. Two physically motivated approximations were considered to be incorporated in the propagator for the quantum system, one was the classical path, or the unperturbed solvent and the other was the time dependent self consistent field or the Ehrenfest model. Although they are incapable of capturing the exact nature of the dynamics, they provide excellent references to construct propagators which allow for larger time steps than conventional bare system, propagators. They lead to the accurate capture of the interplay between classical and quantum mechanics, smoother integrand because of a smaller phase and exponential reduction in the number of terms.

We have extended the method to include the iterative and filtering algorithms with the solvent-driven propagators. These propagators when used with the iterative scheme the decoherence time is achieved in far less number of path integral slices than the bare propagators, leading to further decrease in the number of trajectories in the quasi-Markovian scheme of propagation. The solvent-reference propagators (EACP and TDSCF) which have their weights depend on the position of the classical solvent particle, and would prohibit quantum transitions from taking place in areas of high solvent reorganization, and additionally the TDSCF propagators would prevent these transitions where there is low system-bath coupling. This in turn would lead to an even larger reduction of the weight of the propagator elements leading to a more efficient filtering technique.

2.8 Figures:

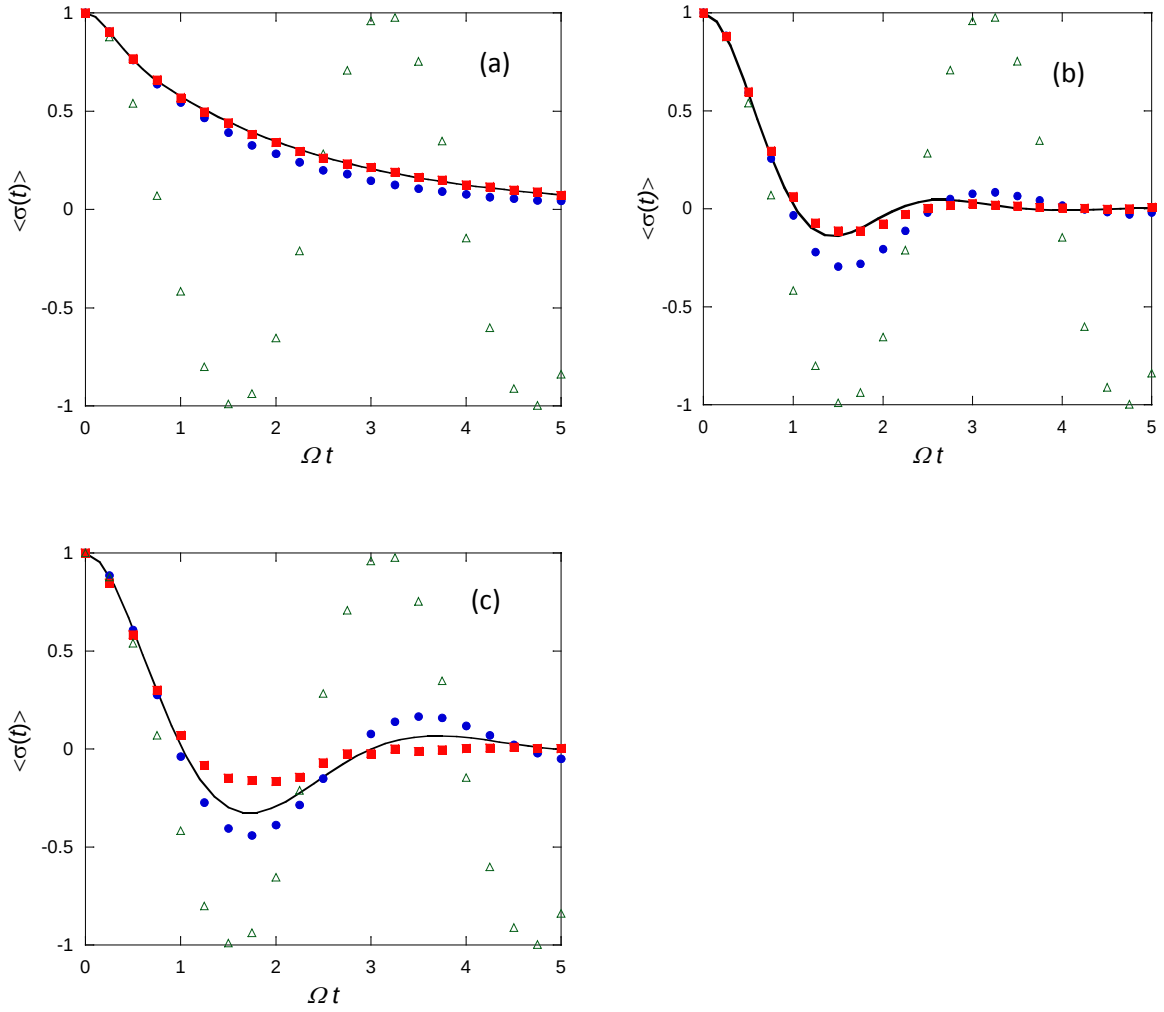

Figure. 2.1: Average position of a symmetric TLS from single-step calculations. Green hollow triangles: propagator for the bare TLS. Blue solid circles: time-dependent reference propagator obtained from unperturbed solvent trajectories (EACP approximation). Red solid squares: time-dependent reference propagator obtained from Ehrenfest trajectories. Black line: exact results obtained via the iterative path integral methodology based on the analytical Feynman-Vernon influence functional. (a) $\omega_c = 2.5\Omega$, $\hbar\Omega\beta = 0.2$, $\xi = 1.2$ (b) $\omega_c = 2.5\Omega$, $\hbar\Omega\beta = 2.5$, $\xi = 0.6$. (c) $\omega_c = 5\Omega$, $\hbar\Omega\beta = 5$, $\xi = 0.3$.

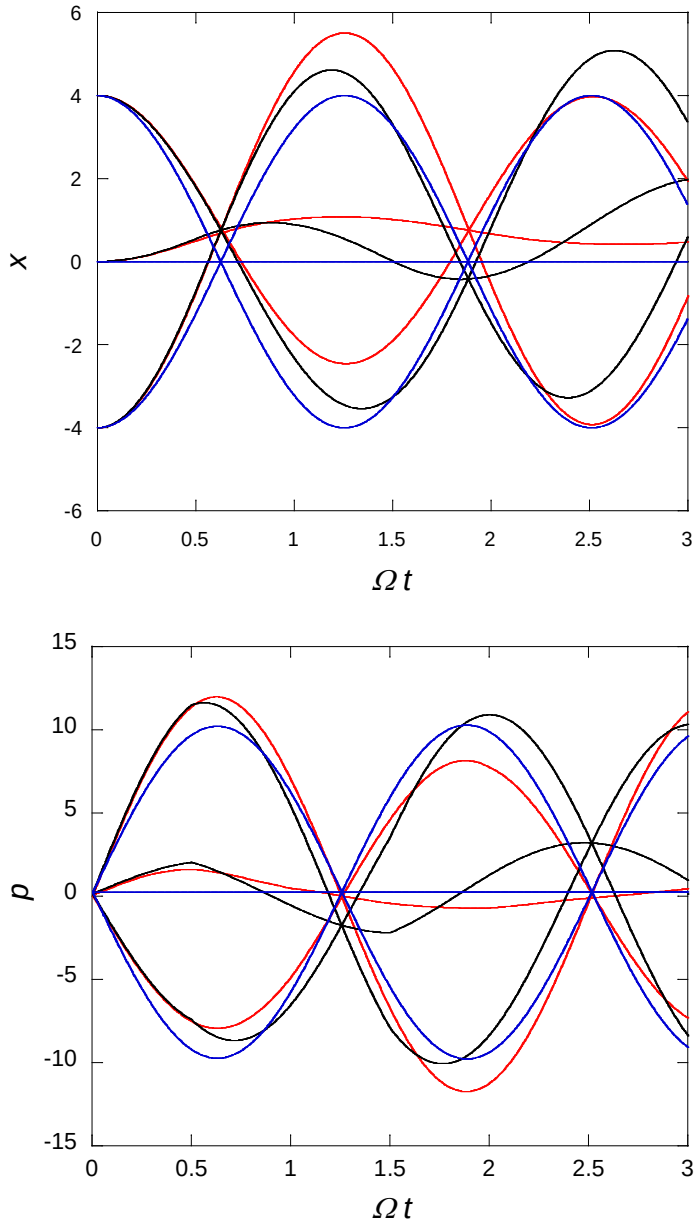

Figure. 2.2: Classical trajectories along arbitrarily chosen forward-backward system paths for a single-oscillator bath with $\omega = 2.5\Omega$ strongly coupled to the TLS. Blue line: free bath trajectory. Red line: trajectory following the Ehrenfest system force. Black line: full trajectory, following the actual force exerted by the TLS.

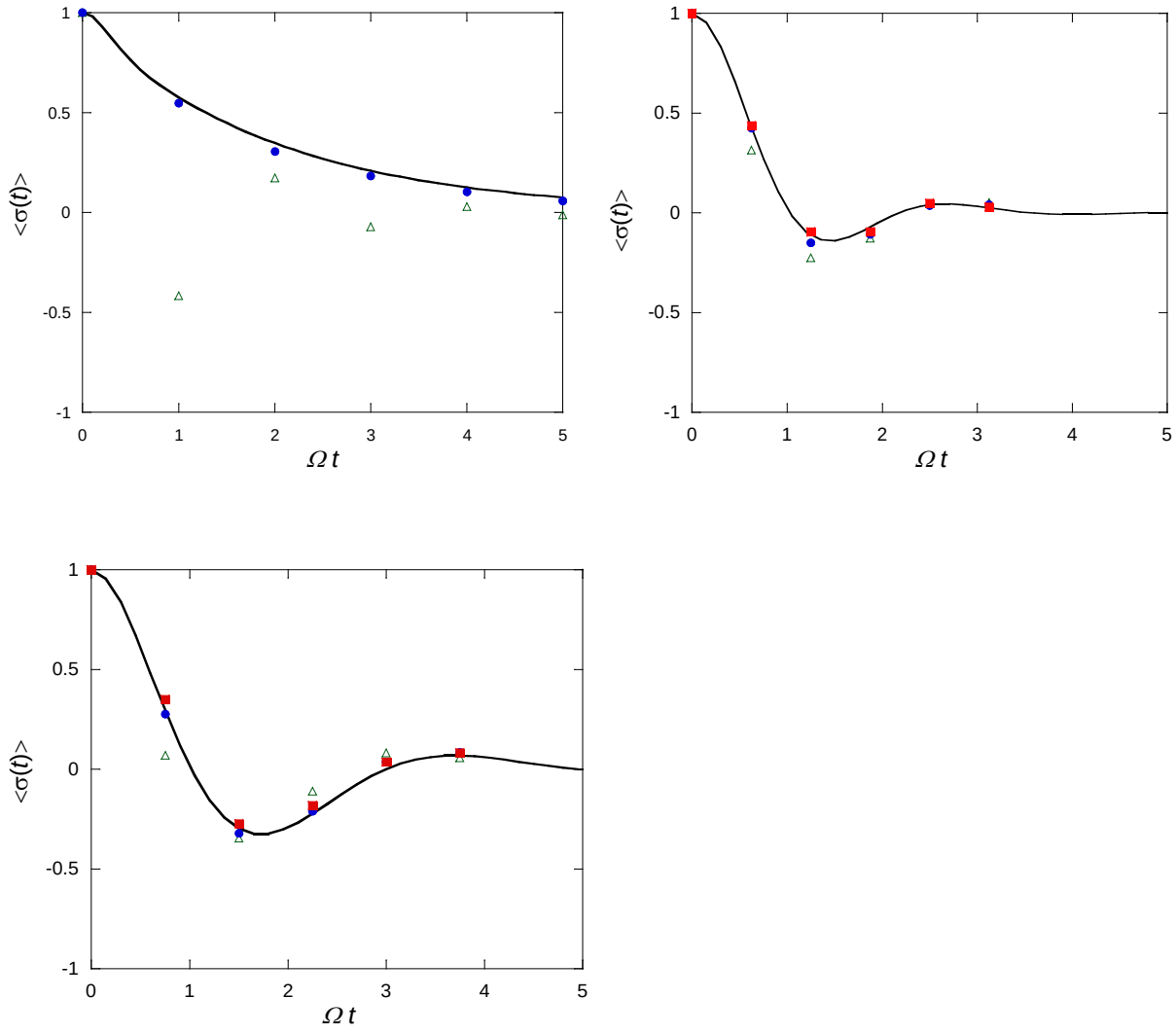

Figure. 2.3: Average position of a symmetric TLS from QCPI calculations. Green hollow triangles: propagator for the bare TLS. Blue solid circles: time-dependent reference propagator obtained from unperturbed solvent trajectories (EACP approximation). Red solid squares: time-dependent reference propagator obtained from Ehrenfest trajectories. Black line: exact results obtained via the iterative path integral methodology based on the analytical Feynman-Vernon influence functional. (a) $\omega_c = 2.5\Omega$, $\hbar\Omega\beta = 0.2$, $\xi = 1.2$, $\Omega\Delta t = 1$. (b) $\omega_c = 2.5\Omega$, $\hbar\Omega\beta = 2.5$, $\xi = 0.6$, $\Omega\Delta t = 0.625$. (c) $\omega_c = 5\Omega$, $\hbar\Omega\beta = 5$, $\xi = 0.3$, $\Omega\Delta t = 0.75$.

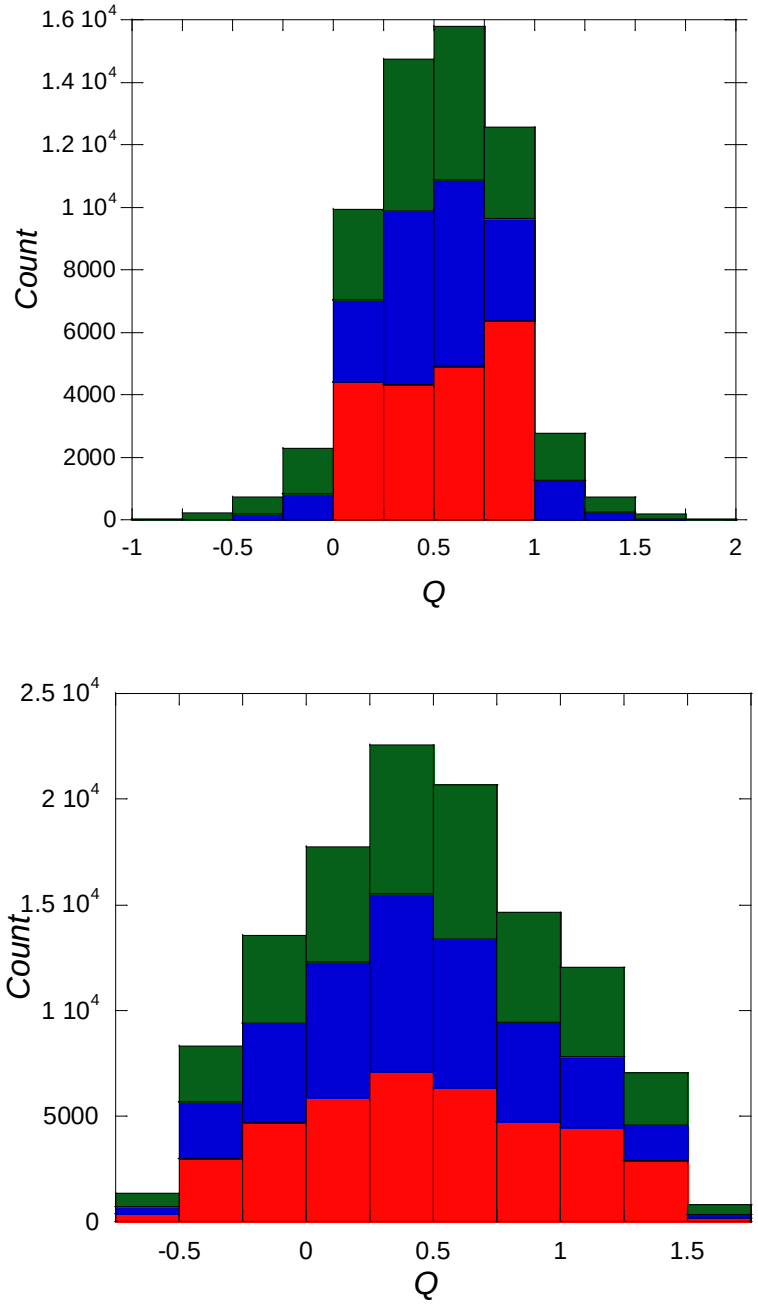

Figure 2.4: Frequency distribution of the Quantum influence functional for different Monte Carlo points sampled. Green section: propagator for the bare TLS. Blue section: time-dependent reference propagator obtained from unperturbed solvent trajectories (EACP approximation). Red section: time-dependent reference propagator obtained from Ehrenfest trajectories. (a) $\omega_c = 2.5\Omega$, $\hbar\Omega\beta = 0.2$, $\xi = 1.2$, $\Omega\Delta t = 1$. (b) $\omega_c = 5\Omega$, $\hbar\Omega\beta = 5$, $\xi = 0.3$, $\Omega\Delta t = 0.75$.

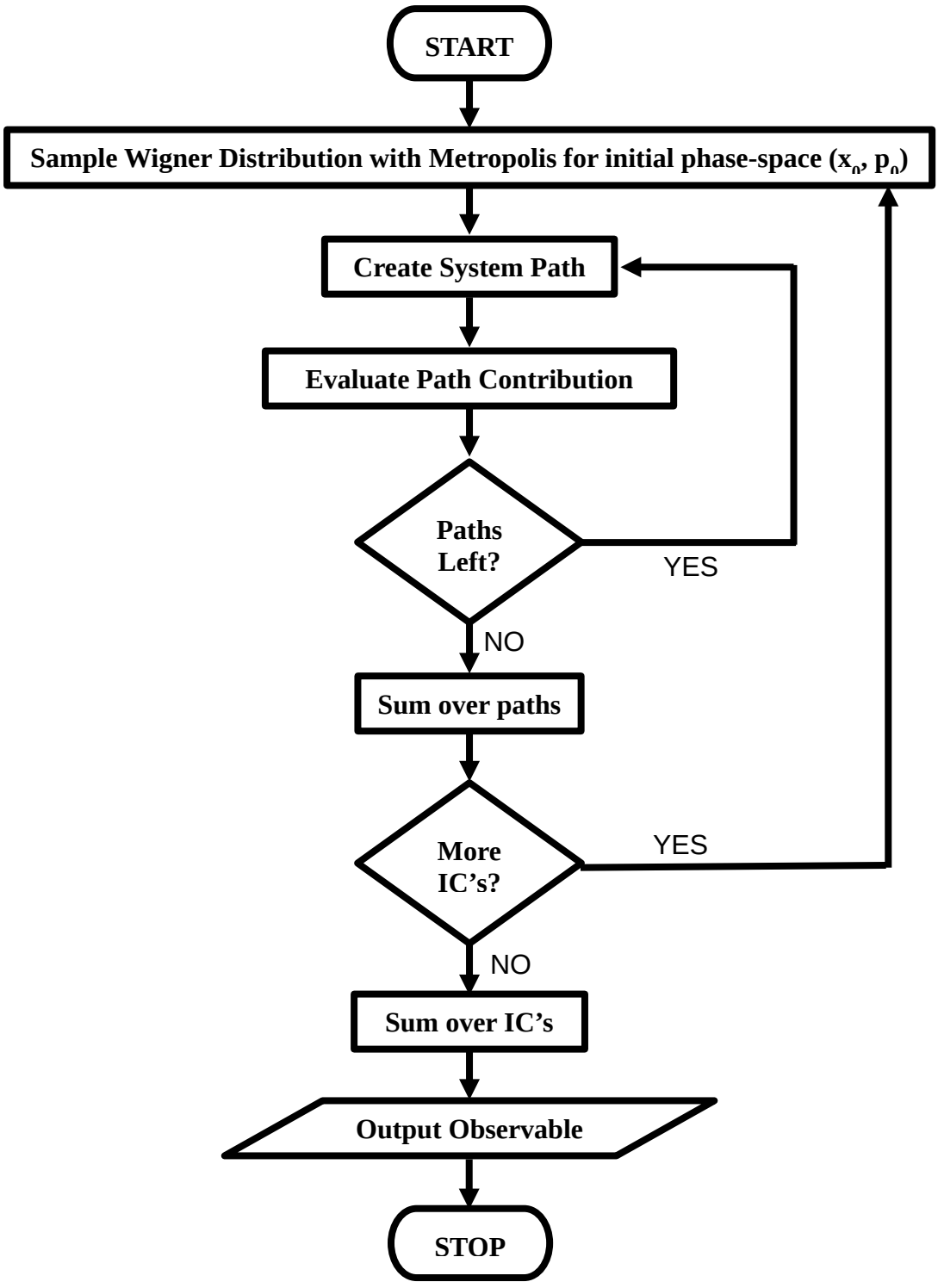

Figure 2.5: Flowchart 1: QCPI Algorithm for computing density matrix for a general system-bath.

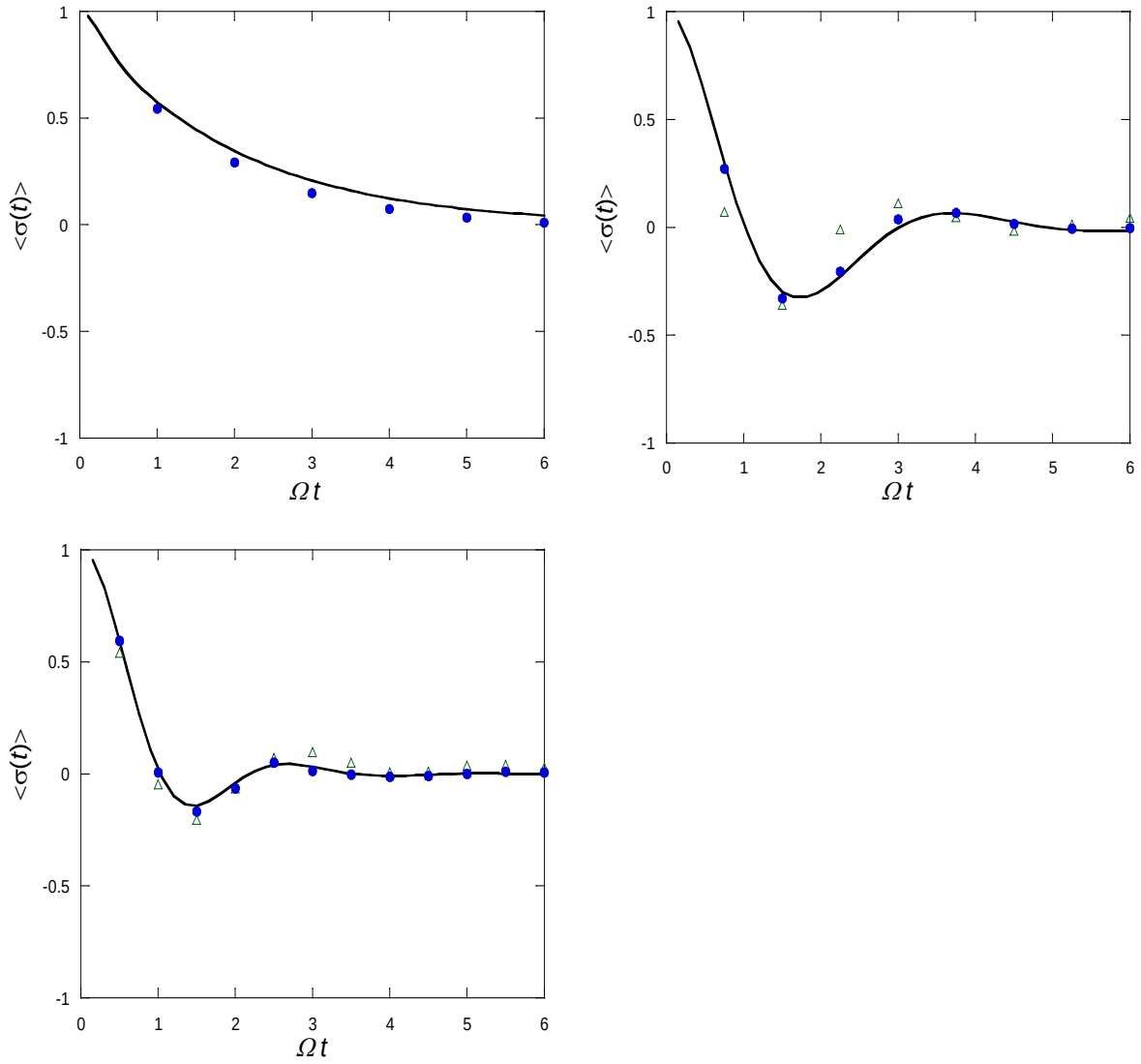

Figure. 2.6: Average position of a symmetric TLS from QCPI calculations. Green hollow triangles: propagator for the bare TLS. Blue solid circles: time-dependent reference propagator obtained from unperturbed solvent trajectories (EACP approximation). Black line: exact results obtained via the iterative path integral methodology based on the analytical Feynman-Vernon influence functional. (a) $\omega_c = 2.5\Omega$, $\hbar\Omega\beta = 0.2$, $\xi = 1.2$, $\Omega\Delta t = 1, m = 1$. (b) $\omega_c = 2.5\Omega$, $\hbar\Omega\beta = 2.5$, $\xi = 0.6$, $\Omega\Delta t = 0.625$, $m = 3$. (c) $\omega_c = 5\Omega$, $\hbar\Omega\beta = 5$, $\xi = 0.3$, $\Omega\Delta t = 0.75$, $m = 2$.

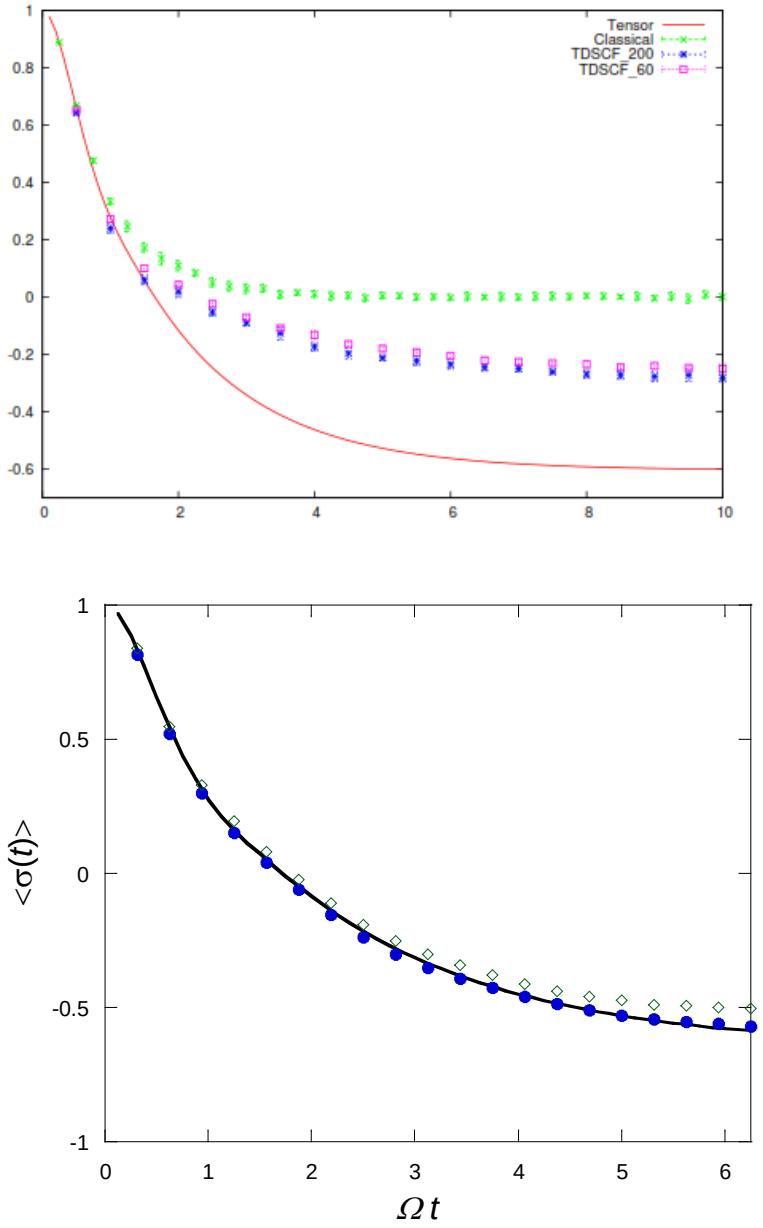

Figure. 2.7: Average position of a symmetric TLS from QCPI calculations. Green hollow triangles: propagator for the bare TLS. Blue solid circles: time-dependent reference propagator obtained from unperturbed solvent trajectories (EACP approximation). Black line: exact results obtained via the iterative path integral methodology based on the analytical Feynman-Vernon influence functional for $\omega_c = 2.5\Omega$, $\hbar\Omega\beta = 1.0$, $\xi = 1.2$, $\varepsilon = 1$ (a) Single step QCPI corresponding to the corresponding approximations. (b) Iterative QCPI calculations with $\Omega\Delta t = 0.25$, $m = 5$

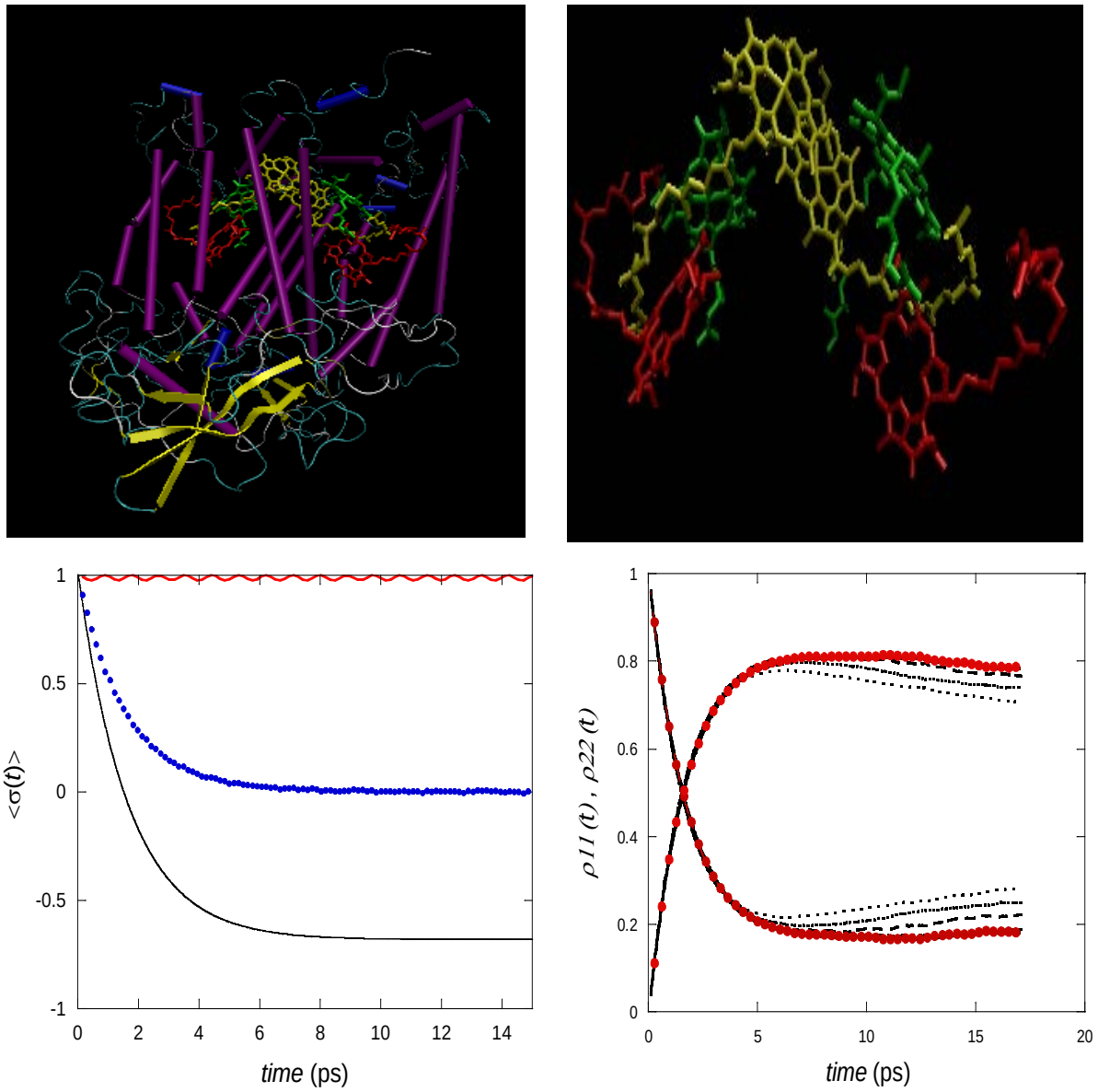

Figure. 2.8: Photosynthetic reaction center containing the protein backbone and the bacteriochlorophylls (b) The 6 bacteriochlorophyll in the reaction centers. Average position of an asymmetric TLS coupled to a sluggish bath (c) Single step propagation- Blue markers: EACP approximation from unperturbed solvent trajectories, red line – bare propagators, black curve –exact Feynman Vernon results with use of iteration and filtering techniques, $\Delta t = 5\, fs$, $m = 20$. (d) Individual population with different number of bath modes (dotted lines using 60, 80, 120, 200 bath modes). The red markers are the EACP-full QCPI with $\Delta t = 10\, fs$, $m = 10$; Use of filtering results in survival of approx. 3000 paths from 2^{20} paths.

2.9 References:

1. Feynman, Richard Phillips. "Space-time approach to non-relativistic quantum mechanics." *Reviews of Modern Physics* 20.2 (1948): 367.

2. R. P. Feynman and A. R. Hibbs, *Quantum Mechanics and Path Integrals*. (McGraw-Hill, New York, 1965).

3. Makri, Nancy, and Dmitrii E. Makarov. "Tensor propagator for iterative quantum time evolution of reduced density matrices. I. Theory." *The Journal of chemical physics* 102.11 (1995): 4600-4610.

4. Makri, Nancy, and Dmitrii E. Makarov. "Tensor propagator for iterative quantum time evolution of reduced density matrices. II. Numerical methodology." *The Journal of chemical physics* 102.11 (1995): 4611-4618.

5. Makri, Nancy, and Keiran Thompson. "Semiclassical influence functionals for quantum systems in anharmonic environments." *Chemical physics letters* 291.1 (1998): 101-109.

6. Thompson, Keiran, and Nancy Makri. "Influence functionals with semiclassical propagators in combined forward–backward time." *The Journal of chemical physics* 110.3 (1999): 1343-1353.

7. Lambert, Roberto, and Nancy Makri. "Quantum-classical path integral. I. Classical memory and weak quantum nonlocality." *The Journal of chemical physics* 137.22 (2012): 22A552.

8. Shi, Qiang, and Eitan Geva. "A relationship between semiclassical and centroid correlation functions." *The Journal of chemical physics* 118.18 (2003): 8173-8184.

9. Poulsen, Jens Aage, Gunnar Nyman, and Peter J. Rossky. "Practical evaluation of condensed phase quantum correlation functions: a Feynman–Kleinert variational linearized path integral method." *The Journal of chemical physics* 119.23 (2003): 12179-12193.

10. Bonella, Sara, Daniel Montemayor, and David F. Coker. "Linearized path integral approach for calculating nonadiabatic time correlation functions." *Proceedings of the National Academy of Sciences of the United States of America* 102.19 (2005): 6715-6719.

11. Shi, Qiang, and Eitan Geva. "Nonradiative electronic relaxation rate constants from approximations based on linearizing the path-integral forward-backward action." *The Journal of Physical Chemistry A* 108.29 (2004): 6109-6116.

12. Wigner, E. J. Calculation of the Rate of Elementary Association Reactions. Chem. Phys. 1937, 5, 720.

13. Sun, Xiong, and William H. Miller. "Semiclassical initial value representation for electronically nonadiabatic molecular dynamics." *The Journal of chemical physics* 106.15 (1997): 6346-6353.

14. Thompson, Keiran, and Nancy Makri. "Rigorous forward-backward semiclassical formulation of many-body dynamics." *Physical Review E* 59.5 (1999): R4729.

15. Bacic, Z., and John C. Light. "Theoretical methods for rovibrational states of floppy molecules." *Annual Review of Physical Chemistry* 40.1 (1989): 469-498.

16. Topaler, Maria, and Nancy Makri. "System-specific discrete variable representations for path integral calculations with quasi-adiabatic propagators." *Chemical physics letters* 210.4 (1993): 448-457.

17. Lambert, Roberto, and Nancy Makri. "Quantum-classical path integral. II. Numerical methodology." *The Journal of chemical physics* 137.22 (2012): 22A553.

18. Sim, Eunji, and Nancy Makri. "Filtered propagator functional for iterative dynamics of quantum dissipative systems." *Computer physics communications* 99.2 (1997): 335-354.

19. Sim, Eunji. "Quantum dynamics for a system coupled to slow baths: On-the-fly filtered propagator method." *The Journal of Chemical Physics* 115.10 (2001): 4450-4456.

20. Lambert, Roberto, and Nancy Makri. "Memory propagator matrix for long-time dissipative charge transfer dynamics." *Molecular Physics* 110.15-16 (2012): 1967-1975.

21. Frauenfelder, Hans, Stephen G. Sligar, and Peter G. Wolynes. "The energy landscapes and motions of proteins." *Science* 254.5038 (1991): 1598-1603.

22. Wolynes, Peter G. "Linearized microscopic theories of nonequilibrium solvation." *The Journal of chemical physics* 86.9 (1987): 5133-5136.

23. Makri, Nancy. "Improved Feynman propagators on a grid and non-adiabatic corrections within the path integral framework." *Chemical physics letters* 193.5 (1992): 435-445.

24. Ilk, Gregory, and Nancy Makri. "Real time path integral methods for a system coupled to an anharmonic bath." *The Journal of chemical physics* 101.8 (1994): 6708-6716.

25. Gerber, R. B., and Mark A. Ratner. "Self-consistent-field methods for vibrational excitations in polyatomic systems." *Advances in Chemical Physics, edited by I. Prigogine and SA Rice (Wiley, 1988)* 70 (2009): 97-132.

26. Billing, Gert D. "Classical path method in inelastic and reactive scattering." *International Reviews in Physical Chemistry* 13.2 (1994): 309-335.

27. Dirac, Paul AM. "Note on exchange phenomena in the Thomas atom." *Mathematical Proceedings of the Cambridge Philosophical Society*. Vol. 26. No. 03. Cambridge University Press, 1930.

28. Makri, Nancy, and William H. Miller. "Time-dependent self-consistent field (TDSCF) approximation for a reaction coordinate coupled to a harmonic bath: Single and multiple configuration treatments." *The Journal of chemical physics* 87.10 (1987): 5781-5787.

29. Wahnström, Göran, Benny Carmeli, and Horia Metiu. "The calculation of the thermal rate coefficient by a method combining classical and quantum mechanics." *The Journal of Chemical Physics* 88.4 (1988): 2478-2491.

30. Haug, Kenneth, and Horia Metiu. "A test of the possibility of calculating absorption spectra by mixed quantum-classical methods." *The Journal of chemical physics* 97.7 (1992): 4781-4791.

31. Leggett, Anthony J., et al. "Dynamics of the dissipative two-state system." *Reviews of Modern Physics* 59.1 (1987): 1.

32. Caldeira, Amir O., and Anthony J. Leggett. "Path integral approach to quantum Brownian motion." *Physica A: Statistical mechanics and its Applications* 121.3 (1983): 587-616.

33. Banerjee, T.; Makri, N.; Quantum-Classical Path Integral with Self-Consistent Solvent-Driven Reference Propagators. *The Journal of Physical Chemistry B* 117.42 (2013): 13357-13366.

Chapter 3. Quantifying Anharmonic Effects Using Ensemble Averaged Classical Path Treatment

3.1 Introduction:

Electron transfer reactions are very important in chemistry, biology and physics. These reactions are fundamental in many catalytic, environmental, solution phase, surface and interface phenomena [1-10]. Thus a detailed theoretical understanding of these reactions at the very molecular level is required. The first of the theoretical descriptions of electron transfer was introduced by Landau-Zener where the non-adiabatic electron transfer between the donor (D) and the acceptor (A) is treated by the Fermi's golden rule [11] and is related to the Franck-Condon factor, FC, that corresponds to the probability of approaching the curve-crossing region.

$$k_{LZ} = \frac{2\pi V^2 FC}{h}$$

The next improvement was made by Marcus, where the rate constants can be described using a small set of parameters quantified from the molecular – level interactions. According to Marcus's model [12-16], which is based on linear approximation theory, the energy distributions are given by identical Gaussians for the donor, acceptor and the uncharged species. Marcus's theory is also based on other approximations: the solvent modes are purely classical; the potential is essentially diabatic with very low diabatic-coupling terms, and the rates are obtained using second order perturbative treatments.

To move beyond Marcus's theory and even the linear approximation, we need to study full-atom simulations of solvent-solute interactions including charge and non-bonding interactions. To exemplify such comparisons, we chose one of the most studied electron transfer reactions. Electron transfer reactions in Fe^{+2} to Fe^{+3} has been studied in the theoretical community over the last few decades [17-21]. We have modeled such electron transfer reaction in its Metallocene framework. Ferrocene is atypical Metallocene complex with the cyclo-pentadienyl rings surrounding the ions on both sides. Ferrocene and its derivatives are widely used as a catalysts, anti-knocking agents and in pharamaceutical industries, among their various other applications. In fact, the electron transfer reaction between Ferrocene and Ferrocenium is so widely studied experimentally, that it is often used as a standard for calibrating reactions in non-aqueous solvents. We have considered the dynamics of such electron transfer reactions in one such solvent, Benzene, because of its high solubility in Benzene.

In the case of such reactions, the quantum mechanical description is restricted to only a few degrees of freedom, thus necessitating the use of mixed quantum-classical treatments. However, since quantum and classical treatments are inherently different, development of rigorous theories are quite challenging. The oldest of these treatments is the Ehrenfest model, [22] where the trajectories of the heavier, hence classical nuclei are subject to average forces from the quantum particles. Pechukas further used the idea of self-consistent determination of the classical trajectory, [23] which is quite rigorous and accurate, but very demanding for large-scale applications. Since the first proposal by Tully in 1970's a lot of surface-hopping techniques have been developed and used for multidimensional systems. [24-30]. However most of these treatments do not correctly account for the accurate interplay between classical and quantum decoherence. Recently, our group have reported rigorous, yet practical quantum-classical path integral techniques to provide a faithful dynamics of highly quantum systems [31-33]. In this chapter, we consider the Ensemble Averaged Classical treatment of this method, to quantify the effects of anharmonicity. By doing so we achieved the following: first, we systematically quantified the anharmonic effects and demonstrated its effect on the dynamics of the system; second, we did a quantitative check on accuracy of Marcus' theory. Using the Ensemble Averaged Classical Path treatment we have analyzed the differences in the dynamics of the same system in the explicit anharmonic bath or the mapped harmonic bath and have also commented on the accurate way of accounting for anharmonicity.

In section 3.2. we include correlation functions and spectral density calculations, while Section 3.3 discusses the energy gap components, and section 3.4. demonstrates their effect on dynamics. Section 3.5. compares rates obtained from different theories and finally we conclude in section 3.6.

3.2 Correlation Functions and Spectral Density Mapping:

The parameterization of the ferrocene - ferrocenium pair was obtained by Peter L. Walters [J. Phys. Chem. Lett. 2015, in press] using the CHARMM General Force Field (CGenFF). These calculations produced geometries in excellent agreement with experimental results [36]. The ferrocene - ferrocenium molecules were held fixed during the simulation with the Fe-Fe distance of 7.0 Å. The diabatic coupling of 32 cm^{-1} was adopted from Friesner et al.[37] We used three different charge configurations for the electron transfer complex: the donor, the acceptor and the mean, where the mean charge configuration is the average of the donor and acceptor configurations. It gives identical charges to both molecules, each having a total charge of 0.5.

Classical trajectories were obtained by Peter L. Walters using NAMD [34]. The simulation cell included a 10.0 Å thick benzene layer (i.e., 55 benzene molecules or 660 atoms). After energy minimization, an equilibration for 100 ps was performed in the NPT ensemble with a pressure of 1 atm and a temperature of

300K allowing the Benzene to move in the external forces from the electron transfer complex. Following equilibration, several different molecular dynamic runs were performed, to calculate the spectral density, and to obtain the EACP reference trajectory. To calculate the spectral density, the dynamics was run for 1.6 ns in the NPT ensemble with a pressure of 1 atm and a temperature of 300K. For the EACP reference trajectory, a 1 ns run was performed in the NVE ensemble. After the dynamics, the interaction energy between the Benzene and the electron transfer complex was calculated twice: once in the donor charge configuration, and again in the acceptor configuration. This is done for each snapshot of the atomic coordinates, captured from the dynamics.

The energy gaps are computed using NAMD, and subsequent analysis is done to provide insight on the system and draw conclusions for its dynamics. First we have mapped the energy gaps to a continuous bath of phonons. In order to do so, we obtained the donor-acceptor energy gap autocorrelation function computed by Peter L. Walters for classical trajectories calculating using NAMD. The expressions below are following the NAMD tutorial on the same.

$$C_{DA}(t) = \frac{1}{\sigma^2}\sum_j \left\langle E\left(x_j(0)\right)E\left(x_j(t)\right) - \overline{E^2}\right\rangle_\beta \tag{3.1}$$

Where the energies for the jth particle at time 0 and t are given by $E\left(x_j(0)\right), E\left(x_j(t)\right)$ respectively and σ is the variance of the energy gaps and is given by,

$$\sigma^2 = \frac{1}{N_t}\sum_{j=1}^{N_t}\left(E^2\left(x_j(t)\right) - \overline{E^2}\right) \tag{3.2}$$

To obtain smoother distribution, “window-averaging” technique is used.

$$C_{DA}(t) = \frac{1}{\sigma^2}\frac{1}{M}\sum_{\alpha=1}^{M}\left\langle E\left(x_j(t+t_\alpha)\right)E\left(x_j(t_\alpha)\right) - \overline{E^2}\right\rangle_\beta \tag{3.3}$$

To calculate the distributions and behavior in the harmonic model, one needs to map the energy gap autocorrelation function obtained from NAMD to the bath response function. The energy gap between the donor and acceptor states linearly coupled to the harmonic bath is given by the following fluctuation [38]

$$const + 2\sum_j c_j x_j(t) \tag{3.4}$$

Where the $x_j(t)$ are the classical trajectories computed using NAMD. The correlation function $C_{DA}(t)$ of the donor-acceptor energy gap function for the harmonic bath linearly coupled to the system is thus given by

$$C_{DA}(t) = 4\sum_j c_j^2 \left\langle x_j(0)\, x_j(t) \right\rangle_\beta^{cl} \tag{3.5}$$

The correlation function dies around 10 ps, which suggests that there is considerable memory in the bath till 10 ps, and hence non-Markovian treatments should be done till this time. Doing such treatments requires the calculation of non-local integrals and hence become very expensive. We can circumvent this problem, by noticing that most of this memory is due to low frequency modes of the bath. These frequency modes are quite accessible at the thermal temperature and are classical in nature. Owing to the classical nature of such memory, it is easily removed by incorporating it into the EACP propagators. We have calculated the correlation function mappings at different charge configurations of the system. In the first mapping scheme, we have used the donor charge configuration of the system, while in the second we have used the average surface mappings. This has been done to facilitate comparison of the two mapping schemes, their spectral densities, their energy gap characteristics, and effect on the EACP dynamics.

The computed correlation function can be expressed in terms of the bath response function which is given by

$$\alpha(t) = \frac{1}{\hbar}\sum_j c_j^2 \left\langle x_j(0)\, x_j(t) \right\rangle_\beta \tag{3.6}$$

Where the $x_j(t)$ is the position operator for the position variable for the jth oscillator and it is averaged at the inverse temperature β. Next, this response function can be mapped to the bath spectral density,

$$J(\omega) = \frac{\pi}{2}\sum_j \frac{c_j^2}{m_j \omega_j}\delta(\omega - \omega_j)$$

Using the relation,

$$\alpha(t) = \frac{1}{\pi}\int_0^\infty d\omega J(\omega)\left(\coth\left(\frac{1}{2}\hbar\omega\beta\right)\cos(\omega t) - i\sin(\omega t)\right) \tag{3.7}$$

To do so we take that the classical limit of the correlation function given by Eqn 3.5 by using the limit $\hbar \to 0$. The correlation function then reverts back to the following expression

$$C_{DA}(t) = \frac{8}{\pi\beta}\int_0^\infty d\omega \frac{J(\omega)}{\omega}\cos\omega t \tag{3.8}$$

Finally the spectral density was obtained by Peter L. Walters as the Fourier Integral of the spectral density and is given by

$$J(\omega) = \frac{\omega\beta}{4}\int_0^\infty dt C_{DA}(t)\cos\omega t \tag{3.9}$$

We find in this system, most of the reorganization energy is obtained from the classical frequencies. For practical purposes the memory can be considered classical, and additionally at such high temperatures, the EACP treatments should be a *very good estimate* of the dynamics of the system. Owing to the high reorganization, the quantum effects may become higher in the long-time dynamics but short time dynamics should be given very well by the EACP limit. Also, when the dynamics of the system is mostly done, a plateau behavior observed in the quantum mechanical system reactions should match exactly EACP limit. Thus the rate extracted from either of these limits should be a good estimate for the rates obtained for fully-converged quantum mechanical answers. For the higher frequency peaks in the spectral density, we refer to the IR- spectra of Benzene. The peaks around 700 cm^{-1} corresponds to the out of plane C-H bending, while those around 1250 cm^{-1}corresponds to the in plane C-H bending, and the peaks centered at 1500 cm^{-1} corresponds to C-C stretches in an aromatic ring. The contribution of all of these peaks combined account for less than a few percent of the reorganization energy.

3.3 Energy Gap Distributions and Anharmonic Components: Moving Beyond Linear Approximation Theory:

To construct the statistical distribution of energy gaps, we take the energy gaps obtained from the NAMD calculations for short runs. We take the sampled energy gaps after 2fs for each of the trajectories, and construct a statistical picture of the distribution, by making histograms and binning them at regular intervals. The curve obtained from the values of these histograms taken for 500 intervals over 10^9 energy gaps sampled is used to obtain smooth-gaussian like curves. The peak of the curves correspond to the reorganization energy and the variance of the curve corresponds to the variance of the correlation function used to map the spectral density.

The curves in Figure 1 correspond to two different mapping schemes and the atomistic simulation result. The mean of the donor-mapped distribution is significantly different from the mean of the atomistic simulation, while the neutral species have a much closer correspondence to the atomistic simulation. This is also evident from the curve-crossing regime shown in Figure 1b. This proves that for mapping to a spectral density the neutral species mapping should be much more accurate than the donor-mapped bath, and this will be proved in subsequent sections and discussions.

The most interesting feature of these curves is the curve-crossing regime. The curve crossing regime, i.e. the negative region of the distribution translates to the region where there is a change from the donor to the acceptor state or vice versa. This is a statistically insignificant portion of the distribution, and can be termed to be a "rare-event" owing to the high reorganization energy. Due to the high reorganization energy of the solvent, this region is minimally sampled and it results in very slow dynamics.

Beyond Linear Approximation:

To motivate this study, we observe that contrary to assumption, the mean and the variance of the neutral and the donor configurations are not equal. If linear approximation were to hold, this would not have been the case, which means there is larger energy gap fluctuations in case of donor state as compared to the neutral state. To move beyond the linear approximation theory, we have computed the third and the fourth order statistical corrections. Skewedness is a measure of asymmetry of the distribution and is quantified by deviation from the mean of the distribution, corresponding to the third standard moment. Kurtosis, on the other hand is the measure of the peakness and is the fourth standardized moment. Although, quite small, the values of skewedness and kurtosis are not negligible for this bath (Table 1)

3.4 Dynamics of Ferrocene - Ferrocenium System in Benzene:

We illustrate the ideas of section 3.2 and see how the anharmonicity in energy gap distributions discussed in the previous section affects the dynamics of the system. To make a quantitative evaluation of anharmonicty on the rates of the electron transfer reaction, we EACP methods described in Chapter 2 using both atomistic bath described by the classical MD trajectories and harmonic bath, which is mapped to the actual bath using the ideas discussed in Section 3.3

The Ferrocene-Ferrocenium system, is described by the Hamiltonian

$$H_0 = -\hbar\Omega\sigma_x\,, \tag{3.10}$$

is characterized by the tunneling splitting $2\hbar\Omega$, where $\Omega = 32cm^{-1}$ and is coupled to a dissipative bath. The bath may be described either using atomistic MD forces or in terms of harmonic oscillator modes linearly coupled to the system given by

$$H_{\mathrm{b}} = \sum_j \left(\frac{\hat{p}_j^2}{2m} + \frac{1}{2} m\omega_j^2 \hat{x}_j^2 \right), \quad V_{\mathrm{int}} = -\sigma_z \sum_j c_j \hat{x}_j\,. \tag{3.11}$$

where σ_x and σ_z are the standard 2×2 Pauli spin matrices. The bath frequencies and coupling coefficients are described collectively by the spectral density function

$$J(\omega) = \frac{\pi}{2}\sum_j \frac{c_j^2}{m_j\omega_j}\delta(\omega-\omega_j)\,. \tag{3.12}$$

The spectral density described in the previous section is dicretized using the procedure developed by Makri. [39]. In order to apply the EACP method, we approximate the bath by a sum of 200 harmonic oscillators whose frequencies and couplings are given by expressions above with a $\omega_{\max}$ of 2000 cm^{-1}.

In case of the atomistic simulations, the Hamiltonian of the bath is given by the kinetic energies of the atoms and different potential terms which consist of both harmonic (bond stretches, dihedrals, etc.) as well as anharmonic (van der Waal's forces, Coulombic forces etc.) In order to carry out calculations, the EACP propagators must be constructed from the shifted intial condition and donor shifted reference. In this case it is worthwhile to note that the instantaneous reference action that has to be included in the propagators is given by the time integrated energy gaps which are easily obtained from the MD calculations. Thus the time dependent Schrödinger Equation given in Eq 3.6 is solved using energy gaps that are updated at every 2fs, which is the time step for the classical MD calculations.

The calculations shown in Fig. 2 compare results obtained from two different mappings to obtain the spectral density and the atomistic simulations. The two different mappings arise from the energy distributions of the solvent that are equilibrated at the donor system configuration and from the energy distribution of the solvent equilibrated at the average system surface and then by shifting it by the reorganization energy λ. Although the dynamics obtained from the two different schemes of mapping are identical, but it is seen that the average system surface equilibrated solvent energy gap distribution provides a much better mapping of the atomistic simulations. This was first pointed out by Makri [38] in which she had obtained the linear response limit by performing a cumulant expansion of the influence functional, where she had done the expansion about the average surface, i.e. $s=0$. In the present context of the EACP method, this observation can be explained from a cumulant expansion of the system-bath interaction, in which the mapping to the average surface $\left(s^+=0; s^-=0\right)$ configuration of the system matches both the mean and the variance of the atomistic simulations, but, the mapping to the donor configuration of the system matches only the variance of the expansion. Although the two different mappings of the spectral density has been used interchangeably in literature, we have for the first time compared the accuracy of the two with the actual dynamics and commented on the exactness of one over the other.

3.5 Rates of the Electron Transfer Reaction:

In this section we compare the rates of electron transfer obtained from the EACP methods and that obtained from Fermi's Golden Rule and Marcus's rate equation. In the non-adiabatic limit, the electron transfer rate can be given by Fermi's Golden rule,

$$k = 2\Delta^2 \,\mathrm{Re}\int_0^\infty dt e^{i\varepsilon t} \exp\left[-\int_0^\infty d\omega \frac{4J(\omega)}{\pi\omega^2}\left[\coth\left(\tfrac{1}{2}\hbar\omega\beta\right)(1-\cos\omega t) - i\sin\omega t\right]\right] \tag{3.13}$$

If we assume the classical limit of the above expression, along with short time approximation we can obtain the well-known Marcus's rate equation

$$k = \frac{2\pi\Delta^2}{\sqrt{4\pi\lambda k_B T}} \exp\left[-\frac{(\varepsilon-\lambda)^2}{4\lambda k_B T}\right] \tag{3.14}$$

The table below shows the rates of the reaction and the time of half reaction for dynamics of the system coupled to the solvent of benzene treated both harmonically and atomistically and the rates obtained from 3.14

It can be clearly seen from Table 2. that the Average Surface mapping produces much more accurate results than the Donor Surface mapping. The differences between the atomistic and the average surface harmonic treatments show slight differences which suggest that the effects of anharmonicity is very low in this case, yet present, and drives the reaction a bit faster. The difference in the rates of the harmonic (mean mapped) to the anharmonic arises from the higher order terms present in the energy distribution, such as the skewedness and kurtosis. The major difference between the two different schemes of mapping comes from the difference in the mean of the energy gap distribution which is a major contributing factor in the rates. The shift in the mean of the energy gap affects the area under the curve crossing regime, which is responsible for the rates of the reaction. There is a considerable difference between the Marcus rate and the atomistic calculations, suggesting that the perturbative type treatments introduced to calculate the Marcus rate equation may not be fully adequate even in such low diabatic coupling case.

3.6 Concluding Remarks:

The concept of developing improved propagators, as described in the last chapter have been extended to study an electron transfer reaction in an atomistic bath by noticing that the energy gap can be obtained from the MD simulations directly. We have investigated the dynamics of an electron transfer reaction in the

widely studied iron complex. Electron transfer reactions of Ferrocene - Ferrocenium complex in non-polar solvent have been studied experimentally. In these calculations we had kept the diabatic coupling fixed, as a result of which the ferrocene - ferrocenium system was not allowed to move. The use of constrained DFT techniques have been utilized by many groups, especially with the work of van Voorhis should allow to remedy this shortcoming and can be investigated later. Though most of these experiments investigate the time scales of the dynamics of these reactions, it is very difficult to classify nature of interactions between the solute and the solvent experimentally and comment on how these interactions affect the dynamics of the reactions. In this chapter we have provided a theoretical description of its dynamics and have shed light to the nature of interaction between the electron transfer complex and the solvent and how it drives these reactions and affects the rates of the reactions. We have systematically classified the order of interactions, by analyzing the energy gap distributions and have commented on how the various ordered interactions makes the dynamics either slower or faster. By mapping the atomistic energy gap correlation function at different system charge configurations, to obtain the spectral density for a harmonic bath we have found the most accurate way of modeling the atomistic bath to a harmonic bath. The energy gap configuration mapped at the average charge distribution of the system produces a mean which is equal to the mean of the energy gap distribution of the atomistic calculation. As a result, the dynamics obtained from discretizing this spectral density is much closer to the dynamics of the atomistic bath. Finally we have also compared the Marcus's rate to those of the harmonic and the atomistic bath, making a note that although rates from bath with linear approximation match quite well with the atomistic bath, the rates from Marcus theory shows a considerable difference which can be attributed to the perturbative treatment of the dynamics.

3.7 Figures, Images, Flowcharts and Tables:

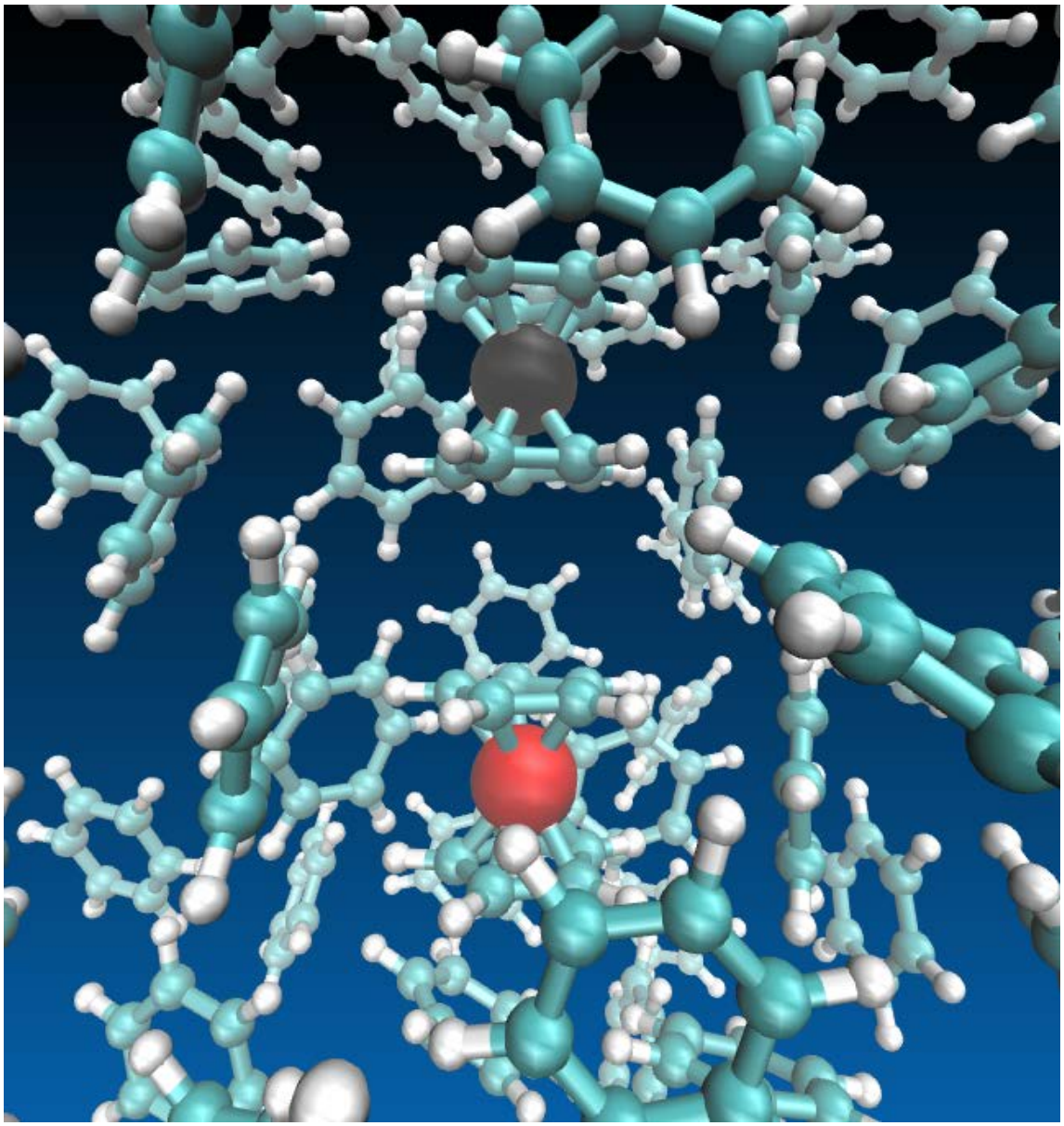

Image 3.1: Ferrocene - Ferrocenium complex in Benzene. The donor Ferrocene is shown in black while the acceptor Ferrocenium is shown in red. Carbon atoms are shown in Teal and Hydrogen in White.

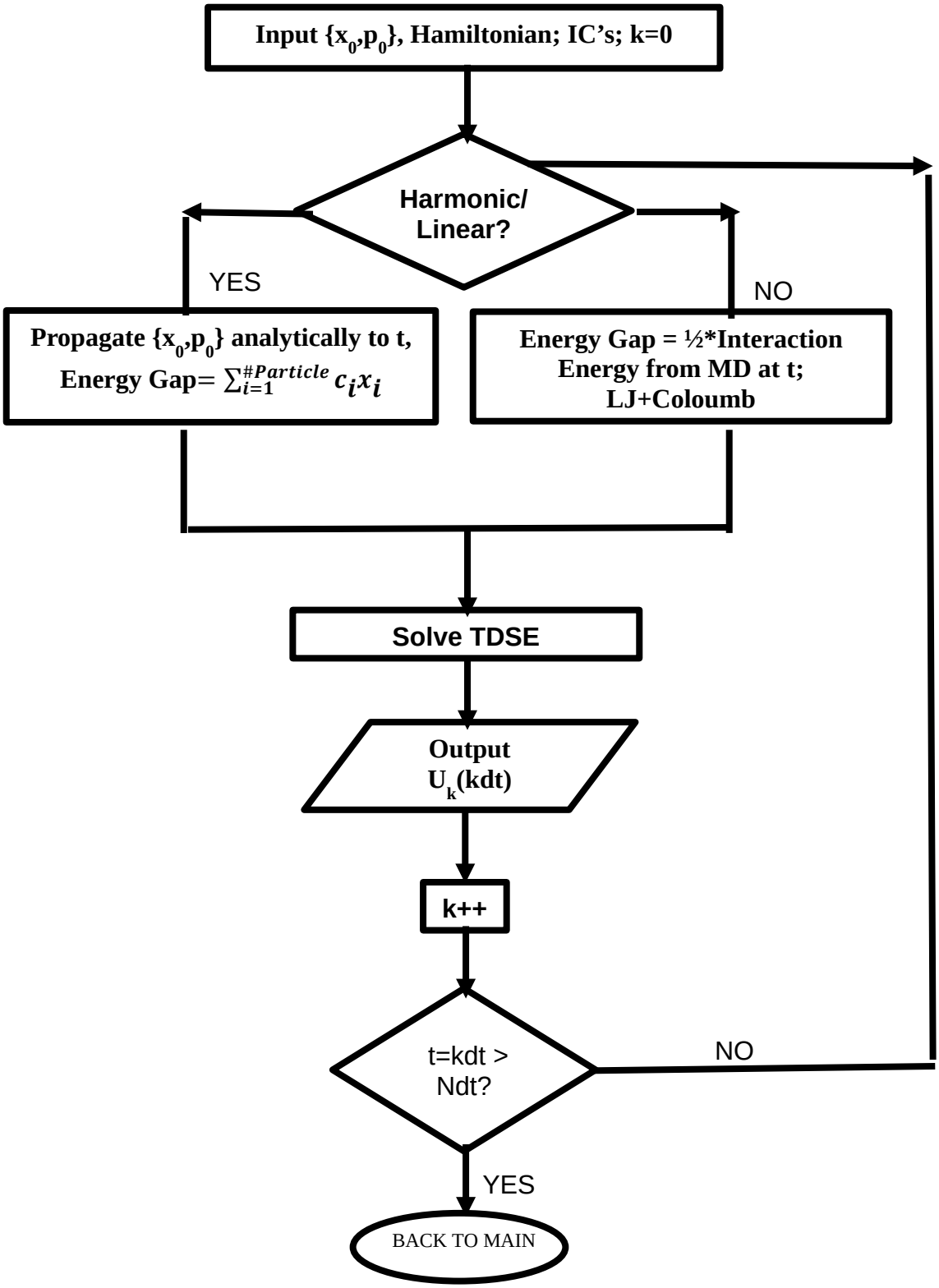

Flowchart 3.1: Construction of improved propagators depending on whether the bath is harmonic or atomistic. Depending on the nature of the bath, the energy gap that is provided as an input is different.

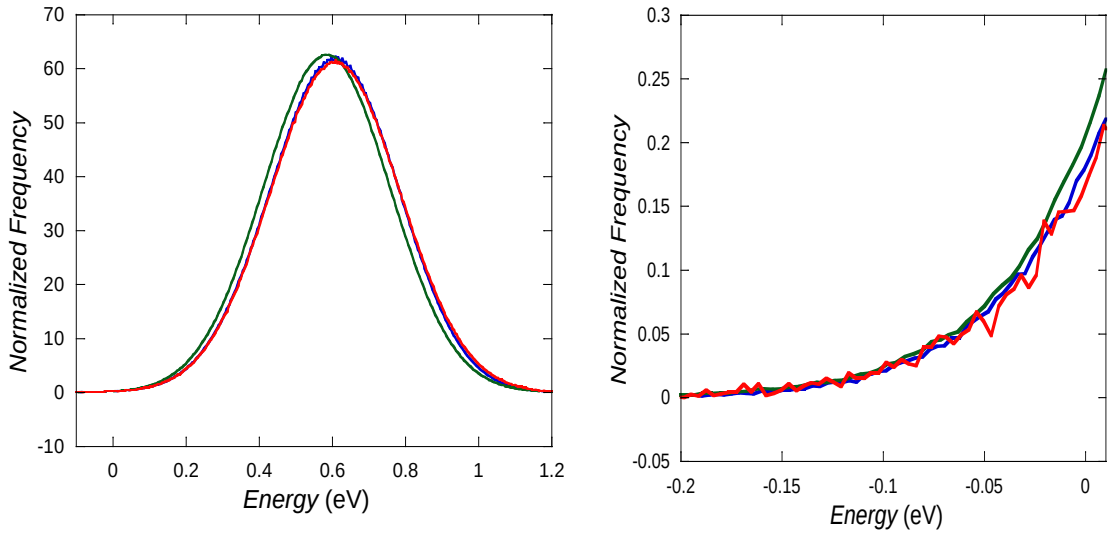

Figure 3.1: a) Energy gap distributions of Benzene experiencing forces from the donor and acceptor configurations obtained by binning 10^9 energy gap values over the entire energy range into 500 binned values. The red curve corresponds to those obtained from the harmonic bath mapped from the solvent experiencing forces from the neutral configurations of the system, green curve corresponds to the harmonic bath mapped from the solvent experiencing forces from the donor configurations of the system, and the blue curve is obtained from the atomistic simulations. b) The curve crossing regime of the same distribution highlighted to compare the area under the curves.

Curve	Mean (eV)	Variance (eV)	Skewness (eV)	Kurtosis (eV)
Harmonic Donor	0.58	1.1 E-03		
Atomistic	0.61	1.1 E-03	-9.51E-05	-0.65
Harmonic Average	0.61	1.1 E-03		

Table 3.1: Statistical quantities corresponding to the first, second, third, and fourth moments of the distribution plotted in Figure 4. The mean and the variance of the energy gap distributions obtained from spectral density mapped from the average/neutral surface map quite well to the atomistic simulation

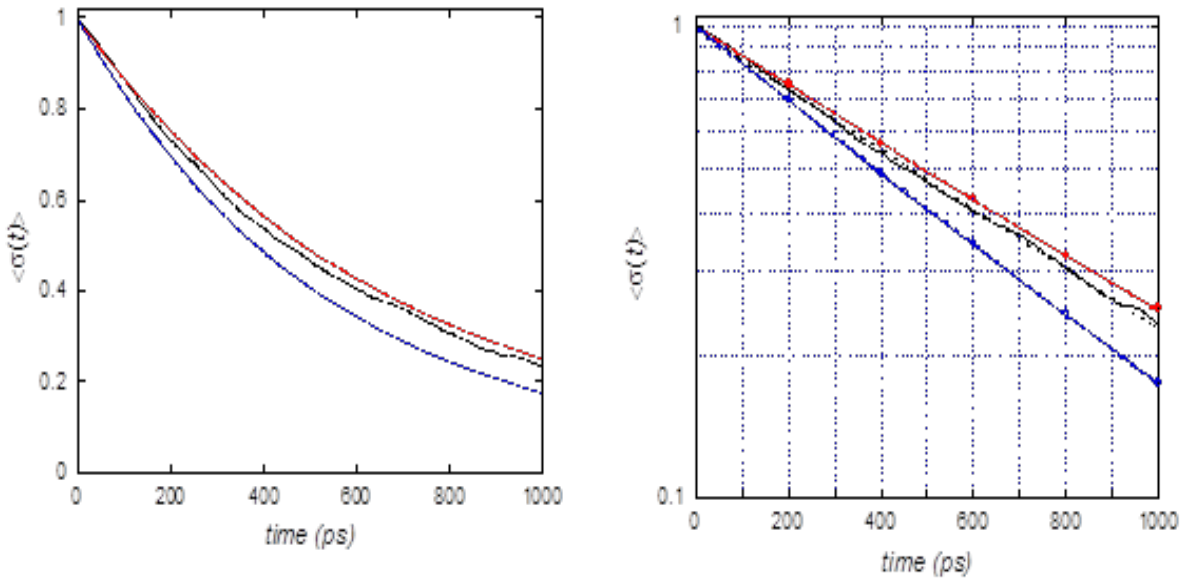

Figure 3.2 : Average position of the Ferrocene-Ferrocenium system mapped to a symmetric TLS. Black Curve - EACP treatment obtained from the atomistic simulations. Red Curve - EACP treatment obtained from the spectral density obtained after mapping the energy gap distribution of the solvent experiencing forces from the average system configuration to harmonic bath. Blue curve –- EACP dynamics obtained from the spectral density obtained after mapping the energy gap distribution of the solvent experiencing forces from the donor system configuration to harmonic bath. b) Log scaling to highlight the exponential nature of the dynamics

Treatment	Rate Constant (ps^{-1})	Half-time of reaction (ps)
Marcus	0.001	1010
Harmonic (Donor)	0.00085	1147
Atomistic	0.00073	1370
Harmonic(Neutral)	0.00070	1435

Table 3.2: Reaction rates obtained from the EACP curves shown in figure 6 along with the computed values from the Marcus theory. The rate constants predicted from the red and the black curves are 0.00070 and 0.00073 ps^{-1}, which suggests that the effects of anharmonicity is only slight in this case. While the Marcus rate constant obtained is 0.001 ps^{-1} which shows a 30% difference.

3.8 References:

1. Bixon, M.; Joshua J. *Electron transfer—from isolated molecules to biomolecules*. John Wiley & Sons, Inc., 2007.

2. D'Souza, F.; Osamu I. Photosensitized electron transfer processes of nanocarbons applicable to solar cells. *Chemical Society Reviews* 41.1 (2012): 86-96.

3. Hush, N. S.; Reimers, J. R. Solvent effects on metal to ligand charge transfer excitations. *Coordination chemistry reviews* 177.1 (1998): 37-60.

4. Astruc, D. Electron-transfer processes in dendrimers and their implication in biology, catalysis, sensing and nanotechnology. *Nature chemistry* 4.4 (2012): 255-267.

5. Zusman, L. D. "Outer-sphere electron transfer in polar solvents." *Chemical Physics* 49.2 (1980): 295-304.

6. Malvankar, N. S.; Lovley, D. R., Microbial nanowires: a new paradigm for biological electron transfer and bioelectronics. *ChemSusChem* 5.6 (2012): 1039-1046.

7. Gray, H. B.; Winkler, J. R. Long-range electron transfer. *Proceedings of the National Academy of Sciences of the United States of America* 102.10 (2005): 3534-3539.

8. Piotrowiak, P. *Electron transfer in chemistry*. Vol. 1. Weinheim, Germany: Wiley-VCH, 2001.

9. Launay, J-P. Long-distance intervalence electron transfer. *Chemical Society Reviews* 30.6 (2001): 386-397.

10. Piotrowiak, P. *Electron transfer in chemistry*. Vol. 1. Weinheim, Germany: Wiley-VCH, 2001.

11. Fermi, E. (1950) Nuclear Physics, University of Chicago Press, Chicago.

12. Marcus, R. A; Sutin, N. Electron transfers in chemistry and biology. *Biochimica et Biophysica Acta (BBA)-Reviews on Bioenergetics* 811.3 (1985): 265-322.

13. Marcus, R. A.; On the theory of oxidation-reduction reactions involving electron transfer. I. *The Journal of Chemical Physics* 24.5 (1956): 966-978.

14. Marcus, R. A. Electron transfer past and future. *Advances in Chemical Physics: Electron Transfer-from Isolated Molecules to Biomolecules. Part 1, Volume 106* (1999): 1-6.

15. Marcus, R. A.; Electron transfer reactions in chemistry. Theory and experiment. *Reviews of Modern Physics* 65.3 (1993): 599.

16. Sumi, H.; R. A. Marcus. Dynamical effects in electron transfer reactions. *The Journal of chemical physics* 84.9 (1986): 4894-4914.

17. Chidsey, Christopher ED. Free energy and temperature dependence of electron transfer at the metal-electrolyte interface. *Science* 251.4996 (1991): 919-922

18. Lovley, D. R., and Blunt-Harris., E. L. Role of humic-bound iron as an electron transfer agent in dissimilatory Fe (III) reduction. *Applied and environmental microbiology* 65.9 (1999): 4252-4254.

19. Saji, T.; Yamada, T. ; Aoyagui. S. "Electron-transfer rate constants for redox systems of Fe (III)/Fe (II) complexes with 2, 2′-bipyridine and/or cyanide ion as measured by the galvanostatic double pulse method." *Journal of Electroanalytical Chemistry and Interfacial Electrochemistry* 61.2 (1975): 147-153.

20. Escax, V. "Photoinduced Ferrimagnetic Systems in Prussian Blue Analogues CI x Co4 [Fe (CN) 6] y (CI= Alkali Cation). 3. Control of the Photo-and Thermally Induced Electron Transfer by the [Fe (CN) 6] Vacancies in Cesium Derivatives." *Journal of the American Chemical Society* 123.50 (2001): 12536-12543.

21. Brunschwig, B. S. "A semiclassical treatment of electron-exchange reactions. Application to the hexaaquoiron (II)-hexaaquoiron (III) system." *Journal of the American Chemical Society* 102.18 (1980): 5798-5809.

22. Ehrenfest, P. Bemerkung über die angenäherte Gültigkeit der klassischen Mechanik innerhalb der Quantenmechanik.

Zeitschrift für Physik A Hadrons and Nuclei, 1927. 45(7): p. 455-457.

23. Pechukas, P. Time-Dependent Semiclassical Scattering Theory. I. Potential Scattering. Physical Review, 1969. 181(1): p. 166-174.

24. Tully, J.C. Molecular dynamics with electronic transitions. The Journal of Chemical Physics, 1990. 93(2): p. 1061-1071.

25. Tully, J.C. ; R.K. Preston, Trajectory Surface Hopping Approach to Nonadiabatic Molecular Collisions: The Reaction of H+ with D2. The Journal of Chemical Physics, 1971. 55(2): p. 562-572.

26. Hammes-Schiffer, S.; J.C. Tully, Proton transfer in solution: Molecular dynamics with quantum transitions. The Journal of Chemical Physics, 1994. 101(6): p. 4657-4667.

27. Hammes-Schiffer, S. Theory of Proton-Coupled Electron Transfer in Energy Conversion Processes. Accounts of Chemical Research, 2009. 42(12): p. 1881- 1889.

28. Coker, D.F.; L. Xiao, Methods for molecular dynamics with nonadiabatic transitions. The Journal of Chemical Physics, 1995. 102(1): p. 496-510.

29. Prezhdo, O.V.; P.J. Rossky, Mean-field molecular dynamics with surface hopping. The Journal of Chemical Physics, 1997. 107(3): p. 825-834.

30. Craig, Colleen F.; Walter R. Duncan; O. V. Prezhdo. "Trajectory surface hopping in the time-dependent Kohn-Sham approach for electron-nuclear dynamics." *Physical review letters* 95.16 (2005): 163001.

31. Lambert, R.; Makri, N. Quantum-Classical Path Integral: Classical Memory and Weak Quantum Nonlocality. The Journal of Chemical Physics, 2012, 137, 22A552

32. Lambert, R.; Makri, N. Quantum-Classical Path Integral: Numerical Formulation. The Journal of Chemical Physics, 2012, 137, 22A553

33. Banerjee, T.; Makri, N.; Quantum-Classical Path Integral with Self-Consistent Solvent-Driven Reference Propagators. *The Journal of Physical Chemistry B* 117.42 (2013): 13357-13366.

34. Phillips, J. C.; Braun, R.; Wang, W.; Gumbart, J.; Tajkhorshid, E.; Villa, E.; Chipot, C.; Skeel, R. D.; Kale, L; Schulten, K.; "Scalable molecular dynamics with NAMD." *Journal of computational chemistry* 26, no. 16 (2005): 1781-1802.

35. Vanommeslaeghe, K; Hatcher, E.; Acharya, C; Kundu, S.; Zhong, S; Shim, J; Darian, E; CHARMM general force field: A force field for drug-like molecules compatible with the CHARMM all-atom additive biological force fields. *Journal of computational chemistry* 31, 4 (2010): 671-690.

36. Seiler, P.; J. D. Dunitz. Low-temperature crystallization of orthorhombic ferrocene: structure analysis at 98 K. *Acta Crystallographica Section B: Structural Crystallography and Crystal Chemistry* 38.6 (1982): 1741-1745.

37. Baik, Mu-Hyun, Joseph B. Crystal, and Richard A. Friesner. Ab Initio Quantum Calculation of the Diabatic Coupling Matrix Elements for the Self-Exchange Redox Couples M (Cp) 20/+ (M= Fe, Co; Cp= C5H5). *Inorganic chemistry* 41.23 (2002): 5926-5927.

38. Sim, Eunji, and Nancy Makri. "Path integral simulation of charge transfer dynamics in photosynthetic reaction centers." The Journal of Physical Chemistry B 101.27 (1997): 5446-5458.

39. Makri, N. The linear response approximation and its lowest order corrections: An influence functional approach. *The Journal of Physical Chemistry B* 103.15 (1999): 2823-2829

Chapter 4. Path Integral Calculations for a System Interacting with a Shifted Dissipative Bath

4.1 Introduction:

Sections 4.1 to 4.3 is based on [Walters, Peter L., Tuseeta Banerjee, and Nancy Makri. "On iterative path integral calculations for a system interacting with a shifted dissipative bath." The Journal of chemical physics 143.7 (2015): 074112.]

The Quasi Adiabatic Path Integral methodology (QuAPI) as the name suggests is a path integral formulation to represent the dynamical quantity of the system, i.e. the reduced density matrix in terms of the localized system states [3]. The spin boson problem [4, 5, 6, 7] in its common treatments, presume that the bath and the system are isolated, and the initial conditions are factorizable. However, this is not a physical picture especially in following the dynamics of a chemically reacting species, where the system is initially prepared in one of the localized state (say the “donor” state) and the dissipative environment is in equilibrium with this state of the system. We will later see in this chapter, that this requires a change of the influence functional [7] coefficients employed in the QuAPI methodology.

In this chapter we will focus on two completely equivalent procedures for achieving the above mentioned aim of equilibrating the Gaussian bath with the localized or the more conveniently called donor state of the system. The first way [8] to achieve this goal would be to shift the bath, this results in evaluation of a phase term, which like other influence functional coefficients is computed in terms of spectral density, but unlike other influence functional coefficients, it is local in time. The second way to approach (which has been proposed earlier in our group [9]) the same would consist of shifting the system states to bring the initial or the donor state to equilibrate with the unshifted bath at the curve crossing region. Fortunately, this approach requires no changes in the influence functional coefficients.

In section 4.2 we derive the influence functional for a shifted bath and in section 4.3. we draw some conclusions.

4.2 Influence Functional for Bath Initially in Equilibrium with Donor:

A general Hamiltonian in continuous coordinates can be represented in terms of the localized discrete states $|\sigma_n\rangle$, or a Discrete Variable Representation, DVR [9,10]. This can be done if the system position operator [8] is represented in the DVR basis, using the following relation

$$\hat{s} = \sum_{n=1}^{M} \sigma_n |\sigma_n\rangle\langle\sigma_n| \tag{4.1}$$

Once we have constructed the DVR basis, the system Hamiltonian can be represented in this basis,

$$\hat{H}_0 = \sum_{n,m}^{M} h_{nm} |\sigma_n\rangle\langle\sigma_m|, \tag{4.2}$$

The next set of components of the QuAPI Hamiltonian comes from the system described above interacting with harmonic oscillators via a coupling in the system-bath coordinates in a bilinear fashion. The total bath and the interaction can be represented using the following expression,

$$\hat{H}_{\text{sb}} = \sum_j \frac{p_j^2}{2m_j} + \frac{1}{2} m_j \omega_j^2 \left(x_j - \frac{c_j \hat{s}}{m_j \omega_j^2} \right)^2. \tag{4.3}$$

The nature of the bath of harmonic oscillators that would have a effect on the dynamics of the system has to now be defined using some function, commonly known as the spectral density function given by,

$$J(\omega) \equiv \frac{\pi}{2} \sum_j \frac{c_j^2}{m_j \omega_j} \delta(\omega - \omega_j). \tag{4.4}$$

Since we are interested in the dynamics of the system, we will consider only the reduced density matrix of the system, $\tilde{\rho}$. This is obtained by integrating out the degrees of freedom (or tracing out the degrees of freedom of the bath), when all the influence of the bath enter via the function F. The reduced density matrix is given by,

$$\begin{aligned} \langle s_N^+ | \tilde{\rho}(N\Delta t) | s_N^- \rangle = \sum_{s_0^\pm} \sum_{s_1^\pm} \cdots \sum_{s_{N-1}^\pm} & \langle s_N^+ | e^{-i\hat{H}_0 \Delta t/\hbar} | s_{N-1}^+ \rangle \cdots \langle s_1^+ | e^{-i\hat{H}_0 \Delta t/\hbar} | s_0^+ \rangle \\ & \times \langle s_0^+ | \tilde{\rho}(0) | s_0^- \rangle \langle s_0^- | e^{i\hat{H}_0 \Delta t/\hbar} | s_1^- \rangle \cdots \langle s_{N-1}^- | e^{i\hat{H}_0 \Delta t/\hbar} | s_N^- \rangle \\ & \times F(s_0^+, s_1^+, \cdots s_N^+, s_0^-, s_1^-, \cdots s_N^-; \Delta t) \end{aligned} \tag{4.5}$$

where *F* is the DVR state discretized version of the Feynman-Vernon influence functional. Here we insist that in literature it is conveniently assumed that the bath is initially in equilibrium with the system and thus the bath is factorizable and hence the initial density matrix is given by $e^{-\beta H_b}/\text{Tr}\, e^{-\beta H_b}$ with

$$H_b = \sum_j \left(\frac{p_j^2}{2m_j} + \frac{1}{2} m_j \omega_j^2 x_j^2 \right) \tag{4.6}$$

With this factorizable initial condition, the influence functional is given by the expression

$$F = \exp\left(-\frac{1}{\hbar}\int_0^t dt' \int_0^{t'} dt'' \left(s^+(t') - s^-(t') \right) \left(\alpha(t'-t'') s^+(t'') - \alpha^*(t'-t'') s^-(t'') \right) \right) \times \exp\left(-\frac{i}{\hbar}\int_0^t dt' \sum_j \frac{c_j^2}{2m_j\omega_j^2} \left(s^+(t')^2 - s^-(t')^2 \right) \right) \tag{4.7}$$

where

$$\alpha(t'-t'') = \sum_j \frac{c_j^2}{2m_j\omega_j} \left(\coth\left(\tfrac{1}{2}\hbar\omega_j\beta \right) \cos\omega_j(t'-t'') - i\sin\omega_j(t'-t'') \right) \tag{4.8}$$

is the response function of the bath. The last exponential in Eq. (4.7) arises from the counterterms [4] included in the system-bath Hamiltonian while completing the square term in the QuAPI expressions. Rewriting Eq. (4.7) in terms of the sum and difference coordinates we can obtain,

$$F = \exp\left(-\frac{1}{\hbar}\int_0^t dt' \int_0^{t'} dt'' \Delta s(t') \left(\mathrm{Re}\,\alpha(t'-t'') \Delta s(t'') + 2i\,\mathrm{Im}\,\alpha(t'-t'') \bar{s}(t'') \right) \right) \times \exp\left(-\frac{i}{\hbar}\int_0^t dt' \sum_j \frac{c_j^2}{m_j\omega_j^2} \Delta s(t') \bar{s}(t') \right) \tag{4.9}$$

where $\Delta s = s^+ - s^-$ and $\bar{s} = \frac{1}{2}(s^+ + s^-)$. Now to minimize the Trotter splitting error, we can factorize the QuAPI propagators, as half step, full step in the middle of propagation and finally ending by half step. so that the error is given as $(\Delta t)^3$. Using this prescription. the system path coordinates are specified by

$$s^{\pm}(t') = \begin{cases} s_0^{\pm}, & 0 \le t' < \frac{1}{2}\Delta t \\ s_k^{\pm}, & (k-\frac{1}{2})\Delta t \le t' < (k+\frac{1}{2})\Delta t \\ s_N^{\pm}, & (N-\frac{1}{2})\Delta t \le t' < N\Delta t \end{cases} \tag{4.10}$$

the influence functional takes the form

$$F = \exp\left(-\frac{1}{\hbar}\sum_{k'=0}^{N}\sum_{k''=0}^{k'} (s_{k'}^+ - s_{k'}^-)(\eta_{k'k''} s_{k''}^+ - \eta_{k'k''}^* s_{k''}^-) \right) = \exp\left[-\frac{1}{\hbar}\sum_{k'=0}^{N}\sum_{k''=0}^{k'} \left(\mathrm{Re}\,\eta_{k'k''} \Delta s_{k'} \Delta s_{k''} + 2i\,\mathrm{Im}\,\eta_{k'k''} \Delta s_{k'} \bar{s}_{k''} \right) \right] \tag{4.11}$$

where the coefficients $\eta_{k'k''}$ have been given in several earlier publications. [13, 14]

However, in chemical reactions, one should take into account that the bath should be in equilibrium with the initially localized state, in common terms, the "donor" state of the system. When the time scale of relaxation of the bath is much faster than the time scale of the electron transfer or the proton transfer process, it really does not matter where the equilibration takes place and can very well be on the curve crossing region, as seen in previous expressions and can be represented by the first figure i.e. 1a) . However, if the

time scale of the relaxation of the bath is much slower than that of the system, then the necessity of the equilibration becomes very pressing and we should think about the two methods of shifting we had introduced before. This two arrangements come either by shifting the coordinates of the bath or the system as shown in Figure 1b) and 1c)

There can be different ways of deriving the influence functional coefficients for a shifted bath. We have used the same analysis in the context of deriving QCPI expressions [15-17] "where the influence functional from a complex polyatomic environment is obtained in terms of classical trajectories within a forward-backward semiclassical [18,19] or quasiclassical [20] approximation". The starting point of the linearized version of QCPI is the equivalence of influence functional given in terms of the phase space integral of the following,

$$F = \prod_j \int dx_{j,0} \int dp_{j,0} W_j(x_{j,0}, p_{j,0}) e^{i\Phi_j(x_{j,0}, p_{j,0})/\hbar} \quad , \tag{4.12}$$

Here Φ_j is the linearized [23] classical action of the solvent trajectory which feels the system force given by the mean of the instantaneous forward and backward system paths. Here W_j is the Wigner function [21] of the initial bath distribution. In case of a harmonic bath (here let us note that QCPI is not restricted to harmonic bath, but to draw the equivalence with Feynman Vernon the harmonic nature of the bath needs to be considered.) the action is given by

$$\begin{aligned} \Phi_j = \sum_j \Bigg[& c_j x_{j,0} \int_0^t \Delta s(t') \cos\omega_j t' dt' + c_j \frac{p_{j,0}}{m_j \omega_j} \int_0^t \Delta s(t') \sin\omega_j t' dt' \\ & + \frac{c_j^2}{2 m_j \omega_j} \int_0^t dt' \int_0^{t'} dt'' \Delta s(t') \left[s^+(t'') + s^-(t'') \right] \sin\omega_j (t' - t'') \\ & - \frac{c_j^2}{2 m_j \omega_j^2} \int_0^t \left(s^+(t')^2 - s^-(t')^2 \right) dt' \Bigg] \end{aligned} \quad . \tag{4.13}$$

The Wigner function is given by the expression

$$W_j(x_{j,0}, p_{j,0}) = (\hbar\pi)^{-1} \tanh\left(\tfrac{1}{2}\hbar\omega_j\beta\right) e^{-\tanh\left(\frac{1}{2}\hbar\omega_j\beta\right)\left(m_j\omega_j x_{j,0}^2/\hbar + p_j^2/m_j\omega_j\hbar\right)} \tag{4.14}$$

Using expression 4.13 and 4.14 in Eq. (4.12), leads to the exact Feynman-Vernon influence functional.

Now let us consider that the system is just given by 2 states, that is ($M = 2$) "right" and "left" states, denoted $|R\rangle$ and $|L\rangle$, respectively. The resulting Two Level System, TLS Hamiltonian has the form

$$\hat{H}_0 = -\hbar\Omega\left(|R\rangle\langle L| + |L\rangle\langle R|\right) + \varepsilon\left(|R\rangle\langle R| - |L\rangle\langle L|\right) = -\hbar\Omega\sigma_x + \varepsilon\sigma_z \tag{4.15}$$

where $-\hbar\Omega$ is the coupling (tunneling) matrix element, the left-right energy difference is 2ε (which introduces asymmetry), and σ_x, σ_z are the usual Pauli spin matrices.

(a) *Influence functional for shifted bath*

Now we can consider that the system position operator is given by, $\hat{s}=\sigma_z$, i.e., with $\sigma_{1,2}=\pm 1$ in Eq. (2.2). The bath can be shifted to be in equilibrium with the system donor state, but shifting the minima of the harmonic parabola, and now the bath is defined by,

$$\hat{H}_{\rm b}=\sum_j \frac{p_j^2}{2m_j}+\frac{1}{2}m_j\omega_j^2\left(x_j-\frac{c_j}{m_j\omega_j^2}\right)^2. \tag{4.16}$$

An relatively easy way to approach the problem is to think that there is a substitution given by the following,

$$x_{j,0}\to x_{j,0}-\lambda_j,\quad \lambda_j=\frac{c_j}{m_j\omega_j^2}. \tag{4.17}$$

Since there is no change in the forces experience by the classical particle, there is no change in the trajectories or the action. Just the initial condition is different. Next we can take the easy way of deriving by just using the above substitution and making $y_{j,0}=x_{j,0}-\lambda_j$, Thus the influence functional for this shifted initial condition is given by

$$\begin{aligned} F_{\rm shifted} &= \prod_j \int dy_{j,0}\int dp_{j,0}\,W_j(y_{j,0},p_{j,0})e^{i\Phi_j(y_{j,0}+\lambda_j,p_{j,0})/\hbar} \\ &= F\exp\left(\frac{i}{\hbar}\sum_j\frac{c_j^2}{m_j\omega_j^2}\int_0^t \Delta s(t')\cos\omega_j t'dt'\right). \end{aligned} \tag{4.18}$$

Using the condition, $\hat{s}=\sigma_z$, the last term in Equations (4.7) becomes 0 as, $\sigma_1^2=\sigma_2^2=1$, and Eq. (4.18) will become

$$\begin{aligned} F_{\rm shifted} &= \exp\left(-\frac{1}{\hbar}\int_0^t dt'\int_0^{t'}dt''\left(s^+(t')-s^-(t')\right)\left(\alpha(t'-t'')s^+(t'')-\alpha^*(t'-t'')s^-(t'')\right)\right) \\ &\times\exp\left(\frac{i}{\hbar}\sum_j\frac{c_j^2}{m_j\omega_j^2}\int_0^t\Delta s(t')\cos\omega_j t'dt'\right) \end{aligned} \tag{4.19}$$

Now that we have arrived at the expression for the shifted influence functional we need to express it in terms of spectral density in order to derive the influence functional coefficients,

$$\begin{aligned} F_{\rm shifted} &= \exp\left(-\frac{1}{\hbar}\int_0^t dt'\int_0^{t'}dt''\left(s^+(t')-s^-(t')\right)\left(\alpha(t'-t'')s^+(t'')-\alpha^*(t'-t'')s^-(t'')\right)\right) \\ &\times\exp\left(\frac{2i}{\pi\hbar}\int d\omega\frac{J(\omega)}{\omega}\int_0^t\Delta s(t')\cos\omega t'dt'\right) \end{aligned}. \tag{4.20}$$

Eq. (4.20) is the result obtained in Ref [8]

Next step would be to derive the discretized version of Eq. (2.19), for which the time is discretized into N segments, $t = N\Delta t$ and each is calculated within each constant system coordinate. If we consider the QuAPI propagator splitting we get the time integral of the following term and is expressed as following

$$\begin{aligned}\int_0^t \Delta s(t')\cos\omega t'dt' = \Delta s_0\int_0^{\frac{1}{2}\Delta t}\cos\omega t'dt' + \Delta s_1\int_{\frac{1}{2}\Delta t}^{\frac{3}{2}\Delta t}\cos\omega t'dt' + \cdots \\ +\Delta s_{N-1}\int_{(N-\frac{3}{2})\Delta t}^{(N-\frac{1}{2})\Delta t}\cos\omega t'dt' + \Delta s_N\int_{(N-\frac{1}{2})\Delta t}^{N\Delta t}\cos\omega t'dt'\end{aligned} \tag{4.21}$$

These integrals are quite simple and can be evaluated analytically to give the new eta coefficients,

$$F_{\text{shifted}}\left(s_0^{\pm}, s_1^{\pm}, \ldots, s_N^{\pm}\right) = \exp\left(-\frac{1}{\hbar}\sum_{k'=0}^{N}\sum_{k''=0}^{k'}(s_{k'}^{+} - s_{k'}^{-})(\eta_{k'k''}s_{k''}^{+} - \eta_{k'k''}^{*}s_{k''}^{-}) + \frac{i}{\hbar}\sum_{k=0}^{N}\gamma_k\Delta s_k\right) \tag{4.22}$$

where the new coefficients are given by the expressions

$$\begin{aligned}\gamma_0 &= \frac{2}{\pi}\int_0^{\infty}\frac{J(\omega)}{\omega^2}\sin(\tfrac{1}{2}\omega\Delta t)\,d\omega \\ \gamma_k &= \frac{2}{\pi}\int_0^{\infty}\frac{J(\omega)}{\omega^2}\left[\sin\left((k+\tfrac{1}{2})\omega\Delta t\right) - \sin\left((k-\tfrac{1}{2})\omega\Delta t\right)\right]d\omega, \quad 0 < k < N \\ \gamma_N &= \frac{2}{\pi}\int_0^{\infty}\frac{J(\omega)}{\omega^2}\left[\sin\left(\omega N\Delta t\right) - \sin\left((N-\tfrac{1}{2})\omega\Delta t\right)\right]d\omega\end{aligned} \tag{4.23}$$

Similar treatments to derive discretized coefficients have been reported in literature [8] but they do not employ QuAPI discretization and hence they are different. Thus, the bath can be easily shifted to the initialized system state, by a small modification in the influence functional coefficients given by (4.22) and (4.23) [24]

(b) Shifting the system Hamiltonian

The other way [11] of achieving the equilibrium between the initial system state and the bath is to shift the states of the system and bring it to the unshifted bath at the origin as shown in Figure 1c. This means the coordinate of the system now become, $\sigma_1 = 0, \sigma_2 = -2$, i.e., setting $\hat{s} = \tilde{\sigma}_z$, where

$$\tilde{\sigma}_z = \begin{pmatrix} 0 & 0 \\ 0 & -2 \end{pmatrix}. \tag{4.24}$$

It has been shown that within the full path integral framework the two approaches of shifting the bath and the system gives us exact analytical results. [24]

4.3 Concluding Remarks:

"Modeling condensed phase environments via a harmonic bath coupled to the system of interest is a common approach that allows numerically exact calculation of dynamical properties. In many such situations, the bath is initially in equilibrium with a localized state of the system, such as the state of the electron donor in the case of charge transfer. We have discussed two straightforward procedures for generalizing the QuAPI methodology to these shifted bath situations. The first approach involves an additional phase, which augments the action (or propagators) of the system, and which is given in terms of time integrals of the spectral density, or, equivalently, in terms of the coefficients that enter the standard influence functional. The second approach consists of shifting the coordinate of the system, to bring the donor state in equilibrium with the unshifted bath. This latter approach requires no additional phase factors."

4.4 Figures:

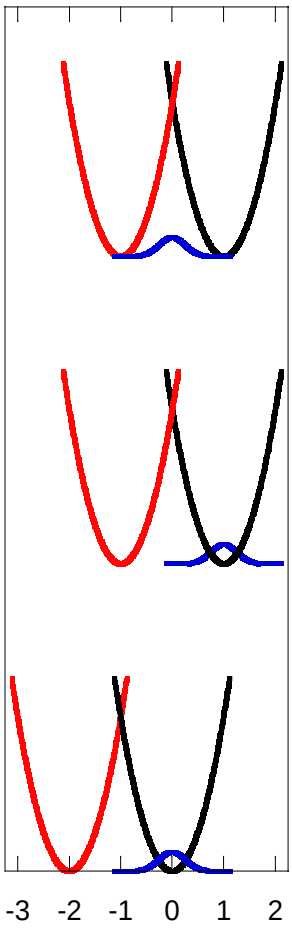

Figure. 4.1: Schematic representation adapted from Ref [24] of the bath potential and the initial state in the case of a TLS. donor potential curve in black, the acceptor potential in red and the bath distribution in blue (a) TLS coordinates set to ± 1 and bath undisplaced. (b) TLS coordinates set to $\pm \mathbf{1}$ and bath in equilibrium with TLS right (donor) state. (c) TLS coordinates set to $-2, 0$ and bath undisplaced, yet in equilibrium with TLS right (donor) state

4.5 References:

1. Feynman, Richard Phillips. "Space-time approach to non-relativistic quantum mechanics." *Reviews of Modern Physics* 20.2 (1948): 367.

2. R. P. Feynman and A. R. Hibbs, *Quantum Mechanics and Path Integrals*. (McGraw-Hill, New York, 1965).

3. Topaler, Maria, and Nancy Makri. "System-specific discrete variable representations for path integral calculations with quasi-

adiabatic propagators." *Chemical physics letters* 210.4 (1993): 448-457.

4. Leggett, Anthony J., et al. "Dynamics of the dissipative two-state system." *Reviews of Modern Physics* 59.1 (1987): 1.

5. Caldeira, Amir O., and Anthony J. Leggett. "Path integral approach to quantum Brownian motion." *Physica A: Statistical mechanics and its Applications* 121.3 (1983): 587-616.

6. U. Weiss, *Quantum Dissipative Systems*. (World Scientific, Singapore, 1993).

7. Feynman, Richard Phillips, and Frank Lee Vernon. "The theory of a general quantum system interacting with a linear dissipative system." *Annals of physics* 24 (1963): 118-173.

8. Nalbach, P., and M. Thorwart. "Ultraslow quantum dynamics in a sub-Ohmic heat bath." *Physical Review B* 81.5 (2010): 054308.

9. Lill, J. V., G. A. Parker, and J. C. Light. "Discrete variable representations and sudden models in quantum scattering theory." *Chemical Physics Letters* 89.6 (1982): 483-489.

10. Light, J. C., I. P. Hamilton, and J. V. Lill. "Generalized discrete variable approximation in quantum mechanics." *The Journal of chemical physics* 82.3 (1985): 1400-1409.

11. Sim, Eunji, and Nancy Makri. "Path integral simulation of charge transfer dynamics in photosynthetic reaction centers." *The Journal of Physical Chemistry B* 101.27 (1997): 5446-5458.

12. Makri, Nancy. "Improved Feynman propagators on a grid and non-adiabatic corrections within the path integral framework." *Chemical physics letters* 193.5 (1992): 435-445.

13. Makri, Nancy, and Dmitrii E. Makarov. "Tensor propagator for iterative quantum time evolution of reduced density matrices. I. Theory." *The Journal of chemical physics* 102.11 (1995): 4600-4610.

14. Makri, Nancy, and Dmitrii E. Makarov. "Tensor propagator for iterative quantum time evolution of reduced density matrices. II. Numerical methodology." *The Journal of chemical physics* 102.11 (1995): 4611-4618.

15. Lambert, Roberto, and Nancy Makri. "Quantum-classical path integral. I. Classical memory and weak quantum nonlocality." *The Journal of chemical physics* 137.22 (2012): 22A552.

16. Lambert, Roberto, and Nancy Makri. "Quantum-classical path integral. II. Numerical methodology." *The Journal of chemical physics* 137.22 (2012): 22A553.

17. Bose, Amartya, and Nancy Makri. "Wigner phase space distribution via classical adiabatic switching." *The Journal of chemical physics* 143.11 (2015): 114114.

18. Makri, Nancy, and Keiran Thompson. "Semiclassical influence functionals for quantum systems in anharmonic environments." *Chemical physics letters* 291.1 (1998): 101-109.

19. Thompson, Keiran, and Nancy Makri. "Influence functionals with semiclassical propagators in combined forward–backward time." *The Journal of chemical physics* 110.3 (1999): 1343-1353.

20. Shi, Qiang, and Eitan Geva. "A relationship between semiclassical and centroid correlation functions." *The Journal of chemical physics* 118.18 (2003): 8173-8184.

21. Wigner, E. J. Calculation of the Rate of Elementary Association Reactions. Chem. Phys. 1937, 5, 720.

22. Sun, Xiong, and William H. Miller. "Semiclassical initial value representation for electronically nonadiabatic molecular dynamics." *The Journal of chemical physics* 106.15 (1997): 6346-6353.

23. Poulsen, Jens Aage, Gunnar Nyman, and Peter J. Rossky. "Practical evaluation of condensed phase quantum correlation functions: a Feynman–Kleinert variational linearized path integral method." *The Journal of chemical physics* 119.23 (2003): 12179-12193.

24. Walters, Peter L., Tuseeta Banerjee, and Nancy Makri. "On iterative path integral calculations for a system interacting with a shifted dissipative bath." The Journal of chemical physics 143.7 (2015): 074112.

Chapter 5. Vibrational Relaxation of a Quantum System in a Dissipative Bath

5.1 Introduction:

Vibrational energy transfer from solute molecules to various modes of motions of solvent plays a crucial role in chemical dynamics. A detailed microscopic and theoretical understanding of the phenomena of this phenomena has been of considerable interest to chemists. [1-6] It is also not surprising that a lot of scientific investigation on this topic has been conducted in the experimental and theoretical communities over the last few decades. Considerable experimental progress has been made to study the vibrational relaxation of small molecules in solution, using recent advances in ultrafast vibrational spectroscopy. [7-13] Owing to the continuing development in the extent of wavelength studied, the increased sensitivity and the time resolution, a large set of parameters can be studied. Theoretical progress in terms of development of different methodologies and the improvement in computational resources has made the simulations of realistic systems possible. Recently, our group has reported rigorous yet practical Quantum Classical Path Integral (QCPI) method which predicts correct product distributions, accurate rate constants by capturing the proper interplay between quantum coherence and dissipation. [14-16] It is an exciting era, where the possible confluence of the two approaches can explain fully the dynamics of such systems.

Vibrational relaxation is essentially caused due to the dissipative nature of the bath. The main quantity of interest in such phenomena is usually the energy or the population relaxation time (*T1*) of the vibrational relaxation states. Experimentally, it is obtained directly from the time-resolved spectroscopic measurements. The relaxation time of the $v=1$ level of a particular mode yields the relaxation time *T1*, which can be calculated theoretically. Perhaps, the easiest way to approach this problem would be to use second order perturbation theory in system-bath coupling, where the equations of motions for the reduced density matrix elements are given by Bloch Equations [17]. For wide range of problems, which deal with low coupling between the system and bath, Bloch Equations provide an exceptionally good description of the dynamics of a two-level system coupled to a dissipative bath. Budimir and Skinner performed a fourth order perturbation theory for a Two-Level System (TLS) coupled, both diagonally and off-diagonally to a Gaussian stochastic bath [18,19]. Later, Laird, Budimir and Skinner have performed fourth order perturbation theory for a TLS coupled to a quantum heat bath [20-23]. While these theories obey the same

Bloch equations, their rate constants are different and they capture a part of the corrections to the second order. Silbey and co-workers have reported further developments and insights using their variational approaches. [24-26] However, none of these theories provide the accurate nature of dynamics beyond the weak coupling regime. Grigolini and co-workers have reported analytic theories, where they study the two-level system linearly interacting with a set of quantum-mechanical bath that capture the nonlinear effects in quantum dissipation[27-29]. They have carefully validated the theory at different regimes, but it fails to provide the exact nature of transition in between these limits.

In this chapter, we propose the application of i-QuAPI method [30-37] with filtering schemes [38-41], to study the exact vibrational dynamics of the TLS coupled diagonally to the harmonic dissipative bath to provide an exact nature of transition between the low-coupled to highly coupled regimes. Harmonic bath model has various analytical approximate treatments, few of which are described earlier, and it can also be numerically solved exactly. One of such numerical methods is the iterative quasi-adiabatic propagator path integral (i-QuAPI) methodology that offers an efficient approach for treating continuous or discrete dissipative systems over extremely long time lengths. The i-QuAPI algorithm is based on iterative methodology, and this avoids the exponential proliferation of quantum paths with propagation time. Since it is based on quadrature based methods, it avoids the Monte Carlo sign problem which arises from the phase in the real-time path integral. The use of filtering algorithms to eliminate the majority of system path segments that span the memory length, often leads to dramatic reduction in storage, enabling applications to more demanding situations with longer memory. [37] The numerical calculations, along with comparisons to different approximate theories are provided for most regimes of parameter space. Finally, we have established the boundary between the coherent and the incoherent behavior.

Section 5.2. discusses the various approximate theories from literature while Section 5.3. reports the mapping of the TLS Hamiltonian to the Spin-Boson Hamiltonian as pointed out by LBS. In section 5.4 we review the i-QuAPI formalism with filtering procedures and Section 5.5. demonstrates the numerical comparisons to the various approximate theories and finally with some concluding remarks in Section 5.6.

5.2 Approximate Theoretical Methods:

The approximate theoretical methods section is mostly summarizes the work in Ref [18-20] and discussed how older theories [17] can also be obtained using similar treatment.

Bloch Redfield Theory: For a generic TLS the ground state is labeled as $|0\rangle$, the excited state is labeled as $|1\rangle$ and their energy difference is given by $\hbar\omega_0$. The dynamics of such system can be completely determined from the density matrix,

$$\sigma(t) = \begin{pmatrix} \sigma_{00}(t) & \sigma_{01}(t) \\ \sigma_{10}(t) & \sigma_{11}(t) \end{pmatrix} \tag{5.1}$$

For a density matrix the diagonal elements represents the populations, thus here $\sigma_{00}(t)$ and $\sigma_{11}(t)$ are of the ground and excited states. The off-diagonal terms are a measure of the coherence between the states. When there is no coupling to the dissipative bath, then the above TLS is in its eigen state and will continue to be in that state, therefore we will not see any dynamics. However, when there is coupling to the bath, the total system and bath do not remain in the eigen state of the system alone, and hence the system decays to the thermal equilibrium and the off-diagonal terms got to zero signifying complete incoherence. The crudest picture of the dynamics of the reduced density matrix of the system then is provided by the Bloch Equations, which are obtained when second order perturbative theory in system-bath coupling is used. The Bloch equations obtained for the diagonal terms in and are given by [17]

$$\begin{aligned} \dot{\sigma}_{00}(t) &= -k_{10}\sigma_{00}(t) + k_{01}\sigma_{11}(t) \\ \dot{\sigma}_{01}(t) &= k_{10}\sigma_{00}(t) - k_{01}\sigma_{11}(t) \end{aligned} \tag{5.2}$$

With k_{10} and k_{01} often referred to as the "up" and the "down" rate constants in literature. In this theory, the population of the ground and excited states decay to the Boltzmann equilibrium values. Also, if the rate of decay of population to equilibrium is defined as $1/T_1$, then it can be shown that it is related to the above "up" and "down" rate constants using the following equation.

$$1/T_1 = k_{01} + k_{10} \tag{5.3}$$

The Bloch-Redfield equations are applicable to a wide range of TLS coupled weakly to a dissipative bath, especially in NMR fields where these equations first appeared.

Laird Budimir and Skinner Theory: We consider the TLS Hamiltonian, as introduced by Skinner and co-workers, [18-20]

$$
\begin{aligned}
H &= H_{TLS} + H_b + H_{\text{int}} \\
H_{TLS} &= \hbar\omega_0 \left|1\right\rangle\left\langle 1\right| \\
H_b &= \sum\nolimits_k \hbar\omega_k \left(b_k^\dagger b_k + \frac{1}{2} \right) \\
H_{\text{int}} &= \hbar\Lambda \left|1\right\rangle\left\langle 0\right| + \hbar\Lambda^\dagger \left|1\right\rangle\left\langle 0\right| \\
\Lambda &= \sum\nolimits_k h_k \left(b_k^\dagger + b_k \right)
\end{aligned}
\tag{5.4}
$$

The Hamiltonian consists of the bare TLS as described above, a harmonic bath that has a linear coupling which is off-diagonal in the system states. The coupling constants which can be either purely imaginary or purely real.

The dynamics of the total density operator is governed by Liouville equation,

$$
\frac{\partial\rho(t)}{\partial t} = -i\left[H, \rho(t) \right] \tag{5.5}
$$

If the harmonic degrees of freedom of the bath are traced out in the interaction representation, then the reduced density operator can be obtained. By accounting for correlations to a particular order the Redfield like coupled equations of motion can be obtained. LBS had shown that when accounting for second order perturbation in the system-bath coupling, one can obtain the Bloch-Redfield Equations. The rate of decay, $1/T_1$ is such treatments, leads to the following expression

$$
1/T_1 = 2\Gamma(\omega_0)\coth\left(\beta\hbar\omega_0/2\right) \tag{5.6}
$$

Where Γ is the weighted density of states (spectral density) and β is the equilibrium temperature. The equilibrium population in this particular treatment leads to the Boltzmann distribution and is given by

Further, fourth order perturbations in the system-bath coupling can be considered with analytical results for the rate of decay given by the following expression,

$$
1/T_1 = \left[\hat{C}_1(\omega_0) + \hat{C}_1(-\omega_0) \right] + 1/2\pi \left\{ \begin{array}{l}
\omega_0^{-1}\left[\hat{C}_2(\omega_0) + \hat{C}_2(-\omega_0) \right]\left[P_2(\omega_0) - P_2(-\omega_0) \right] \\
-\left[\hat{C}_1'(\omega_0) - \hat{C}_1'(-\omega_0) \right]\left[P_1(\omega_0) - P_1(-\omega_0) \right] \\
-\left[\hat{C}_1(\omega_0) + \hat{C}_1(-\omega_0) \right]\left[P_1'(\omega_0) + P_1'(\omega_0) \right]
\end{array} \right\} \tag{5.8}
$$

Where

$$\hat{C}_i(\omega) = 2\left\{\Gamma_i(\omega)\left[n(\omega)+1\right] + \Gamma_i(-\omega)n(-\omega)\right\}$$
$$n(\omega) = 1/\left(e^{\hbar\beta\omega} - 1\right)$$
$$P_i(\omega) = P\int_{-\infty}^{\infty} d\omega' \frac{\hat{C}_i(\omega')}{\omega' - \omega} \tag{5.9}$$
$$\hat{C}_1'(\omega) = \frac{\partial \hat{C}_i(\omega)}{\partial\omega}$$
$$P_1'(\omega) = \frac{\partial P_i(\omega)}{\partial\omega}$$

5.3 Mapping to the Spin Boson Problem:

Another generic TLS is given by the Spin Boson (SB) Problem, where the total Hamiltonian is expressed in the "right" $|r\rangle$ and the "left" $|l\rangle$ basis. The quantum system is given by

$$H_0 = -\hbar\Omega\sigma_x \tag{5.10}$$

where σ_x and σ_z are the standard 2×2 Pauli spin matrices and the bare TLS is characterized by the tunneling splitting $2\hbar\Omega$. The TLS is coupled to a harmonic bath described by the Hamiltonian

$$H_b = \sum_j \left(\frac{\hat{p}_j^2}{2m} + \frac{1}{2}m\omega_j^2\hat{x}_j^2 - c_j\sigma_z\hat{x}_j \right) \tag{5.11}$$

We assume that the bath is at thermal equilibrium at the temperature $k_B T = \beta^{-1}$.

This is the prototypical TLS model used to study the tunneling behavior across symmetric or asymmetric potentials. In order to map the LBS Hamiltonian to the SB problem, they applied the following transformation to the LBS Hamiltonian,

$$|r\rangle = 1/\sqrt{2}\left(|0\rangle + |1\rangle\right)$$
$$|l\rangle = 1/\sqrt{2}\left(|0\rangle - |1\rangle\right) \tag{5.12}$$

By doing so, LBS Hamiltonian in the "right" $|r\rangle$ and the "left" $|l\rangle$ basis is obtained,

$$H = -\frac{\hbar\omega_0\sigma_x}{2} + \sum\nolimits_k \hbar\omega_k\left(b_k^\dagger b_k + \frac{1}{2}\right) + \frac{\delta\hbar\left(\Lambda + \Lambda^\dagger\right)}{2}\sigma_z + \frac{i\delta\hbar\left(\Lambda - \Lambda^\dagger\right)}{2}\sigma_y \tag{5.13}$$

A simple comparison with Eqn. 5.10 and Eqn 5.11 and Eqn 5.13 shows that if we have Λ as Hermitian, and set $\omega_0 = \Delta$ and $h_k\left(2m_k\hbar\omega_k\right)^{1/2} = c_k/2$ then both of them are equivalent.

5.4 Iterative Quasi-Adiabatic Path Integral (i-QuAPI) with Filtering:

The method of i-QuAPI with filtering has been described in previous publication [37] and has been summarized here for completeness. Using the system-bath Hamiltonian, as described in Section 5.3., the time evolution of the system is obtained from the reduced density operator given by,

$$\rho_{\mathrm{red}}(\mathrm{s}_N^{\pm};\mathrm{N}\Delta t)=\mathrm{Tr}_{\mathrm{b}}\left\langle s_N^{+}\left|e^{-i\hat{H}t/\hbar}\hat{\rho}(0)e^{i\hat{H}t/\hbar}\right|s_N^{-}\right\rangle \tag{5.14}$$

Where $\rho(0)$ is the initial density operator and the expression is traced over all bath degrees of freedom to obtain the reduced degrees of freedom of the system. Two assumptions are made in this particular initialization: i) the system and bath are uncorrelated at the initial time, and the density operator is simply expressed as a product of the bath and the system density matrix;. ii) the system bath is in thermal equilibrium. Using the assumptions we can have the following expressions,

$$\hat{\rho}(0)=\hat{\rho}_{sys}(0)\hat{\rho}_b(0)=\hat{\rho}_{sys}(0)e^{-\beta H_{\mathrm{b}}}/\mathrm{Tr}\,e^{-\beta H_{\mathrm{b}}} \tag{5.15}$$

The quasi-adiabatic splitting of the Hamiltonian is given by the following form,

$$\begin{aligned}\hat{H}&=\hat{H}_0+\sum_j\left(\frac{\hat{p}_j^2}{2m}+\frac{1}{2}m\omega_j^2\left(\hat{x}_j-\frac{c_j\sigma_z}{m\omega_j^2}\right)\right)\\ \hat{H}_0&=\hat{H}_{sys}-\sum_j\frac{c_j\sigma_z}{2m\omega_j^2}\end{aligned} \tag{5.16}$$

In order to reduce the error coming from the Trotter splitting, we propagate the reduced density matrix by propagating it in N small increments of time length $\Delta t=t/N$, such that each of the exponential of the forward and backward propagation is replaced by a product of exponentials,

$$\begin{aligned}\left\langle s_N^{+}\left|\hat{\rho}(\mathrm{N}\Delta\mathrm{t})\right|s_N^{-}\right\rangle=\mathrm{Tr}_{\mathrm{b}}\sum_{s_0^{\pm}}\sum_{s_1^{\pm}}\cdots\sum_{s_{N-1}^{\pm}}&\left\langle s_N^{+}\left|e^{-i\hat{H}_0\Delta t/\hbar}\right|s_{N-1}^{+}\right\rangle\cdots\left\langle s_1^{+}\left|e^{-i\hat{H}_0\Delta t/\hbar}\right|s_0^{+}\right\rangle\\ &\times\left\langle s_0^{+}\left|\tilde{\rho}(0)\right|s_0^{-}\right\rangle\left\langle s_0^{-}\left|e^{i\hat{H}_0\Delta t/\hbar}\right|s_1^{-}\right\rangle\cdots\left\langle s_{N-1}^{-}\left|e^{i\hat{H}_0\Delta t/\hbar}\right|s_N^{-}\right\rangle\end{aligned} \tag{5.17}$$

Next if we use all the three of the above concepts: the factorized initial density, quasi-adiabatic splitting of the time evolution operator, and the time discretization to obtain the reduced density matrix in the following form,

$$\left\langle s_N^+ \left| \tilde{\rho}(N\Delta t) \right| s_N^- \right\rangle = \sum_{s_0^\pm} \sum_{s_1^\pm} \cdots \sum_{s_{N-1}^\pm} \left\langle s_N^+ \left| e^{-i\hat{H}_0 \Delta t/\hbar} \right| s_{N-1}^+ \right\rangle \cdots \left\langle s_1^+ \left| e^{-i\hat{H}_0 \Delta t/\hbar} \right| s_0^+ \right\rangle$$
$$\times \left\langle s_0^+ \left| \tilde{\rho}(0) \right| s_0^- \right\rangle \left\langle s_0^- \left| e^{i\hat{H}_0 \Delta t/\hbar} \right| s_1^- \right\rangle \cdots \left\langle s_{N-1}^- \left| e^{i\hat{H}_0 \Delta t/\hbar} \right| s_N^- \right\rangle$$
$$\times F(s_0^+, s_1^+, \cdots s_N^+, s_0^-, s_1^-, \cdots s_N^-; \Delta t) \tag{5.18}$$

where F is the Feynman-Vernon influence functional and is given by the form,

$$F\left(s_0^\pm, s_1^\pm, \ldots, s_N^\pm\right) = \exp\left(-\frac{1}{\hbar} \sum_{k'=0}^{N} \sum_{k''=0}^{k'} (s_{k'}^+ - s_{k'}^-)(\eta_{k'k''} s_{k''}^+ - \eta_{k'k''}^* s_{k''}^-) \right) \tag{5.19}$$

Where $\eta_{k'k''}$ the discretized version of the response are function and has been given explicitly in many of the previous publications. The double sum in the expressions originate from time-nonlocality which occurs due to the coupling between the system and the bath, and is often referred to as "memory". The length of the memory depends on the numerical value of these coefficients.

This correlation or memory as observed earlier in the group decays to zero beyond a certain time interval $\tau_{\text{mem}} = m\Delta t$. This results in the observation that the coefficients $\eta_{k'k''}$ becomes lesser than threshold value when two time points are separated by a time gap greater than m. Thus the double integral goes to being a single integral beyond the memory, and hence the resultant dynamics is quasi-Markovian in nature. The reduced density matrix R, (a tensor of rank *m*) containing all interactions within the time span m is accounted for in the following expression,

$$R_m\left(s_{k+1}^\pm, \ldots, s_{k+m}^\pm; (m+1)\Delta t\right) = \sum_{s_1^\pm} S_m\left(s_k^\pm, s_{k+1}^\pm, \ldots, s_{k+m}^\pm\right) R_{m-1}\left(s_k^\pm, s_{k+1}^\pm, \ldots, s_{k+m-1}^\pm; \mathrm{k}\,\Delta\,\mathrm{t}\right) \tag{5.20}$$

A propagator matrix that can propagate R to the next step is given by S_m is a multi-time propagator matrix (a tensor of rank $m+1$) with the elements given by the following expression

$$S_m\left(s_k^\pm, s_{k+1}^\pm, \ldots, s_{k+m}^\pm\right) = \left\langle s_{m+1}^+ \left| e^{-i\hat{H}_0 \Delta t/\hbar} \right| s_m^+ \right\rangle \left\langle s_m^- \left| e^{i\hat{H}_0 \Delta t/\hbar} \right| s_{m+1}^- \right\rangle$$
$$\times \exp\left(-\frac{1}{\hbar} \sum_{k'=k}^{k+m} (s_{k'}^+ - s_{k'}^-)(\eta_{k'k} s_k^+ - \eta_{k'k}^* s_k^-) \right) \tag{5.21}$$

Another propagator matrix which is used to terminate the iteration, is formed by including connections from the last time point up to the memory length.

$$T_m\left(s_k^{\pm},s_1^{\pm},\ldots,s_{k+m}^{\pm}\right)=\prod_{k'=k}^{k+m}\left\langle s_{k'}^{+}\left|e^{-i\hat{H}_0\Delta t/\hbar}\right|s_{k'-1}^{+}\right\rangle\left\langle s_{k'-1}^{-}\left|e^{i\hat{H}_0\Delta t/\hbar}\right|s_{k'}^{-}\right\rangle \times\exp\left(-\frac{1}{\hbar}\sum_{k'=k}^{k+m}\sum_{k''=0}^{k'}(s_{k'}^{+}-s_{k'}^{-})(\eta_{k'k''}s_{k''}^{+}-\eta_{k'k''}^{*}s_{k''}^{-})\right) \tag{5.22}$$

The termination procedure to obtain the reduced density matrix is given using the following expression

$$\rho_{\mathrm{red}}(\mathrm{s}_N^{\pm};\mathrm{N}\Delta t)=\sum_{s_{N-m}^{\pm}}\sum_{s_{N-m+1}^{\pm}}\cdots\sum_{s_{N-1}^{\pm}}T_m\left(s_{N-m}^{\pm},\ldots,s_N^{\pm}\right)\times\mathrm{R}_m\left(s_{N-m}^{\pm},\ldots,s_{N-1}^{\pm};(N-m)\Delta t\right) \tag{5.23}$$

This procedure requires storage of matrices that scale exponentially with a factor of 2m. For very slow and sluggish bath, even normal iterative procedure can be very demanding and impractical. For many regimes, a vast majority of these paths have negligible weight and can be omitted. The weight of a path is defined by

$$p_{\alpha}^{(n)}=\prod_{k'=1}^{n-1}\left\langle s_{k'}^{+}\left|e^{-i\hat{H}_0\Delta t/\hbar}\right|s_{k'-1}^{+}\right\rangle\left\langle s_{k'-1}^{-}\left|e^{i\hat{H}_0\Delta t/\hbar}\right|s_{k'}^{-}\right\rangle \times\exp\left(-\frac{1}{\hbar}\sum_{k'=1}^{n}\sum_{k''=1}^{k}(s_{k'}^{+}-s_{k'}^{-})(\eta_{k'k''}s_{k''}^{+}-\eta_{k'k''}^{*}s_{k''}^{-})\right) \tag{5.24}$$

If this weight is greater than the threshold θ then it is accepted otherwise it is rejected. The procedure is deterministic, and often results in elimination of majority of the non-important paths. All paths within the memory m, which is greater than the threshold are selected, and all of these segments are use for further propagation. This procedure is particularly advantageous for slow bath with long propagation time required to complete the dynamics. The threshold value, θ, is a convergence parameter and propagations are done using different values of θ till convergence is achieved.

5.5 Numerical Example:

Using the methodology described in section 5.4. We study the SB Hamiltonian for relaxation process which is a defined by

$$H_0=-\hbar\Omega\sigma_z$$

$$H_{\mathrm{b}}=\sum_j\left(\frac{\hat{p}_j^2}{2m}+\frac{1}{2}m\omega_j^2\left(\hat{x}_j+c_j\sigma_x\Big/m_j\omega_j^{\,2}\right)^2\right) \tag{5.25}$$

The relevant quantity of interest here is the population difference in the energy levels, and is given by $\rho_{1,2} = \frac{1}{2}(1 \pm \sigma_z)$. Also, we assume that the initial state of the system is created in the excited state.

To study the rates and the asymptotic values we chose the ohmic spectral density with exponential cutoff, given by the following expression, (equivalence to Ohmic-Lorentzian spectral density used by LBS will also be shown for comparisons and to provide the complete picture

$$J(\omega) = \frac{1}{2}\pi\hbar\xi\omega\, e^{-\omega/\omega_c} \tag{5.26}$$

where the dimensionless Kondo parameter ξ provides a measure of the dissipation strength (i.e., the magnitude of the system-bath coupling) and ω_c gives the maximum of the spectral density.

Low coupled regime:

In the very low coupling regime, , we find there is considerable qualitative agreement between the quantum results and the second-order perturbative results. In Fig. 1, we report the relaxation dynamics for various cutoff frequencies, $\omega_c = 1, 2.5, 5, 7.5$ at a high temperature $\beta = 0.2$, moderate temperature, $\beta = 1.0$ and very low temperature, $\beta = 2.5$ for two coupling strengths, $\xi = 0.03, 0.05$. Since the coupling is very low, we find almost no difference in the equilibrium population between those obtained from quantum curve and from the analytic expressions in the second order treatments. The curves more or less depict prototypical exponential dynamics, with exceptions observed in the higher temperature regime. The initial dynamics start deviating from the Markovian limit and hence the Redfield-Bloch limit. This was also reported by LBS, where they pointed out that only under even lower coupling regimes, will Markovian limit fully hold[19]. Fig 1a, b, and c, shows the dynamics of the TLS at a very low coupling strength, $\xi = 0.03$. This regime map very well to the Ohmic-Lorentzian spectral density parameters reported by LBS[19]. In fact, for figure 1b) the parameters predict very similar results to the fourth order changes reported in their paper. They claimed a 20% change from the Redfield-Bloch equations due to second order corrections and further predicted a 2% change for the sixth ordered terms. The full quantum mechanical results match this prediction, thus proving that higher order perturbative treatments are not required in this parameter regime.

In Figure 1a), for the highest temperature scenario, the convergence of the system coupled to a bath with $\omega_c = 1$ required a quantum mechanical time step of $\Omega\Delta t = 0.75$ and the Non-Markovian nature of the dynamics spanned 8 path integral time steps, while $\omega_c = 2.5, 5$ required $\Omega\Delta t = 0.25$ and $\omega_c = 7.5$ required $\Omega\Delta t = 0.125$, the Non-Markovian character extended for 8 time steps. In Figure 1b) for the intermediate temperature, we required similar time steps and non-Markovian memory. As we lowered temperatures in

Figure 1c) we see that although the path integral time step remained the same, the Non-Markovian memory time span increased mostly by a single path integral time step. In Fig 1d - f) we increased the coupling strength slightly. Even with this slight increase in the coupling, the deviation from perturbative treatments become significant especially in the higher temperature, lower frequency ranges and during the initial decay time. In Figure 1e) the convergence for the system dynamics with the bath with $\omega_c = 1$ required a path integral time step of $\Omega\Delta t = 0.75$ and the Non-Markovian nature spanning 11 path integral time steps, while $\omega_c = 2.5, 5$ required $\Omega\Delta t = 0.25$ and $\omega_c = 7.5$ required $\Omega\Delta t = 0.125$ the Non-Markovian character spanned for 8-9 time steps.

The table 1 shows a comprehensive data of the rate and equilibrium values of i-QuAPI and the Redfield methodologies. A point to be noted is that contrary to expectation, we find that at lower temperature and higher frequencies the rates match quite well, while they tend to deviate a lot in the higher temperature and lower frequency range. This can be attributed to the fact, that as the temperature is raised and the frequency lowered there is a considerable deviation from exponential-kinetics, and even at such low coupling strengths, perfect exponential behavior as predicted by Bloch-Redfield Equations are not obtained. For the lowest coupled regime, $\xi = 0.03$, we find differences between the Bloch-Redfield and i-QuAPI methods to be anywhere between (0-40)%, the lowest being reported for the coldest bath frequency modes, and the highest difference is observed for the high temperature classical bath modes. We report the change of rates from anywhere between 50 % from the high temperature, low frequency ranges to almost non-negligible difference for the low temperature high frequency ranges, for $\xi = 0.05$

Moderately Coupled Regime:

In the moderately coupled regime, we find significant deviation from the exponential behavior at high temperature and low frequency regime. In fact, the quantitative agreement between the quantum results and the second-order perturbative results decreases even in low temperature and the high frequency regions. We report the relaxation dynamics for various cutoff frequencies - from high temperatures $\beta = 0.2$, moderate temperatures $\beta = 1.0$, to low temperatures $\beta = 2.5$ in figure 2. With increase in the coupling, the curves tend to deviate from the exponential kinetics. This effect is heavily pronounced for the lower cutoff frequencies when we compare the dynamics of $\omega_c = 1, 2.5, 5, 7.5$ behavior in Figure 2. The higher frequency ranges still show exponential behavior and their rates match the Redfield rates much better than the lower frequency ranges.

Fig 2a, b, and c, shows the dynamics of the TLS at a lower value of the coupling strength in this regime, where coupling strength, $\xi = 0.1$ In Figure 2a), for the highest temperature scenario, the convergence of the system coupled to a bath with $\omega_c = 1$ required a quantum mechanical time step of $\Omega\Delta t = 0.5$ and the Non-Markovian nature spanned 8 path integral time steps, while $\omega_c = 2.5, 5, 7.5$ required $\Omega\Delta t = 0.125$ and the Non-Markovian character extended from anywhere between 8-10 time steps. In Figure 2b) for the intermediate temperature, we converged with relatively larger time steps and the Non-Markovian memory was also greater than at higher temperatures. While the convergence of a bath with $\omega_c = 1$ required a quantum mechanical time step of $\Omega\Delta t = 0.5$ and the Non-Markovian dynamics spanning 8 path integral time steps, while $\omega_c = 2.5, 5.0, 7.5$ required $\Omega\Delta t = 0.25$ and the Non-Markovian character spanned for anywhere between 8-10 time steps. As we lowered temperatures even further in Figure 2c) we see that although the path integral time step remained the same, the Non-Markovian memory time span increased only slightly. In Fig 2d - f) we increased the coupling strength slightly to $\xi = 0.3$. Even with this slight increase in the coupling, the appearance of coherences become quite distinct especially significant in the higher temperature, lower frequency ranges and it is present throughout the entire decay. In Figure 2d), the convergence for the bath with $\omega_c = 1$ required a path integral time step of $\Omega\Delta t = 0.25$ and the Non-Markovian nature spanning 10 path integral time steps, while $\omega_c = 2.5, 5$ required $\Omega\Delta t = 0.125$ and $\omega_c = 7.5$ required $\Omega\Delta t = 0.0625$ the Non-Markovian character spanned for 10 time steps. In Figure 2e) for the intermediate temperature, we converged with relatively similar or larger time steps and the Non-Markovian memory was also greater than at higher temperatures. While the convergence of a bath with $\omega_c = 1$ required a quantum mechanical time step of $\Omega\Delta t = 0.5$, the Non-Markovian nature dynamics spanning 9 path integral time steps, while $\omega_c = 2.5, 5.0, 7.5$ required $\Omega\Delta t = 0.125$ and the Non-Markovian character spanned for anywhere between 8-10 time steps. For lower temperature in Figure 2f) we see that although the path integral time step remained the same, the Non-Markovian memory time span increased only slightly.

Table 2 shows the rate and equilibrium values of i-QuAPI and the Redfield methodologies. We have reported the rates for i-QuAPI methodology where we have seen exponential decay kinetics. The higher coupling, higher temperature lower frequency ranges are here not presented, because they start to deviate significantly from exponential kinetics. For the coupling of $\xi = 0.1$, we find deviations anywhere between 1-50% depending on the temperature and the frequencies, 1% being at almost quantum mechanical temperatures and higher frequency bath, while 50% being for the most classical of the regimes. For the

coupling of $\xi = 0.3$, we find deviations anywhere between 2-75% depending on the temperature and the frequencies, 1% being at almost quantum mechanical temperatures and higher frequency bath, while 50% being for the most classical of the regimes.

Strongly Coupled Regime:

In the highly coupled regime, we find even the qualitative agreement between the exact quantum mechanical results and perturbative approaches does not hold. Redfield-type equations are coupled differential equation and predicts exponential kinetics. The Redfield type equations cannot predict the coherent behavior which persists in these regime and have been demonstrated using exact iQuAPI methodologies. This can be justified from the bath parameters entering the system Hamiltonian via the diagonal terms, which is numerically responsible for coherences. So greater the strength of coupling, greater is the coherent nature of the dynamics.

Fig 3a, b, and c, shows the dynamics of the TLS where coupling strength, $\xi = 0.6$ In Figure 3a), for the highest temperature, where $\beta = 0.2$, the system dynamics coupled to a bath with $\omega_c = 1$ required a quantum mechanical time step of $\Omega\Delta t = 0.25$ and the Non-Markovian nature dynamics spanning 10 path integral time steps for convergence, while $\omega_c = 2.5$ required $\Omega\Delta t = 0.125$ and the Non-Markovian character spanned for anywhere between 9 time steps, while $\omega_c = 5.0, 7.5$ required $\Omega\Delta t = 0.0625$ and the Non-Markovian character spanned for 6 and 9 time steps respectively and . In Figure 3b) for the intermediate temperature, we converged the lower frequency regime with relatively larger time steps and the Non-Markovian memory was also greater than at higher temperatures. While the convergence of a bath with $\omega_c = 1$ required a quantum mechanical time step of $\Omega\Delta t = 0.375$ and the Non-Markovian nature dynamics spanning 10 path integral time steps, while $\omega_c = 2.5$ required $\Omega\Delta t = 0.125$ and the Non-Markovian character spanned for anywhere between 8 time steps, and $\omega_c = 5.0, 7.5$ required $\Omega\Delta t = 0.0625$ and the Non-Markovian character spanned for anywhere between 8-10 time steps. As we lowered temperatures even further in Figure 3c) we see that we require higher path integral time step as well as higher Non-Markovian memory time span for convergence. For the convergence of system dynamics coupled to a bath with a cutoff frequency, $\omega_c = 1$ required a quantum mechanical time step of $\Omega\Delta t = 0.375$ and the Non-Markovian nature spanning 10 path integral time steps, while $\omega_c = 2.5, 5.0, 7.5$ required $\Omega\Delta t = 0.125$ and the Non-Markovian character spanned for anywhere between 8-10 time steps, In Fig 3d - f) we increased the coupling strength slightly to $\xi = 1.2$. In this regime, the exponential kinetics is hardly present at higher

temperatures. Even for lower temperatures, the lower frequency regions, deviate a lot from the exponential kinetics especially in the initial decay time. In Figure 3d), the convergence for the bath with $\omega_c = 1$ required a path integral time step of $\Omega\Delta t = 0.125$ and the Non-Markovian nature spanning 11 path integral time steps, while $\omega_c = 2.5$ required $\Omega\Delta t = 0.125$ and $\omega_c = 5, 7.5$ required $\Omega\Delta t = 0.0625$ the Non-Markovian character spanned for 10 time steps. In Figure 3e) for the intermediate temperature, we converged with relatively similar or larger time steps and the Non-Markovian memory length. While the convergence of a bath with $\omega_c = 1$ required a quantum mechanical time step of $\Omega\Delta t = 0.25$ and the Non-Markovian nature dynamics spanning 9 path integral time steps, while $\omega_c = 2.5$ required $\Omega\Delta t = 0.125$ and $\omega_c = 5, 7.5$ required $\Omega\Delta t = 0.0625$, the Non-Markovian character spanned for anywhere between 8-10 time steps. As we lowered temperatures even further in Figure 3f) we could converge with larger time step, but required longer time non-locality. For $\omega_c = 1$ required a path integral time step of $\Omega\Delta t = 0.25$ and the Non-Markovian nature spanning 10 path integral time steps, while $\omega_c = 2.5$ required $\Omega\Delta t = 0.125$, Non-Markovian spanned 10 steps, and $\omega_c = 5, 7.5$ required $\Omega\Delta t = 0.0625$ the Non-Markovian character spanned for 6-10 time steps.

Table 3 shows the rate and equilibrium values of i-QuAPI and the Redfield methodologies. For the highest coupling regime, $\xi = 1.2$ exponential dynamics is not seen and hence rates are not reported. Only for the lower temperature, and higher frequencies do we see exponential kinetics, and for these the rates differ from the Redfield theory from anywhere between 7-40 %. For the coupling strength, $\xi = 0.6$, we have seen the rates differ from anywhere between 7-40%, only for lower temperature and high frequency baths.

For the couple of parameters where a memory of 11 path integral time steps were required, a code generated for filtering by Dr. Roberto Lambert was used. For the rest of the parameters which involved using Non-Markovian dynamics spanning 10 path integral time steps, simple i-QuAPI procedures were used.

Comparison of Classical and Quantum Decoherence:

To gain a complete understanding of the decoherence process it is important to revisit the response function expression. If we consider the equivalence of Quantum-Classical Path Integral formalism[38] for harmonic bath then the influence functional is given by,

$$F = \prod_j \int dx_{j,0} \int dp_{j,0} W_j(x_{j,0}, p_{j,0}) e^{i\Phi_j(x_{j,0}, p_{j,0})/\hbar}$$

Where the forward-backward action is given by,

$$\Phi = cx_0 \int_0^t dt' \left[s^+(t') - s^-(t') \right] \cos \omega t' + c \frac{p_0}{m_b \omega} \int_0^t dt' \left[s^+(t') - s^-(t') \right] \sin \omega t'$$
$$+ \frac{c^2}{2m_b \omega} \int_0^t dt' \int_0^{t'} dt'' \left[s^+(t') - s^-(t') \right] \left[s^+(t'') + s^-(t'') \right] \sin \omega (t' - t'')$$

It was shown in Ref [38] the first two terms of the action arises from the "free" or the classical trajectory which is not subject to any system force, while the third term comprising of the double integral consists the explicit system force experienced along each unique combination of the system paths. When integrated over the phase space density we obtain the following non-discretized version of influence functional given by,

$$F = \exp\left[-\frac{1}{\hbar} \int_0^t dt' \int_0^{t'} dt'' \left[s^+(t') - s^-(t') \right] \left[\alpha(t' - t'') s^+(t'') - \alpha(t' - t'')^* s^-(t'') \right] \right]$$

where

$$\alpha(t' - t'') = \frac{c^2}{2m_b \omega} \coth\left(\tfrac{1}{2} \hbar \omega \beta \right) \cos \omega (t' - t'') - i \sin \omega (t' - t'')$$

The first two terms or the classical path of the action, gives rise to the Real part of the Influence functional while the system-force dependent part gives rise to the imaginary part of the Influence Functional. Since we are interested in the off-diagonal terms of the density matrix the classical part of the decoherence contributes as a phase, as a result this results in oscillatory behavior of the dynamics. The oscillatory nature is more pronounced at higher temperature and as the ratio of $\frac{c}{\omega}$ increases, which implies increase in the coupling strength and/or decrease in the frequency modes of the bath. The classical part of the influence functional also predicts the equal equilibrium values. These predictions are quite accurate at higher temperatures, and at very high temperatures indeed we can see equal population distribution and highly oscillatory behavior. However, as we increase the temperature the quantum part of the influence functional which brings about the quenching effects becomes more predominant. This is just opposite to what was observed when seeing the dynamics of the diagonal elements of the SB problem.[39] This captures the transition from the coherent to the exponential dynamics, and remedies the classical decoherence to capture the total effect in a quantitative fashion. The quantum effects is also expected to become more important in case of strong system-bath coupling and/or higher frequency modes of bath. This predicted behavior is exactly what we observe in Figure 4. Figure 4 shows comparison of the classical and quantum part of decoherence for a highly coupled ohmic bath, $\xi = 1.2$, with low cut-off frequency . For high temperatures the dynamics is oscillatory and quite close to the equal population as predicted by classical theory, while

as we decrease the temperature, the quantum part of the memory quenches these oscillations and we obtain the decay kinetics and a larger shift from the equilibrium population.

Equilibrium Population

Figure 5 shows the equilibrium values for low temperature $\beta = 2.5$ and high cut off frequency $\omega_c = 7.5\Omega$; calculations for different Kondo parameters. While second order perturbative theory predicts complete localization at low temperature, the classical treatment predicts equal distribution between the excited and the ground state. We find the exact quantum results to span the entire range, with the very low couplings matching the Redfield limit. As we increase the coupling strength, we see a lot of deviations from the Redfield limit, and see how the second order perturbative treatment is not at all successful in calculating the equilibrium population. A similar analogy has be drawn to the dissipative dynamics, where the NIBA prediction to the equilibrium population for asymmetric systems deviates from the accurate quantum mechanical results as asymmetry is increased. [31-32]

5.6 Concluding Remarks:

Vibrational energy transfer in condensed phases is important in deciding the rates and routes of various chemical processes. These energy transfer reactions usually take place over a considerable number of degrees of freedom, and in such conditions the central limit theorem can be invoked and the bath can be treated in its Gaussian form. This has been taken into account in many perturbative approaches developed in early 90's using harmonic semiclassical and quantum mechanical bath, where explicit analytical expressions for the fourth order perturbative approaches had been developed. Since then several variants of the numerically exact path integral methods to treat Gaussian baths with the influence functional approach have been developed and applied to study tunneling dynamics. We have used one such variant, namely the iterative Quasi-Adiabatic-Path Integral approach coupled with deterministic filtering algorithm to explore an extensive parameter space for such energy relaxation processes.

We have explored the dependence of the energy transfer from an excited state to the ground state in presence of a dissipative bath. Vibrational relaxation is essentially a dissipative process and is guided by the strength of friction from the bath.

1) For a highly dissipative bath, these relaxations are much faster and coherent oscillations are present. The oscillatory behavior is magnified in presence of smaller bath frequency modes. This behavior persists from high to moderate coupling strengths which is in fact the opposite for tunneling dynamics. In tunneling

dynamics the high coupled bath quenches the oscillatory nature, while in a weakly coupled bath coherences are present.

2) The perturbative approaches on the other hand solve coupled differential equations and hence always predict exponential kinetics, with the rates increasing with increase in coupling strengths.

3) The coherent-incoherent boundary is also not very well defined and it depends strongly on coupling strengths and cut-off frequencies, and considerably on temperature.

4) At higher temperatures, the rate of the decay kinetics increases.

A similar analysis was done for a TLS coupled to a TLS bath, but in that case, the diagonal elements of the reduced density matrix was seen. The results are quite different as in this case, high temperature and strong quenching increase the oscillatory behavior while it is the opposite for a diagonal element coupling [40]. The presence of coherent oscillations arising during the short time dynamics in these system come from the Non-Markovian nature of the bath and cannot be suitably explained using perturbative approaches, which limit this Non-Markovian character to explicitly treat only a few degrees of correlations. These oscillations play an important role in deciding the mechanism of such energy transfer and need to be investigated using accurate theoretical methods.

5.7 Figures and Tables:

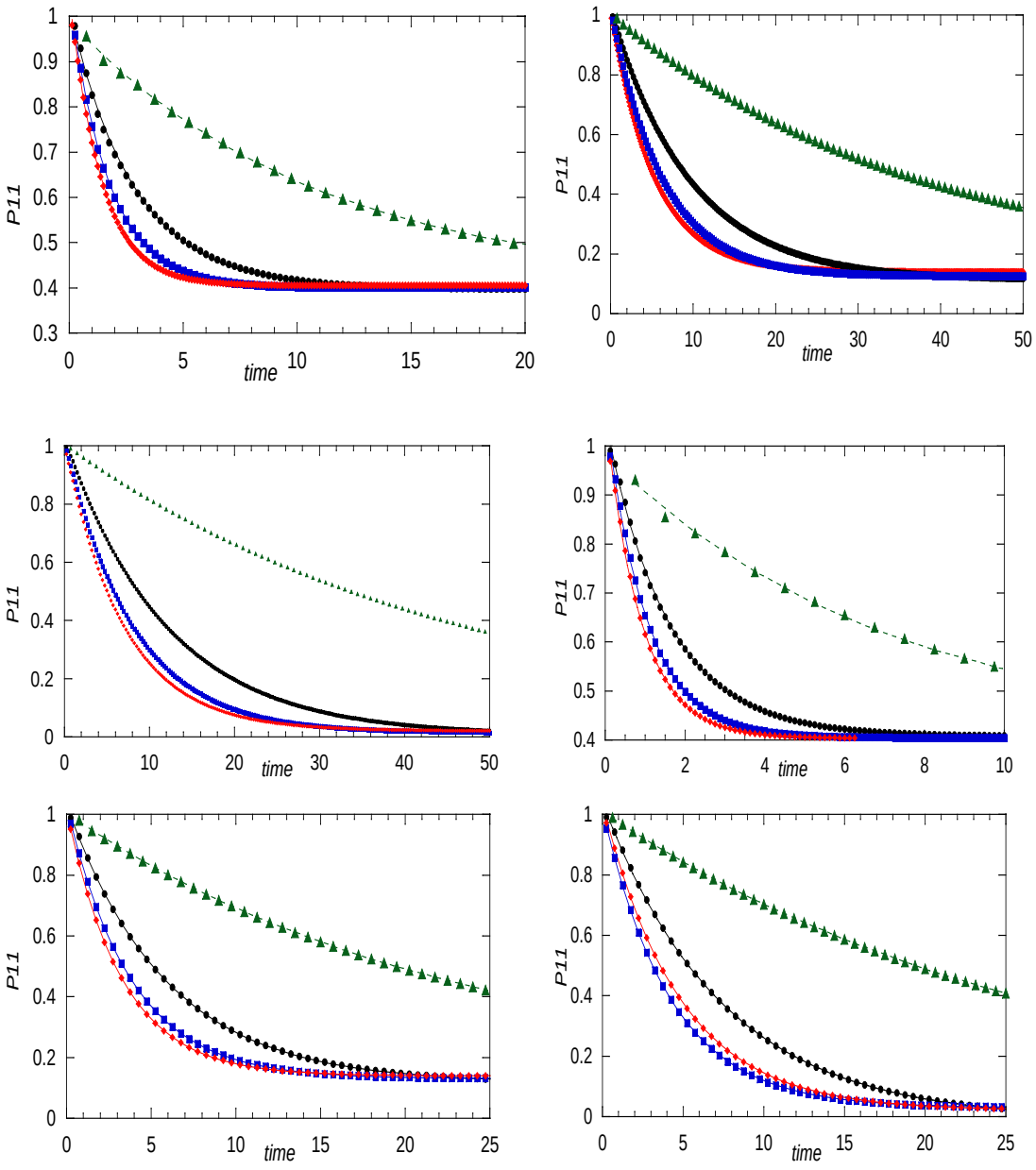

Figure 5.1: Evolution of relaxation population for a TLS with $\hbar\Omega = 1$, $\varepsilon = 0$, initially at the excited state coupled to an Ohmic bath. Green filled triangles, black filled circles, blue filled circles, red filled circles are $\omega_c = 1.0\Omega, 2.5\Omega, 5.0\Omega, 7.5\Omega$. Dashed lines are the exponential fit to the i-QuAPI data. a) $\beta = 0.2; \xi = 0.03$; b) $\beta = 1.0; \xi = 0.03$; c) $\beta = 2.5; \xi = 0.03$; d) $\beta = 0.2; \xi = 0.05$; b) $\beta = 1.0; \xi = 0.05$; c) $\beta = 2.5; \xi = 0.05$;

β	ω_c	Rate (iQuAPI)	Eqm (iQuAPI)	Rate (BR)	Eqm (BR)	Change %
			ξ = 0.03			
0.2	1	0.093	0.4	0.13	0.4	40
	2.5	0.35	0.4	0.43	0.4	23
	5	0.58	0.4	0.64	0.4	10
	7.5	0.71	0.4	0.73	0.4	2
1	1	0.027	0.13	0.033	0.12	22
	2.5	0.104	0.11	0.111	0.12	6
	5	0.161	0.12	0.166	0.12	3
	7.5	0.191	0.14	0.19	0.12	0.5
2.5	1	0.021	0.02	0.026	0.006	23
	2.5	0.084	0.005	0.086	0.006	2.4
	5	0.13	0.015	0.13	0.006	
	7.5	0.144	0.02	0.143	0.006	
			ξ = 0.05			
0.2	1	0.14	0.4	0.21	0.4	50
	2.5	0.64	0.4	0.72	0.4	12.5
	5	0.97	0.4	1.07	0.4	10
	7.5	1.13	0.4	1.22	0.4	8
1	1	0.044	0.13	0.056	0.12	27
	2.5	0.17	0.12	0.185	0.12	9
	5	0.27	0.12	0.28	0.12	3.7
	7.5	0.30	0.14	0.32	0.12	2
2.5	1	0.036	0.02	0.04	0.006	11
	2.5	0.13	0.005	0.14	0.006	7.7
	5	0.21	0.015	0.21	0.006	
	7.5	0.24	0.02	0.24	0.006	

Table 5.1: Equilibrium population and rates of relaxation of population for a TLS with $\hbar\Omega = 1$, $\varepsilon = 0$, initially at the excited state and coupled to an Ohmic bath for the coupling regime $\xi = 0.03; \xi = 0.05$. It shows the comparison with Bloch-Redfield Equations and reports the changes between the two theories.

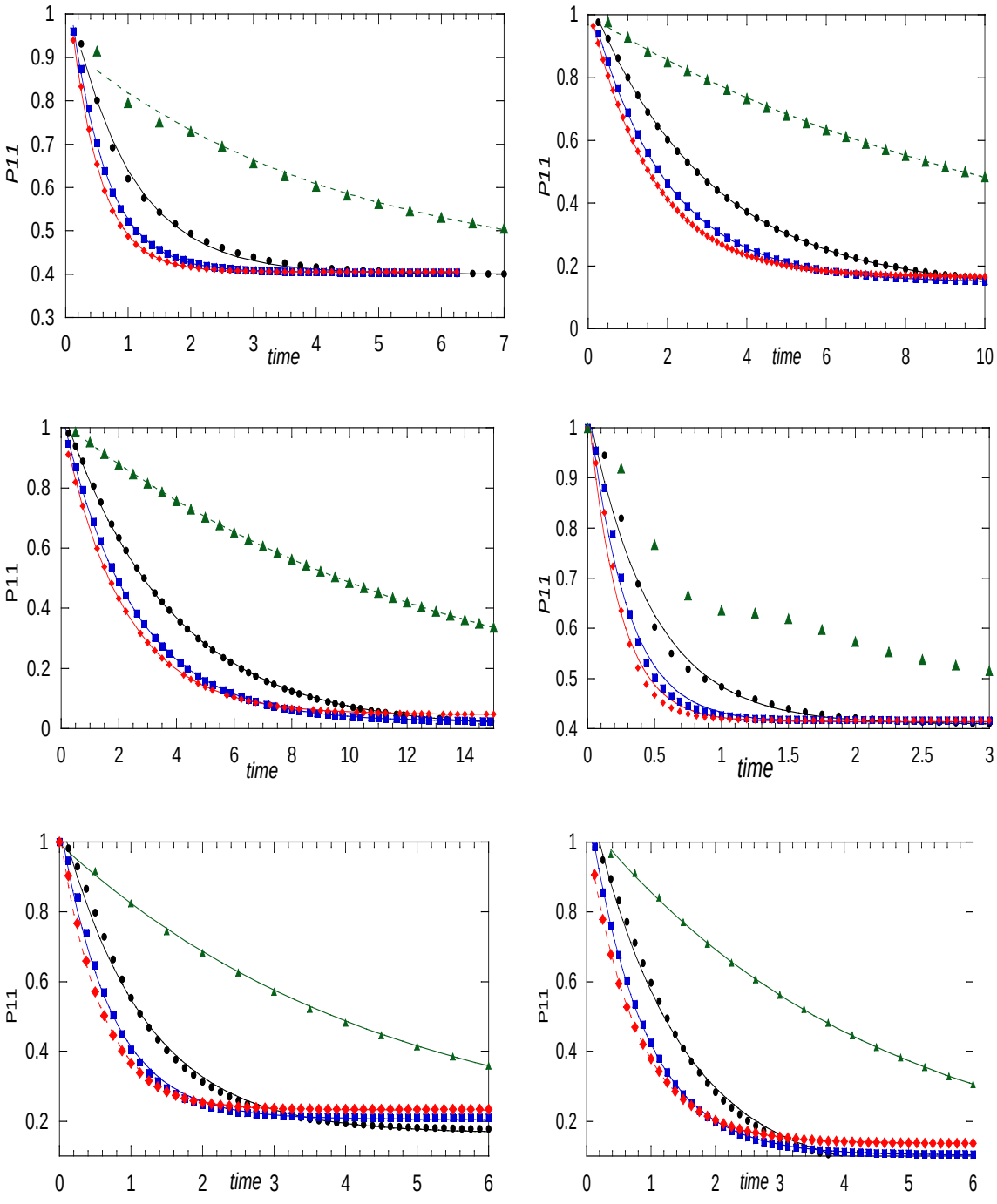

Figure 5.2: Evolution of relaxation population for a TLS with $\hbar\Omega = 1$, $\varepsilon = 0$, initially in the exited state coupled to an Ohmic bath. Green filled triangles, black filled circles, blue filled circles, red filled circles are $\omega_c = 1.0\Omega, 2.5\Omega, 5.0\Omega, 7.5\Omega$. Dashed lines are the exponential fit to the i-QuAPI data. a) $\beta = 0.2; \xi = 0.1$; b) $\beta = 1.0; \xi = 0.1$; c) $\beta = 2.5; \xi = 0.1$; d) $\beta = 0.2; \xi = 0.3$; e) $\beta = 1.0; \xi = 0.3$; f) $\beta = 2.5; \xi = 0.3$;

β	ω_c	Rate (iQuAPI)	Eqm (iQuAPI)	Rate (BR)	Eqm (BR)	Change %
			ξ = 0.1			
0.2	1	0.23	0.4	0.43	0.4	
	2.5	1.02	0.4	1.43	0.4	40
	5	1.76	0.4	2.13	0.4	21
	7.5	2.11	0.41	2.44	0.4	16
1	1	0.07	0.12	0.056	0.12	20
	2.5	0.33	0.12	0.37	0.12	12
	5	0.53	0.15	0.55	0.12	4
	7.5	0.64	0.16	0.63	0.12	1
2.5	1	0.088	0.006	0.086	0.006	22
	2.5	0.29	0.001	0.27	0.006	7
	5	0.41	0.02	0.43	0.006	5
	7.5	0.48	0.05	0.49	0.006	2
			ξ = 0.3			
0.2	1			1.29	0.4	
	2.5	2.45	0.41	4.29	0.4	75
	5	4.00	0.41	6.4	0.4	60
	7.5	4.95	0.41	7.31	0.4	48
1	1		0.21	0.33	0.12	
	2.5	1	0.17	1.11	0.12	11
	5	1.53	0.2	1.66	0.12	8
	7.5	1.85	0.23	1.89	0.12	2
2.5	1	0.22	0.13	0.29	0.006	31
	2.5	0.73	0.14	0.86	0.006	18
	5	1.17	0.14	1.31	0.006	12
	7.5	1.28	0.1	1.46	0.006	14

Table. 5.2: Equilibrium population and rates of relaxation of the population for a TLS with $\hbar\Omega = 1$, $\varepsilon = 0$, initially at the excited state and coupled to an Ohmic bath for the coupling regime $\xi = 0.1; \xi = 0.3$. It shows the comparison with Bloch-Redfield Equations and reports the changes between the two theories

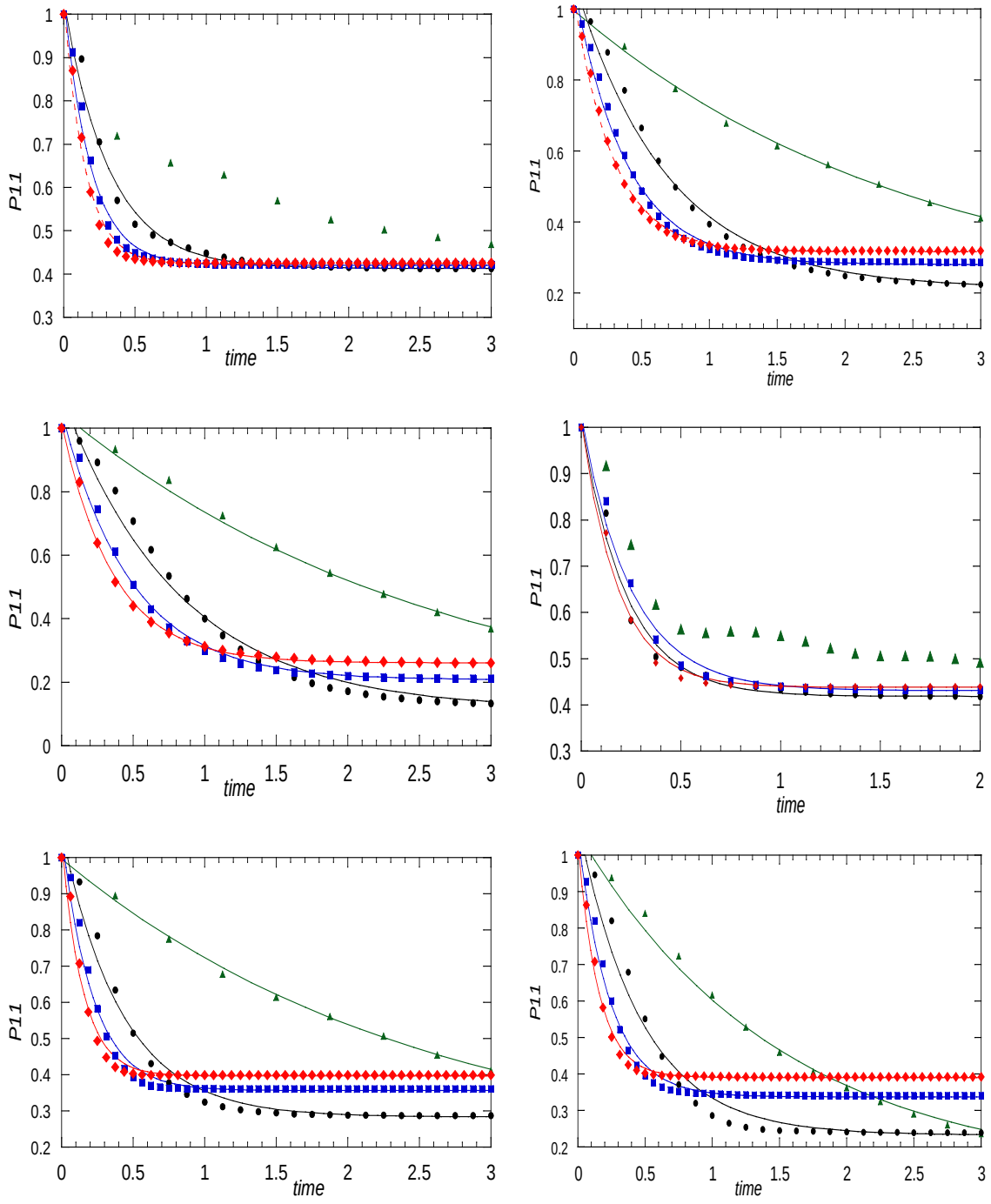

Figure 5.3: Evolution of relaxation population for a TLS with $\hbar\Omega = 1$, $\varepsilon = 0$, initially at excited state coupled to an Ohmic bath. Green filled triangles, black filled circles, blue filled circles, red filled circles are $\omega_c = 1.0\Omega, 2.5\Omega, 5.0\Omega, 7.5\Omega$. Dashed lines are the exponential fit to the i-QuAPI data. a) $\beta = 0.2; \xi = 0.6$; b) $\beta = 1.0; \xi = 0.6$; c) $\beta = 2.5; \xi = 0.6$; d) $\beta = 0.2; \xi = 1.2$; e) $\beta = 1.0; \xi = 1.2$; f) $\beta = 2.5; \xi = 1.2$;

β	ω_c	Rate (iQuAPI)	Eqm (iQuAPI)	Rate (BR)	Eqm (BR)	Change %
			ξ = 0.6			
0.2	1		0.40	2.58	0.4	
	2.5	3.11	0.41	8.58	0.4	
	5	5.31	0.42	12.80	0.4	
	7.5	6.74	0.42	14.63	0.4	
1	1			0.67	0.12	
	2.5	1.83	0.21	2.22	0.12	21
	5	2.86	0.28	3.32	0.12	16
	7.5	3.78	0.32	3.79	0.12	0.2
2.5	1			0.52	0.006	
	2.5	1.22	0.11	1.72	0.006	41
	5	2.06	0.21	2.56	0.006	24
	7.5	2.74	0.26	2.93	0.006	7
			ξ = 1.2			
0.2	1		0.38	5.17	0.4	
	2.5	3.48	0.42	17.16	0.4	
	5	7.98	0.43	25.61	0.4	
	7.5	10.73	0.44	29.26	0.4	
1	1			1.34	0.12	
	2.5	2.92	0.29	4.45	0.12	52
	5	5.6	0.36	6.63	0.12	18
	7.5	8.68	0.4	7.58	0.12	13
2.5	1		0.006	1.03	0.006	
	2.5	2.14	0.23	3.43	0.006	60
	5	4.23	0.34	5.12	0.006	21
	7.5	6.44	0.39	5.85	0.006	9

Table. 5.3: Equilibrium population and rates of relaxation of the population for a TLS with $\hbar\Omega = 1$, $\varepsilon = 0$, initially at the excited state and coupled to an Ohmic bath for the coupling regime $\xi = 0.6; \xi = 1.2$. It shows the comparison with Bloch-Redfield Equations and reports the changes between the two theories.

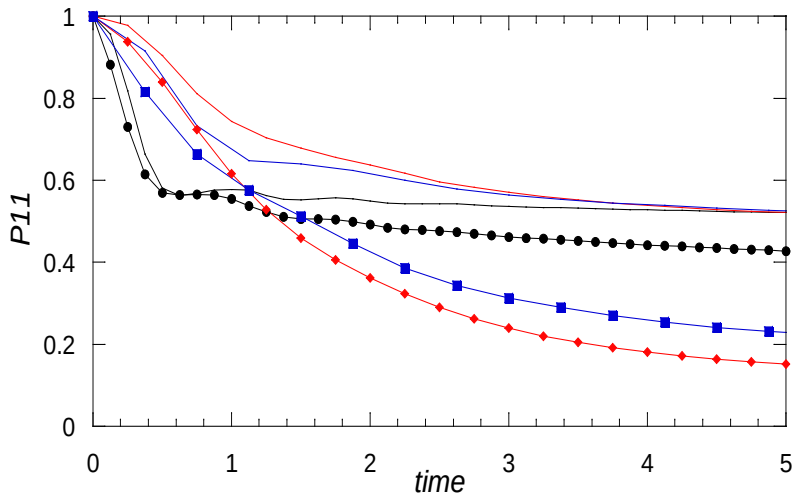

Figure 5.4: Evolution of relaxation population for a TLS with $\hbar\Omega = 1$, $\varepsilon = 0$, initially at excited state coupled to an Ohmic bath. Green filled triangles, black filled circles, blue filled circles, red filled circles are $\omega_c = 1.0\Omega$. Solid lines are the classical coherence, while line with markers is the total dynamicsi-QuAPI data. a) Red: $\beta = 2.5; \xi = 1.2$; b) Blue: $\beta = 1.0; \xi = 1.2$; c) Black: $\beta = 0.2; \xi = 1.2$;

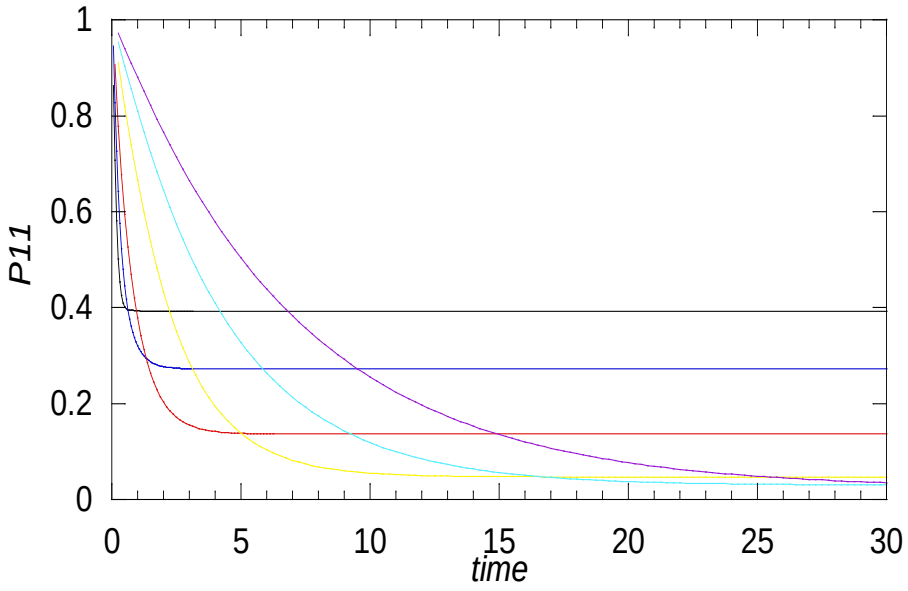

Figure 5.5: Evolution of relaxation population for a TLS with $\hbar\Omega = 1$, $\varepsilon = 0$, initially at excited state coupled to an Ohmic bath. Green filled triangles, black filled circles, blue filled circles, red filled circles are $\omega_c = 7.5\Omega; \beta = 2.5$ a) Black: $\xi = 1.2$; b) Blue: $\xi = 0.6$; c) Red: $\xi = 0.3$; d) Yellow: $\xi = 0.1$; b) Cyan: $\xi = 0.05$; c) Purple: $\xi = 0.03$;

5.8 References:

1. Hamm, Peter, Manho Lim, and Robin M. Hochstrasser. Vibrational energy relaxation of the cyanide ion in water. *The Journal of chemical physics* 107.24 (1997): 10523-10531.

2. Egorov, S. A., and J. L. Skinner. A theory of vibrational energy relaxation in liquids. *The Journal of chemical physics* 105.16 (1996): 7047-7058.

3. Harris, A. L., and N. J. Levinos. Vibrational energy relaxation in a molecular monolayer at a metal surface. *The Journal of Chemical Physics* 90.7 (1989): 3878-3879.

4. Heilweil, E. J., F. E. Doany, R. Moore, and R. M. Hochstrasser. Vibrational energy relaxation of the cyanide ion in aqueous solution. *The Journal of Chemical Physics* 76, no. 11 (1982): 5632-5634.

5. Owrutsky, J. C., Y. R. Kim, M. Li, M. J. Sarisky, and R. M. Hochstrasser. Determination of the vibrational energy relaxation time of the azide ion in protic solvents by two-color transient infrared spectroscopy. *Chemical physics letters* 184, no. 5 (1991): 368-374.

6. Genberg, L., Q. Bao, S. Gracewski, and R. J. D. Miller. Picosecond transient thermal phase grating spectroscopy: a new approach to the study of vibrational energy relaxation processes in proteins. *Chemical physics* 131, no. 1 (1989): 81-97.

7. Owrutsky, J. C., D. Raftery, and R. M. Hochstrasser. "Vibrational relaxation dynamics in solutions." Annual review of physical chemistry 45.1 (1994): 519-555.

8. Gai, Huadong, and Gregory A. Voth. Vibrational energy relaxation of Si–H stretching modes on the H/Si (111) 1× 1 surface. *The Journal of chemical physics* 99.1 (1993): 740-743.

9. Zhong, Q., A. P. Baronavski, and J. C. Owrutsky. Reorientation and vibrational energy relaxation of pseudohalide ions confined in reverse micelle water pools. *The Journal of Chemical Physics* 119.17 (2003): 9171-9177.

10. Skinner, J. L., & Park, K. Calculating vibrational energy relaxation rates from classical molecular dynamics simulations: quantum correction factors for processes involving vibration-vibration energy transfer. *The Journal of Physical Chemistry B*, (2001), *105*(28), 6716-6721.

11. Banin, Uri, Amir Waldman, and Sanford Ruhman. Ultrafast photodissociation of I3− in solution: Direct observation of coherent product vibrations. *The Journal of chemical physics* 96.3 (1992): 2416-2419.

12. Alfano, Joseph C., Y. Kimura, P. K. Walhout, and Paul F. Barbara. Photodissociation and vibrational relaxation of I− 2 in water, ethanol, and ethanol-d 1. *Chemical physics* 175, no. 1 (1993): 147-155.

13. Lian, T., Bromberg, S. E., Asplund, M. C., Yang, H., & Harris, C. B. (1996). Femtosecond infrared studies of the dissociation and dynamics of transition metal carbonyls in solution. *The Journal of Physical Chemistry*, *100*(29), 11994-12001.

14. Banin, Uri, Ronnie Kosloff, and Sanford Ruhman. Femtosecond Chemical Dynamics in Solution: Photodissociation of I3-. *Israel journal of chemistry* 33, no. 2 (1993): 141-156.

15. Redfield, Alfred G. On the theory of relaxation processes. *IBM Journal of Research and Development* 1.1 (1957): 19-31.

16. Bloch, Felix. Nuclear induction. *Physical review* 70.7-8 (1946): 460.

17. Blum, K. Density matrix theory and its application. (1981).

18. Budimir, J., and J. L. Skinner. On the relationship betweenT 1 andT 2 for stochastic relaxation models. *Journal of statistical physics* 49, no. 5-6 (1987): 1029-1042.

19. Laird, Brian B., Jane Budimir, and James L. Skinner. Quantum-mechanical derivation of the Bloch equations: Beyond the weak-coupling limit. *The Journal of chemical physics* 94, no. 6 (1991): 4391-4404.

20. Chang, T-M., and J. L. Skinner. Non-Markovian population and phase relaxation and absorption lineshape for a two-level system strongly coupled to a harmonic quantum bath. *Physica A: Statistical Mechanics and its Applications* 193.3 (1993): 483-539.

21. Sevian, H. M., and J. L. Skinner. T2 can be greater than 2T1. *The Journal of chemical physics* 91.3 (1989): 1775-1782.

22. Egorov, S. A., K. F. Everitt, and J. L. Skinner. Quantum dynamics and vibrational relaxation. *The Journal of Physical Chemistry A* 103.47 (1999): 9494-9499.

23. Reichman, David R., and Robert J. Silbey. On the relaxation of a two-level system: Beyond the weak-coupling approximation. *The Journal of chemical physics* 104.4 (1996): 1506-1518.

24. Reichman, David, Robert J. Silbey, and Alberto Suárez. On the nonperturbative theory of pure dephasing in condensed phases at low temperatures. *The Journal of chemical physics* 105.23 (1996): 10500-10506.

25.Vitali, David, Paolo Allegrini, and Paolo Grigolini. Nonlinear quantum mechanical effects: real or artefact of inaccurate approximations? *Chemical physics* 180.2 (1994): 297-318.

26. Vitali, D., L. Bonci, R. Mannella, and P. Grigolini. Localization breakdown as a joint effect of nonlinear and quantum dissipation. *Physical Review A* 45, 4 (1992): 2285.

27. Bonci, L., P. Grigolini, R. Roncaglia, and D. Vitali. Nonlinear Schrödinger equation and wave-function collapse: An unreliable consequence of the semiclassical approximation. *Physical Review A* 47, no. 5 (1993): 3538.

28. Topaler, Maria, and Nancy Makri. System-specific discrete variable representations for path integral calculations with quasi-adiabatic propagators. *Chemical physics letters* 210.4 (1993): 448-457.

29. Topaler, Maria, and Nancy Makri. Quasi-adiabatic propagator path integral methods. Exact quantum rate constants for condensed phase reactions. *Chemical physics letters* 210.1 (1993): 285-293.

30. Makarov, Dmitrii E., and Nancy Makri. Path integrals for dissipative systems by tensor multiplication. Condensed phase quantum dynamics for arbitrarily long time. *Chemical physics letters* 221.5 (1994): 482-491.

31. Makri, Nancy, and Dmitrii E. Makarov. Tensor propagator for iterative quantum time evolution of reduced density matrices. I. Theory. *The Journal of chemical physics* 102.11 (1995): 4600-4610.

32. Makri, Nancy, and Dmitrii E. Makarov. Tensor propagator for iterative quantum time evolution of reduced density matrices. II. Numerical methodology. *The Journal of chemical physics* 102.11 (1995): 4611-4618.

33. Makarov, Dmitrii E., and Nancy Makri. Tunneling dynamics in dissipative curve-crossing problems. *Physical Review A* 48.5 (1993): 3626.

34. Sim, Eunji, and Nancy Makri. Tensor propagator with weight-selected paths for quantum dissipative dynamics with long-memory kernels. *Chemical physics letters* 249.3 (1996): 224-230.

35. Sim, Eunji, and Nancy Makri. Filtered propagator functional for iterative dynamics of quantum dissipative systems. *Computer physics communications* 99.2 (1997): 335-354.

36. Sim, Eunji. Quantum dynamics for a system coupled to slow baths: On-the-fly filtered propagator method. *The Journal of Chemical Physics* 115.10 (2001): 4450-4456.

37. Lambert, Roberto, and Nancy Makri. "Memory propagator matrix for long-time dissipative charge transfer dynamics." *Molecular Physics* 110.15-16 (2012): 1967-1975.

38. Lambert, Roberto, and Nancy Makri. "Quantum-classical path integral. I. Classical memory and weak quantum nonlocality." *The Journal of chemical physics* 137.22 (2012): 22A552.

39. Makri, Nancy. "Exploiting classical decoherence in dissipative quantum dynamics: Memory, phonon emission, and the blip sum." Chemical Physics Letters 593 (2014): 93-103.

40. Forsythe, Kelsey M., and Nancy Makri. "Dissipative tunneling in a bath of two-level systems." Physical Review B 60.2 (1999): 972.

Chapter 6. Conclusion

Path Integral formulation of quantum mechanics provide an excellent tool for developing system-bath formalisms. System-bath formalisms circumvent the problem of exponential scaling with the number of degrees of freedom which is commonly encountered in quantum mechanics. The degrees of freedom of the total ensemble is partitioned into system of interest (treated quantum mechanically) and environment (bath), where the exponential scaling problem is restricted only to the few system modes. Unlike wave-based methods, path integral methods can intuitively account for all bath correlations on the system. However, while integrating out the degrees of freedom of the bath, the detailed dynamics of the system at a particular time point depends on the entire trajectory of the system. This results in exponential growth in the number of integration terms as the system is propagated forward in time. A natural way of tackling such problem is to increase the system time step. The allowed system time step in numerical evaluation of such problems is determined by the error arising from splitting the total Hamiltonian into the system part and the remaining terms. The work reported in this thesis deals with methods of increasing the time step as compared to the conventional system-bath splitting within the quantum-classical framework of path integrals, by allowing a part of the system-bath interaction to be considered inside the system part, and evaluated by solving the time dependent Schrodinger equation. The first of such methods deal with incorporating the interaction between an unperturbed solvent and the system inside the system propagators. This reference itself captures all bath-induced decoherence of a classical origin and can lead to nearly quantitative results at high temperatures or when the system-bath interaction is weak. To go beyond the unperturbed *ansatz*, we considered the trajectories that take into account the interaction between system and solvent following the *average* system path. These two prescriptions of the references revert back to the EACP and the TDSCF approximations, when used in itself. Incorporating them into the full path integral expressions lead to larger time steps (which motivated its development) and lower phase. Lowering of the phase reduces the number of Monte Carlo points required to converge the multidimensional phase space integral of the bath degrees of freedom, leading to linear reduction in computational costs. The increase of time steps, on the other hand, results in exponential reduction in the number of terms (integrals) required to propagate the ensemble from an initial to the final point, and account for majority of the savings.

Another physically motivated approach to obtain reduction in the exponential growth is by utilizing the observation made in the Makri group, that the memory has a finite length and correlations among time points longer than this memory or decoherence time can be neglected. This allowed for iterative decomposition of the path integral algorithm. All effects of the bath, within the time scale of the decoherence time is taken into account to construct a multidimensional tensor. This tensor can then be propagated forward in time using a matrix-vector multiplication scheme thus restricting the exponential

growth only within the decoherence time limit. This scheme was adapted in the Quantum Classical framework of Path Integral methods using the improved propagators described earlier. The decoherence time was reached in much fewer path integral time steps allowing for a further exponential reduction, facilitating much easier iterative decomposition. Further advantage comes from the lower ranked tensors and propagators to be stored, which is often the restricting criteria for allowing larger memory calculations.

A third physical motivation that deals with the exponential scaling problem arise from the observation that many of the paths generated (either in the full path framework or within the deoherence time window) have low weight and can be neglected. Conventional system propagators constructed in the energy truncated basis utilize the fact that the weight of the path that undergoes many system transitions are low and can be neglected. For the improved reference propagators being dependent of the solvent dynamics, additionally. the state-to-state transitions are controlled by the magnitude of solvent reorganization. This is crucial for efficiency, as the interplay between nonadiabatic transitions and dissipative effects is known to play an important role in determining reaction rates. Also, this implies that phase-space areas of large reorganization can easily be filtered out. The above advantages have been carefully validated using spin-boson models in various parameter regimes that highlight the physical motivation dealt with.

The main advantage of the quantum classical treatment of path integrals come from the fact that it can treat any generic bath and the methodology is not restricted to a harmonic bath bi-lineraly coupled to a system. The ideas developed for the QCPI framework was further integrated by our group with molecular dynamics packages like NAMD. It was used to study the electron transfer reaction in Ferrocene and Ferrocenium complex in Benzene via the classical path treatment of the fully atomistic QCPI and also via a harmonic bath model mapped to the atomistic solvent. By doing we achieved the following: first it was conclusively proved, both from theoretical intuition and statistical distribution, how to map the inherently anharmonic bath to produce a Gaussian bath with the closest resemblance to initial potential. Second, the anharmonic effects was quantified and its effect on the dynamics of the system was demonstrated. Third, a quantitative check on accuracy of Marcus' theory revealed that even in this 'classical like' system there is a 30% difference in the Marcus rate and the exact calculated rate.

To correctly account for the initial distribution of the solvent on the dynamics of the system, we compared two simple ways of applying the Quasi-Adiabatic Path Integral (QuAPI) method designed for a harmonic bath bilinearly coupled to the system, to an environment initially in equilibrium with the localized state of the system (e.g., the donor in the case of charge transfer, or the protonated species). Motivated by the analysis of equivalence of the QCPI methods for harmonic model with the Feynman Vernon influence functional, the work involved deriving the phase of the system via a time-local component. This approach requires the evaluation of new coefficients obtained from the shifted influence functional. The second,

alternative approach involves shifting the coordinate of the system, to bring the donor state in equilibrium with the bath. When applied in the Quasi-Adiabatic Path Integral framework the two approaches are equivalent.

The concepts of filtering and iteration in the Quasi-Adiabatic Path Integral (QuAPI) framework has been used to model the vibrational relaxation process using the Spin Boson Hamiltonian where relaxation between two energy levels occurs due to the off-diagonal coupling to the bath. The exact quantum mechanical results for population relaxation times (T1) were compared to previously reported approximate methods, including the Redfield approximations and the fourth order perturbative treatments. These approximate methods are correct only in the lower temperature and lower coupling regimes, while there is a considerable quantitative difference of these methods to the accurate answers for highly quantum mechanically coupled regimes. The perturbative approaches are based on coupled differential equations and hence always predict exponential kinetics, with the rates increasing with increase in coupling strengths. Thus the diffused coherent-incoherent phase transition observed using fully quantum mechanical methods cannot be captured by them. The boundary between the coherent and incoherent transition is also not very well defined and it depends strongly on coupling strengths and cut-off frequencies, and considerably on temperature. Ongoing work on the exact quantum mechanical nature of phase relaxation times (T2), the pure dephasing component (T2') will help develop further insights on regions of negativity of T2' especially for strongly correlated regimes in non-ohmic spectral densities.